



**Calhoun: The NPS Institutional Archive**  
**DSpace Repository**

---

Theses and Dissertations

1. Thesis and Dissertation Collection, all items

---

1972

# A discrete potential element approach to nonsteady subsonic lifting surface theory

Breckon, Richard Louis

Monterey, California. Naval Postgraduate School

---

<http://hdl.handle.net/10945/16092>

---

This publication is a work of the U.S. Government as defined in Title 17, United States Code, Section 101. Copyright protection is not available for this work in the United States.

*Downloaded from NPS Archive: Calhoun*



<http://www.nps.edu/library>

Calhoun is the Naval Postgraduate School's public access digital repository for research materials and institutional publications created by the NPS community. Calhoun is named for Professor of Mathematics Guy K. Calhoun, NPS's first appointed -- and published -- scholarly author.

**Dudley Knox Library / Naval Postgraduate School**  
**411 Dyer Road / 1 University Circle**  
**Monterey, California USA 93943**

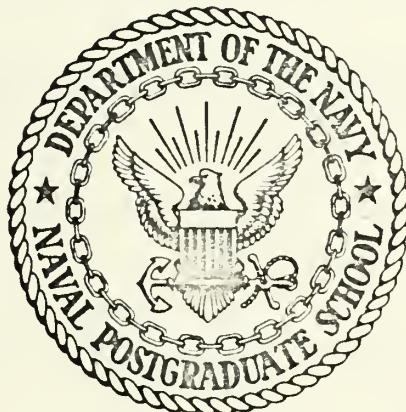
A DISCRETE POTENTIAL ELEMENT APPROACH TO  
NONSTEADY SUBSONIC LIFTING SURFACE THEORY

Richard Louis Breckon



# NAVAL POSTGRADUATE SCHOOL

## Monterey, California



# THESIS

A DISCRETE POTENTIAL ELEMENT APPROACH  
TO  
NONSTEADY SUBSONIC LIFTING SURFACE THEORY

by

Richard Louis Breckon

Thesis Advisor:

L. V. Schmidt

June 1972

*Approved for public release; distribution unlimited.*





A Discrete Potential Element Approach  
to  
Nonsteady Subsonic Lifting Surface Theory

by

Richard Louis Breckon  
Commander, United States Navy  
B.S.M.E., University of California, 1957  
M.S.A.E., Naval Postgraduate School, 1965

Submitted in partial fulfillment of the  
requirements for the degree of

DOCTOR OF PHILOSOPHY

from the  
NAVAL POSTGRADUATE SCHOOL  
June 1972



## ABSTRACT

A discrete potential element approach to subsonic numerical lifting surface theory has been developed and shown to be practical in predicting the nonsteady loading on harmonically oscillating, medium to low aspect ratio wings. A unique method of including the wake effect in the wing kernel function matrix prior to solution of the singular integral downwash equation was devised, thus greatly simplifying the velocity potential formulation. In addition, termination of the effective wake a finite distance downstream of the wing was investigated, with wing loading found to converge to within one per cent in an effective wake length of four root chords.

This discrete element method has also been extended to the case of an oscillating wing, cantilevered from a cylindrical fuselage, to investigate nonplanar interference effects. This interference in wing loading, while of relatively small magnitude, does exist in both pressure amplitude and phase angle distributions, and is, therefore, of importance in three-dimensional stability analyses of wing/body configurations.



## TABLE OF CONTENTS

I.	INTRODUCTION -----	14
II.	GENERAL PROBLEM DEVELOPMENT -----	17
	A. POTENTIAL FLOW EQUATIONS -----	17
	B. SMALL PERTURBATION THEORY -----	19
	C. LINEARIZED BOUNDARY CONDITIONS -----	21
III.	LIFTING SURFACE THEORY -----	27
	A. BASIC APPROACH -----	27
	B. NUMERICAL SOLUTIONS TO LIFTING SURFACE THEORY -----	30
	C. SOLUTIONS BASED ON DISCRETE LOADING LINES -----	32
	D. NONPLANAR CONFIGURATIONS -----	33
IV.	DISCRETE POTENTIAL ELEMENT DEVELOPMENT -----	35
	A. WING ANALYSIS -----	35
	1. Basic Formulation -----	35
	2. Wake Effect -----	29
	3. Matrix Equation for Symmetric Motion ----	43
	4. Doublet Singularity -----	46
	5. Section and Wing Coefficients -----	49
	B. WING/BODY ANALYSIS -----	52
	1. Basic Formulation -----	52
	2. Governing Matrix Equation -----	56
	3. Symmetry -----	58
	4. Effective Body Length -----	61



5.	Body Singularities -----	62
6.	Kernel Functions -----	63
V.	DESCRIPTION OF COMPUTER PROGRAMS -----	66
A.	GENERAL DESCRIPTION -----	66
B.	WING PROGRAM -----	67
C.	WING/BODY PROGRAM -----	69
VI.	RESULTS AND DISCUSSION -----	73
A.	WING ANALYSIS -----	73
1.	Comparison with Lifting Surface Theory -----	73
2.	Convergence -----	98
3.	Wake Effect -----	107
B.	WING/BODY ANALYSIS -----	111
1.	Comparison with Steady Analyses -----	111
2.	Extension to Nonsteady Interference -----	118
VII.	CONCLUSIONS -----	126
APPENDIX A:	KERNEL FUNCTION DEVELOPMENT -----	130
1.	Stationary Singularity -----	131
2.	Moving Singularity -----	133
3.	Wing-Fixed Periodic Singularities -----	135
4.	Kernel Functions for Wing/Body Doublets -----	136
APPENDIX B:	INPUT INSTRUCTIONS FOR COMPUTER PROGRAMS -----	141
1.	Wing Program -----	141
2.	Wing/Body Program -----	142
APPENDIX C:	COMPUTER PROGRAM FLOW DIAGRAMS -----	144
APPENDIX D:	LISTING OF THE FORTRAN CODE FOR THE WING PROGRAM -----	155





APPENDIX E: LISTING OF THE FORTRAN CODE FOR THE WING/BODY PROGRAM -----	166
LIST OF REFERENCES -----	183
INITIAL DISTRIBUTION LIST -----	188
FORM DD 1473 -----	189



## LIST OF FIGURES

### Figure

1.	Coordinate System and Boundary Conditions of General Lifting Surface Problem -----	25
2.	Wing/Wake Discrete Element Grid -----	37
3.	Boundary Conditions for Linearized Harmonic Motion -----	40
4.	Discrete Potential Representation of Wake Effect -----	42
5.	Wing/Wake Planform for Analysis of Symmetric Wing Motion -----	44
6a.	Singularity in Doublet Upwash -----	48
6b.	Discrete Element Representation of Doublet Singularity -----	48
7.	Wing/Wake/Body Discrete Element Grid -----	54
8.	Wing/Body Configuration in Cylindrical Coordinates -----	55
9a.	Representation of Wing/Body Potential Singularities -----	60
9b.	Wing/Body No-Flow Boundary Condition -----	60
10.	Wing Program Diagram -----	68
11.	Wing/Body Program Diagram -----	71
12.	Chordwise Pressure Distribution - Pitching - Swept, Tapered Wing - 0.1 Mach Number -----	80
13.	Spanwise Loading - Pitching - Swept, Constant Chord Wing	
a.	0.1 Mach Number -----	81
b.	0.8 Mach Number -----	82



14.	Spanwise Loading - Plunging - Swept, Constant Chord Wing	
a.	0.1 Mach Number -----	83
b.	0.8 Mach Number -----	84
15.	Steady Spanwise Loading - Swept, Tapered Wing 0.1 Mach Number -----	85
16.	Rectangular Wing - Bending - 0.24 Mach Number	
a.	Chordwise Pressure Distribution - Amplitude -----	86
b.	Chordwise Pressure Distribution - Phase Angle -----	87
c.	Spanwise Loading -----	88
17.	Rectangular Wing - Bending - 0.7 Mach Number	
a.	Chordwise Pressure Distribution - Amplitude -----	89
b.	Chordwise Pressure Distribution - Phase Angle -----	90
c.	Spanwise Loading -----	91
18.	Spanwise Loading - Bending - Rectangular Wing - 0.9 Mach Number -----	92
19.	Rectangular Wing - Pitching - 0.1 Mach Number	
a.	Chordwise Pressure Distribution - Amplitude -----	93
b.	Chordwise Pressure Distribution - Phase Angle -----	94
c.	Spanwise Loading -----	95
20.	Spanwise Loading - Plunging - Rectangular Wing - 0.1 Mach Number -----	96
21.	Frequency Response - Flapping - Rectangular Wing -----	97
22.	Convergence - Pitching	
a.	Spanwise Loading - Amplitude -----	100
b.	Spanwise Loading - Phase Angle -----	101



23.	Convergence - Bending	
a.	Spanwise Loading - Amplitude -----	102
b.	Spanwise Loading - Phase Angle -----	103
24.	Convergence - Flapping	
a.	Spanwise Loading - Amplitude -----	104
b.	Spanwise Loading - Phase Angle -----	105
25.	Convergence - Steady Angle of Attack -----	106
26.	Wake Effect - Example - Bending -----	109
27.	Wake Effect - Maximum Deviation -----	110
28.	Steady Wing/Body Spanwise Loading -----	115
29.	Convergence - Steady Wing/Body -----	116
30.	Effect of Body Size - Steady Case -----	117
31.	Unsteady Wing/Body Spanwise Loading - Wing Bending	
a.	Amplitude -----	120
b.	Phase Angle -----	121
32.	Effect of Body Size - Wing Bending	
a.	Spanwise Loading Amplitude -----	122
b.	Phase Angle -----	123
33.	Unsteady Wing/Body Spanwise Loading - Wing Torsion	
a.	Amplitude -----	124
b.	Phase Angle -----	125
34.	Wing Program - MAIN Flow Diagram -----	145
35.	Subroutine PRES Flow Diagram -----	146
36.	Wing Program - DINCO Flow Diagram -----	147
37.	Subroutine COMAT Flow Diagram -----	148
38.	Subroutines SECLM and WINGLM Flow Diagram -----	149





39.	Wing/Body Program - MAIN Flow Diagram -----	150
40.	Wing/Body Program - DINCO Flow Diagram -----	151
41.	Subroutine UTHETA Flow Diagram -----	152
42.	Subroutine URAD1 Flow Diagram -----	153
43.	Subroutine URAD2 Flow Diagram -----	154



# TABLE OF SYMBOLS

$a$	speed of sound
$AR$	aspect ratio
$b$	wing semispan
$c$	wing chord
$c_r$	wing root chord
$c_t$	wing tip chord
$c_\ell$	section lift coefficient ( $\ell/qc$ )
$C_L$	wing lift coefficient ( $L/qS$ )
$c_m$	section pitching moment coefficient ( $m/qc^2$ )
$C_M$	wing pitching moment coefficient ( $M/qSc_r$ )
$c_p$	coefficient of pressure ( $p/q$ )
$c_{p\chi}, c_{\ell\chi}$	coefficients normalized with respect to indicated motion amplitude ( $\chi$ )
$h$	wing vertical translation, positive upwards in $+z$ direction
$i$	$\sqrt{-1}$ in complex valued variables
$k$	reduced frequency parameter ( $\omega c_r/2U_\infty$ )
$K$	kernel function
$\ell$	sectional lift force per unit span
$L$	wing lift force, or wing loading in kernel function formulation wing forces are positive upwards in $+z$ direction
$m$	sectional pitching moment per unit span
$M$	wing pitching moment moments are positive in nose up sense
$M_\infty$	free stream Mach number
$p$	pressure



$\Delta p$	pressure difference across lifting surface
$q$	dynamic pressure ( $\frac{1}{2}\rho_{\infty}U_{\infty}^2$ )
$R$	modified radius, defined in each case where used
$r_B$	radius of body
$S$	wing planform area, or surface of integration
$t$	time
$\vec{U}$	total velocity vector
$\vec{u}$	perturbation velocity vector
$(u,v,w)$	perturbation velocity components in cartesian coordinate system
$(u_r, u_{\theta}, u_x)$	perturbation velocity components in cylindrical coordinate system
$(x,y,z)$	cartesian coordinates, normally dimensional
$(\xi,\eta,\zeta)$	cartesian coordinates, normally non-dimensionalized with respect to $(c,b,c)$
$(r,\theta,x)$	cylindrical coordinate system, normally dimensional
$\alpha$	angle of attack
$\beta$	compressibility factor $\sqrt{1-M_{\infty}^2}$
$\gamma_{\chi}$	phase angle between force $\chi$ and wing motion, positive for force leading motion displacement
$\nabla$	gradient operator, $\hat{i} \left( \frac{\partial}{\partial x} \right) + \hat{j} \left( \frac{\partial}{\partial y} \right) + \hat{k} \left( \frac{\partial}{\partial z} \right)$ in cartesian coordinates
$\nabla^2$	Laplacian operator, $\frac{\partial^2}{\partial x^2} + \frac{\partial^2}{\partial y^2} + \frac{\partial^2}{\partial z^2}$ in cartesian coordinates
$\lambda$	taper ratio ( $c_t/c_r$ )
$\rho$	density
$\phi$	velocity potential
$\psi$	acceleration potential
$\omega$	circular frequency (radians per second)
$\Lambda$	angle of sweep, wing leading edge



$\exp(\chi)$	$e^{(\chi)}$	
[ ]	matrix symbol	
{ }	vector symbol	
$[\ ]^{-1}$	inverse of indicated matrix	
notation convention		
$P, U, \phi$	total stream values	
$U_{\infty}, \rho_{\infty}, a_{\infty}$	steady free stream values	
$\bar{p}, \bar{u}, \bar{\phi}$	perturbation values	
$p, u, \phi$	complex perturbation amplitude for harmonic motion $\bar{p}(x, y, z, t) = p(x, y, z)e^{i\omega t}$	





## ACKNOWLEDGEMENT

To my friend and advisor, Professor L. V. Schmidt, I wish to offer my deep appreciation for the invaluable aid and encouragement he has given me throughout all phases of my graduate education.

To the members of my Doctoral Committee, Professors Ball, Collins, Eller, Platzner, and Stewart, I express my gratitude for the assistance so freely given in this effort.

For my wife, Judi, and my children, Bill, Terrie, Lori, Mike, John, and Francie, I can only humbly acknowledge the unwavering faith and personal commitment each has invested in the quest.

Finally, I dedicate this thesis, whatever it's worth, to the memory of my father, Louis A. Breckon. Pax Dómini sit semper vo bíscum.

A handwritten signature in cursive script, appearing to read "L. A. Breckon", with a long horizontal flourish extending to the right.



## I. INTRODUCTION

The aerodynamic analysis of the forces over an oscillating wing, situated in a steady flow, is the basic problem considered by nonsteady lifting surface theory. The determination of these nonsteady pressure distributions is of prime importance in the consideration of stability. A basic objective of flutter analysis, for example, is to determine the aerodynamic loading on a wing oscillating with small amplitudes in a definite mode and with a given frequency. Thus the problem is formulated on the basis that the motion and deformation of the lifting surface are either known or composed of known elemental modes, and is amenable to harmonic modal analysis. A downwash integral equation, based on the transformed wave equation for linearized potential flow, relates loading (either in terms of velocity potential or pressure) over the oscillating wing to the normal velocity induced by the wing motion, and must be solved numerically to obtain this wing loading.

The analysis of this paper will deal primarily with the subsonic case, this being the one in which the largest number of applications of lifting surface theory to engineering problems are to be found [1]. Most of the work in subsonic nonsteady lifting surface theory is based on the development of the general kernel function approach by Küssner in 1940 [2], which was first formulated successfully



for the computer by Watkins, Runyan, and Woolston in 1955 [3]. More recent techniques have been developed by Stark in 1964 [4] and Laschka in 1963 [5]. Solution of the singular downwash integral equation by the usual lifting surface methods is accomplished through assuming the loading to be a series of preselected functions with unknown coefficients, and then determining these by satisfying the normal velocity condition with some sort of collocation technique. The downwash and the loading are related by kernel functions, which are themselves singular, and which must be numerically evaluated.

In spite of the fact that lifting surface theory has enjoyed a great deal of success, certain shortcomings, discussed in Refs. 1, 6, and 7, do exist:

(i) Lifting surface theory is not as computationally economic as steady or two-dimensional methods.

(ii) Wing loading functions, which incorporate the proper singular behavior, have to be assumed a priori.

(iii) Uncertainty exists as to the method of locating collocation points.

(iv) Techniques for analyzing control surface effects have not been adequately developed, partly because of (ii).

(v) Lifting surface theory has been primarily restricted to planar surfaces.

In order to attack these problems, Houbolt [6] proposed that the wing loading be represented by concentrated pressure loads in the form of Dirac delta functions. Using this loading representation, the kernel function and downwash



equation were formulated and analyzed for certain restricted cases. However, no general numerical solution of the lifting surface problem was developed.

The present study is concerned with developing such a method of solution to the subsonic, nonsteady lifting surface problem, in terms of discrete loading elements. However in this case wing loading is expressed in terms of velocity potential, rather than pressure, since this formulation allows a more direct approach to nonplanar configurations. Haviland [8] reports using a similar approach to the steady planar case with consistent results.

The aim of this discrete potential element method is to provide a new approach to nonsteady, subsonic lifting surface theory which eliminates, or minimizes, the problems previously indicated. Theoretical development of this approach was made from basic principles, and the resulting formulation applied in a computer program which analyzes harmonically oscillating wings in subsonic flow. A unique way of including the wake effect was also developed which greatly simplified the velocity potential solution of the numerical problem. As an extension of the theory, and an indication of the versatility of this discrete element approach, a second computer program was developed to analyze interference effects on oscillating wings mid-mounted from steady bodies. To the author's knowledge, this type of wing/body interference investigation has not previously been presented for the nonsteady case.





## II. GENERAL PROBLEM DEVELOPMENT

Following the method of development by Garrick [9], the governing equations and boundary conditions are linearized by application of small perturbation theory.

### A. POTENTIAL FLOW EQUATIONS

The governing equations for adiabatic, irrotational, inviscid flow, as developed in Ref. 10 are:

Continuity

$$\frac{\partial \rho}{\partial t} + \nabla \cdot \rho \vec{U} = 0 \quad (2.1)$$

Momentum

$$\frac{\partial \vec{U}}{\partial t} + \vec{U} \cdot \nabla \vec{U} = - \frac{1}{\rho} \nabla P \quad (2.2)$$

Energy

$$\frac{P}{\rho^\gamma} = \text{constant} \quad (\gamma \text{ the specific heat ratio}) \quad (2.3)$$

Since the flow is irrotational, the curl of the velocity vector vanishes ( $\nabla \times \vec{U} = 0$ ) and a velocity potential function can be defined, such that

$$\vec{U} = \nabla \phi \quad (2.4)$$

If further, a perfect gas is assumed, then from the energy equation the well known relationship

$$\partial P / \partial \rho = a^2 \quad (2.5)$$

is obtained for constant entropy flows.



The continuity and momentum equations can now be rewritten as

$$\frac{1}{\rho} \frac{D\rho}{Dt} + \nabla^2 \phi = 0 \quad (2.6)$$

$$\nabla \left( \frac{\partial \phi}{\partial t} + \frac{U^2}{2} \right) = - \frac{a^2}{\rho} \nabla \rho \quad (2.7)$$

where  $\frac{D}{Dt}$  is the substantial derivative defined by  $\left( \frac{\partial}{\partial t} + \vec{U} \cdot \nabla \right)$ .

Combining equations (2.6) and (2.7), a single equation in  $\phi$  is obtained.

$$\nabla^2 \phi - \frac{1}{a^2} \left( \frac{\partial}{\partial t} + \vec{U} \cdot \nabla \right)^2 \phi = 0$$

or

$$\nabla^2 \phi - \frac{1}{a^2} \frac{D^2 \phi}{Dt^2} = 0 \quad (2.8)$$

This is the governing partial differential equation for general nonsteady, nonviscous, potential flow of a perfect gas. Equation (2.8) is not limited to small disturbances, and has the form of the classic wave equation in terms of the substantial, or convective derivative. Thus, the flow disturbance represented by the velocity potential is convected by the local fluid, or stream velocity, and propagated as a wave which spreads at a rate equal to the local speed of sound.

In this general form, equation (2.8) is highly nonlinear due both to the quadratic terms in the convective operator  $\vec{U} \cdot \nabla$ , and to the interdependence of the velocity potential and the local speed of sound. Boundary conditions, in general, will depend on the location and form of the moving



body, on discontinuities along streamlines, on shock waves, and on flow conditions at infinity. There exist no general methods for obtaining solutions to equation (2.8), and it is necessary to consider small perturbations, to linearize, to reduce the number of equations, or to try schemes of successive approximations to attack the general problem.

## B. SMALL PERTURBATION THEORY

Most of the theoretical developments in aerodynamics, including nonsteady aerodynamics, are based on the concept of small perturbations. There are two aspects to the problem of flow past a body creating small disturbances in an undisturbed mainstream, linearization of the governing differential equations and further linearization of the boundary conditions.

Linearization of the governing equations requires the problem to be posed with a compressible fluid in a uniform stream flowing with velocity  $U_\infty$  in the positive  $x$  direction. Small disturbances in the flow are defined by

$$\vec{U} = (U_\infty + \bar{u})\hat{i} + \bar{v}\hat{j} + \bar{w}\hat{k} = U_\infty\hat{i} + \vec{u}$$

$$\rho = \rho_\infty + \bar{\rho} \qquad \phi = \phi_\infty + \bar{\phi}$$

$$P = p_\infty + \bar{p} \qquad \text{with } \vec{u} = \nabla \bar{\phi}$$

The perturbation velocities are considered small with respect to  $U_\infty$ ,  $a_\infty$ , and  $U_\infty - a_\infty$ , thus ruling out transonic flow. The perturbation density and pressure are also restricted, so that



$$\bar{\rho}/\rho_{\infty} \quad \text{and} \quad \bar{p}/p_{\infty} \ll 1$$

Considering  $\bar{\phi}$  as the perturbation velocity potential, the governing equation (2.8) becomes

$$\nabla^2 \bar{\phi} - \frac{1}{a_{\infty}^2} \left( \frac{\partial}{\partial t} + U_{\infty} \frac{\partial}{\partial x} \right)^2 \bar{\phi} = 0 \quad (2.9)$$

where higher order terms in the  $\vec{U} \cdot \nabla$  operator have been neglected. This linearized governing equation may now be applied to flow problems within the initial small perturbation assumptions. Although equation (2.9) was developed for a uniform flow in the positive  $x$  direction relative to a space-fixed coordinate system, it also applies to the case of a wing moving with uniform velocity  $U_{\infty}$  in the negative  $x$  direction with the coordinate system fixed to the wing.

Within the concept of small perturbations, the momentum equation becomes

$$\frac{\partial \vec{u}}{\partial t} + U_{\infty} \frac{\partial \vec{u}}{\partial x} = - \frac{1}{\rho_{\infty}} \nabla \bar{p} \quad (2.10)$$

Substituting the perturbation velocity potential ( $\vec{u} = \nabla \bar{\phi}$ ) into this equation, a linear relationship between potential and pressure is obtained.

$$\bar{p} = -\rho_{\infty} \left( \frac{\partial}{\partial t} + U_{\infty} \frac{\partial}{\partial x} \right) \bar{\phi} \quad (2.11)$$

Therefore  $\bar{p}$  satisfies the same differential equation (2.9) as does  $\bar{\phi}$ .

If harmonic motion were considered, the perturbation variables would have the form





$$\bar{\phi} = \phi(x,y,z)e^{i\omega t}, \quad \bar{p} = p(x,y,z)e^{i\omega t}$$

$$\bar{u} = u(x,y,z)e^{i\omega t}, \text{ etc.}$$

and the governing equation would become

$$\nabla^2 \phi - \frac{1}{a_\infty^2} (U_\infty \frac{\partial}{\partial x} + i\omega)^2 \phi = 0 \quad (2.12)$$

with the relationship between pressure and velocity potential

$$p = -\rho_\infty (U_\infty \frac{\partial}{\partial x} + i\omega) \phi \quad (2.13)$$

In the above equations the time dependence  $e^{i\omega t}$  has been factored out. This relationship between  $p$  and  $\phi$  can be integrated to give

$$\phi(x,y,z) = - \frac{e^{-i\omega x/U_\infty}}{\rho_\infty U_\infty} \int_{-\infty}^x p(\xi,y,z) e^{i\omega \xi/U_\infty} d\xi \quad (2.14)$$

where far ahead of the disturbance, the perturbation potential is assumed to be zero.

### C. LINEARIZED BOUNDARY CONDITIONS

The small disturbance assumption, resulting in the linearized governing differential equation (2.9), implies small deviations from the uniform flow. Therefore it is also necessary to linearize the boundary conditions for the physical problems considered, such as properly oriented thin wings and slender bodies. These boundary conditions consist of the mathematical formulation of several physical and phenomenological statements which are normally grouped as follows:



(i) Surface boundary conditions. No flow can pass through the wing or body surface, that is to say the total flow is tangential to the body surface.

(ii) Edge conditions. Sufficient viscosity is present in the "nonviscous" flow to determine the flow pattern near sharp edges. Thus in subsonic flow the well known Kutta Condition can be applied to the wing trailing edge, requiring that the surface pressure difference remains continuous near, and vanishes at, the trailing edge. A similar condition should be satisfied at the side edges. Through the method of matched asymptotic expansions, Landahl [11] verified that at trailing and side edges the pressure difference will approach zero with infinite slope due to weak singularities in the first derivative. Conditions at the leading edge have not been fully explored, but for small disturbances to rounded leading edges it is sufficient to require that the total integrated force be finite and the singularities in the pressure distribution be of the proper order [9]. This latter requirement is fulfilled with the pressure varying as the inverse square root of the distance downstream of the leading edge [12].

(iii) Wake conditions. The free vorticity shed from the trailing edge in the wake is such that its circulation together with the bound circulation vanishes in accordance with the Helmholtz-Kelvin Theorem. It is assumed that the shed wake remains where it is formed, floats without mutual interference along streamlines, and forms a continuous sheet



of discontinuity coplanar with the wing in the direction of flight. Edge effects and roll-up of the sheet at infinity are ignored.

(iv) Conditions at infinity. The flow is considered uniform at infinity, and perturbation waves are required to propagate away from the sources of disturbances and to behave properly at infinity.

In addition to the above, for supersonic flow account must be taken of zones of influence and dependence, as in the method of characteristics. In supersonic flow there are also other problems which do not arise in the subsonic analysis, such as the difference between subsonic and supersonic edges.

To formulate the main boundary conditions, a thin wing is considered lying in the  $x$ - $y$  plane, creating small disturbances in a uniform stream  $U_\infty$  flowing in the positive  $x$  direction. The linearized tangential flow condition on the wing surface  $\bar{z}_s$  takes the form

$$\bar{w}(x, y, z_s, t) = \frac{\partial \bar{z}_s}{\partial t} + U_\infty \frac{\partial \bar{z}_s}{\partial x} \quad (2.15)$$

The normal fluid velocity  $\bar{w}$  can be expanded in a power series about  $z = 0$ , so that

$$\begin{aligned} \bar{w}(x, y, z_s, t) = & \bar{w}(x, y, 0, t) + \left( \frac{\partial \bar{w}}{\partial z} \right)_{z=0} \bar{z}_s \\ & + \frac{1}{2!} \left( \frac{\partial^2 \bar{w}}{\partial z^2} \right)_{z=0} \bar{z}_s^2 + \dots \end{aligned} \quad (2.16)$$



In addition, problems of camber and thickness can be separated from wing motion and angle of attack in the linearized formulation. Therefore, neglecting higher order terms in equation (2.16), the tangential flow condition becomes

$$\bar{w}(x,y,0,t) = \frac{\partial \bar{z}_c}{\partial t} + U_\infty \frac{\partial \bar{z}_c}{\partial x} \quad (2.17)$$

where  $\bar{z}_c(x,y,0,t)$  represents the mean camber surface position of the wing.

Since  $\bar{w}$  is an even function of  $z$  (its value is unchanged for the top or the bottom side of the mean surface), the velocity potential  $\bar{\phi}$  is an odd function of  $z$ , as is the perturbation pressure  $\bar{p}$  through the linear relationship of equation (2.11). Therefore, in the plane of the wing  $\bar{\phi}$  equals zero outside of the wing and wake.  $\bar{\phi}$  does not equal zero in the wake because of the discontinuity in the  $\bar{u}$  component of the perturbation velocity across the wake. The perturbation pressure is also zero in the  $x$ - $y$  plane, except at the lifting surface where the pressure difference  $\Delta \bar{p}$  between the top and bottom surfaces is given by

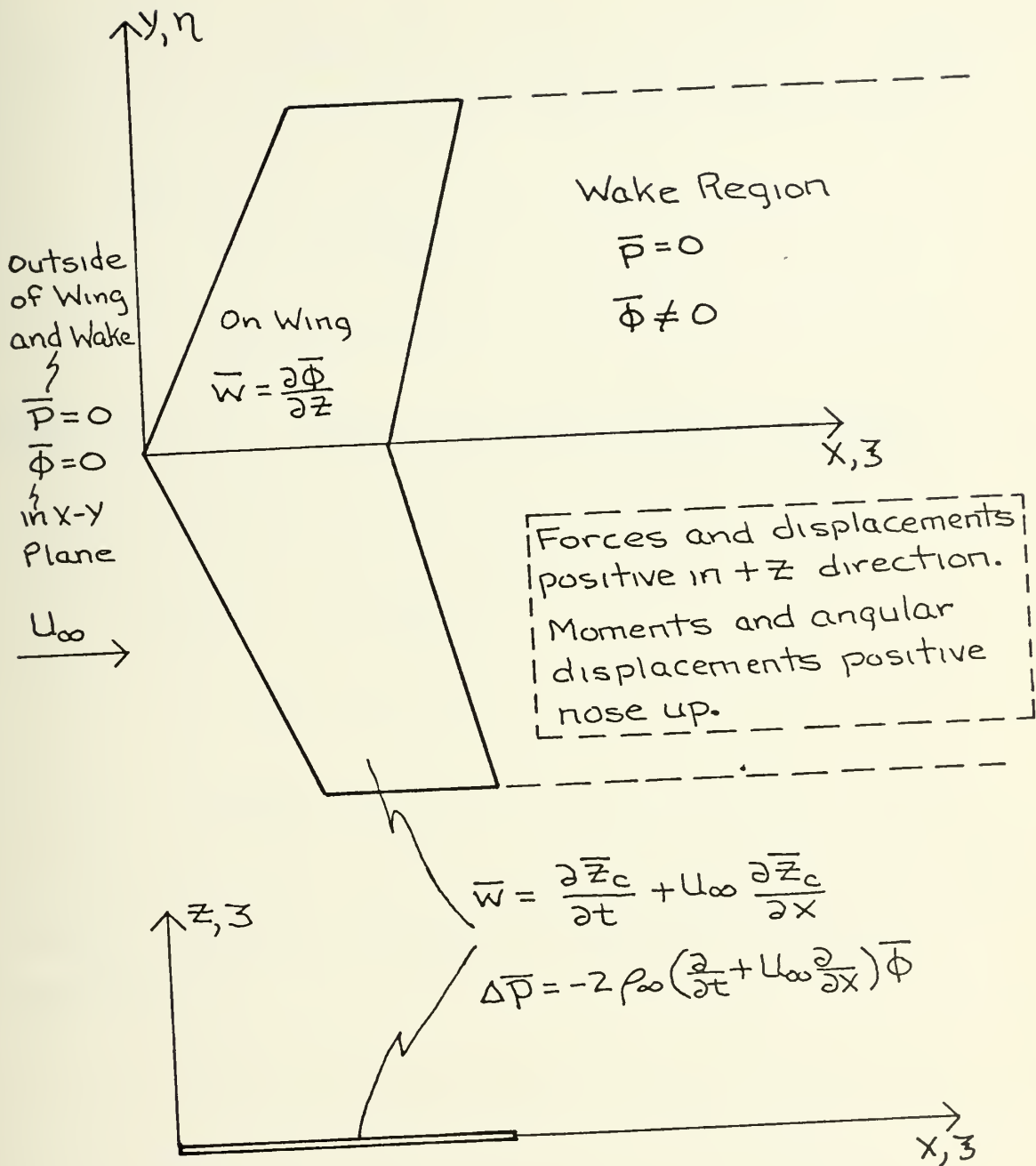
$$\begin{aligned} \Delta \bar{p}(x,y,t) &= \bar{p}(x,y,0-,t) - \bar{p}(x,y,0+,t) \\ &= 2\bar{p}(x,y,0,t) = -2\rho_\infty \left( \frac{\partial}{\partial t} + U_\infty \frac{\partial}{\partial x} \right) \bar{\phi} \end{aligned} \quad (2.18)$$

Figure 1 summarizes the formulation of these boundary conditions for a lifting surface in the  $x$ - $y$  plane.

These linearized boundary conditions along with the linearized governing differential equation (2.9) can be used to attack a wide range of perturbation problems in subsonic







Governing Equation

$$\nabla^2 \bar{\Phi} - \frac{1}{a_\infty^2} \left( \frac{\partial}{\partial t} + U_\infty \frac{\partial}{\partial x} \right)^2 \bar{\Phi} = 0$$

FIGURE 1  
COORDINATE SYSTEM AND BOUNDARY CONDITIONS  
OF GENERAL LIFTING SURFACE PROBLEM



and supersonic flow. Miles [13] has shown that a sufficient condition for linearization of the equations for the perturbation potential is any one or combination of the factors

$$|M_{\infty}^2 - 1| \gg 0 \quad (\delta^{2/3})$$

$$k \gg 0 \quad (\delta^{2/3})$$

$$\frac{1}{AR} \gg 0 \quad (\delta^{1/3})$$

where  $\delta$ ,  $M_{\infty}\delta$ ,  $k\delta$ , and  $kM_{\infty}\delta$  must be sufficiently small.

The perturbation equation is nonlinear only when the following conditions are jointly satisfied

$$|M_{\infty}^2 - 1| = 0 \quad (\delta^{2/3})$$

$$k = 0 \quad (\delta^{2/3})$$

$$\frac{1}{AR} = 0 \quad (\delta^{1/3})$$

$\delta$  is here intended to be a thickness, angle of attack, camber, or motion parameter serving as a measure of the flow disturbance.



### III. LIFTING SURFACE THEORY

#### A. BASIC APPROACH

The basic nonsteady problem considered in lifting surface theory is that of a linearized thin wing harmonically oscillating in the normal direction in some prescribed deflection mode, creating small disturbances in the uniform mainstream. Particular solutions to the linearized governing differential equation (2.9) are required which give perturbation velocity potential or perturbation pressure distributions on the wing, and which satisfy the essential boundary conditions discussed in Section III-C. Such a direct solution has been possible for only a few special cases, such as two-dimensional incompressible flow as in Refs. 14 and 15. For the more general three-dimensional case, an integral equation formulation must be employed which makes use of a downwash kernel function, analogous to an influence coefficient development.

Considering the time dependence  $e^{i\omega t}$  in the harmonic analysis as being factored out, the integral equation relating the downwash amplitude to the wing loading has the form

$$w(x,y,0) = \iint_S L(\xi,\eta,0)K(x-\xi, y-\eta,0)d\xi d\eta \quad (3.1)$$

The loading  $L$  can either be the velocity potential or the pressure distribution over the surface, and  $K$  is the kernel function which denotes the normal velocity (downwash) on the wing at  $(x,y,0)$  due to a unit acoustic singularity located



at  $(\xi, \eta, 0)$ . In other words, the surface is modeled by a distribution of radiators, formulated in terms of either potential or pressure which satisfy the linearized governing equation

$$\nabla^2 \phi - \frac{1}{a_\infty^2} (U_\infty \frac{\partial}{\partial x} + i\omega)^2 \phi = 0 \quad (2.12)$$

$w$  is the downwash at point  $(x, y, 0)$  on the wing, determined by the harmonic motion of the surface in fulfilling the tangential flow requirement. All of these quantities are complex in the spatial domain due to the nonsteady nature of the problem.

Employing the velocity potential approach, the kernel function is defined by

$$K = w(x, y, 0) = \partial \phi / \partial z \quad (3.2)$$

where  $\phi$  is the solution to equation (2.12) for an acoustic radiator of unit strength. In this formulation, the integration (3.1) must be carried out over the surface of both wing and wake, since the potential does not go to zero in the wake region. This complicates the integration process and has proven a major disadvantage of the potential approach.

If the wing is modeled by a pressure distribution, the kernel function is denoted by

$$K = w(x, y, 0) = \frac{-e}{\rho_\infty U_\infty} \lim_{z \rightarrow 0} \frac{\partial}{\partial z} \int_{-\infty}^x p(\xi, y, z) e^{\frac{i\omega \xi}{U_\infty}} d\xi \quad (3.3)$$

from equation (2.14) where  $p$  is now the solution to equation (2.12) for an acoustic radiator of unit strength. The





integration here need only be carried out over the wing surface, since the pressure goes to zero in the wake. Because of this, methods based on the pressure formulation have been more widely employed. This kernel function (3.3) is more complicated than that developed from equation (3.2) and has not been integrated in closed form due to singularities at  $(y-\eta)=0$  and  $(x-\xi)\geq 0$ . However these singularities have been isolated and expressed in forms which can be handled by numerical procedures [3].

The acoustic singularities used to model the wing surface in subsonic flow are harmonically pulsating doublets (dipoles) oriented in the  $z$ , or wing-normal, direction. Doublets are employed in order to represent the pressure difference between the two surfaces of the wing, while in supersonic flow acoustic sources, or monopoles, are used due to the independence of the two wing surfaces in that flow regime. Küssner [2] developed the general formulation of the pressure doublet kernel function, through use of the Lorentz transformation, in order to apply solutions to the classical wave equation of physics

$$\nabla^2 \phi - \frac{1}{a^2} \frac{\partial^2 \phi}{\partial t^2} = 0$$

to the governing differential equation of lifting surface theory (2.9). This method of attack is used in Appendix A to develop the kernel functions used in this report.



## B. NUMERICAL SOLUTIONS TO LIFTING SURFACE THEORY

To find the potential or pressure loading on the lifting surface actually requires the inverse solution of equation (3.1), since the downwash velocity distribution is determined by the type of surface motion prescribed through equation (2.15). The numerical methods that have been developed in subsonic lifting surface theory rest on this inverse solution to the singular integral equation. The usual procedure is to assume the loading to be a series of preselected functions with unknown coefficients and then to determine these by satisfying the downwash velocity distribution exactly in a set of collocation points [16, 17], or approximately in the least squares sense in a larger set of control points [4, 18], or by satisfying certain integral relations derived from variational procedures [19, 20].

Ashley and Landahl [21], and Landahl and Stark [1] have presented survey papers summarizing the status of numerical lifting surface theory, and presenting formulations of the integral downwash equation and the kernel function in the various methods of attack, such as:

(i) Velocity potential. As previously discussed, the kernel function used in this formulation, while singular, is much simpler than that employed with the pressure loading approach. However, integration must be carried out over both wing and wake. The velocity potential formulation has been employed by Jones [22] for  $M_\infty = 0$  in 1952.

(ii) Acceleration potential. Formulating this approach in terms of an acceleration potential defined by  $c_p = -2\psi$  [23],



allows the use of the same kernel function as in the velocity potential formulation, but removes the necessity of integrating over the wake, since  $c_p = 0$  there. However, the solution is not unique, since multiples of eigen solutions with  $\frac{\partial \psi}{\partial z} = 0$  on the wing may be added, and integration must be extended into the region ahead of the leading edge to achieve uniqueness. This formulation has been used for two-dimensional cases and also for certain three-dimensional cases [24].

(iii) Pressure formulation. The original development by Küssner [2] has been formulated for the computer by Watkins, et al [3] and by Richardson [16]. This procedure provides direct determination of the pressure with integration required only over the wing surface, but the kernel function is highly singular and needs to be evaluated through numerical quadrature, thereby increasing computer time considerably.

Various refinements of the basic approaches discussed above have been developed, such as the integrated acceleration potential by Stark [4] and the advanced velocity potential [1], but these do not change the basic problem formulation, nor the basic advantages and disadvantages of the continuous loading function methods.

In lifting surface theory the loading is expressed as a linear combination of preselected functions, with coefficients to be determined by satisfying the tangential flow condition through the integral equation (4.1). In selecting



the loading functions, known results from two-dimensional incompressible flow theory have been used. The loading is separated into chordwise and spanwise functions, so that a pressure function element would be represented as

$$p_{mn} = f_m(\xi)g_n(\eta)$$

These loading functions have been represented by Fourier expansions [17], power series [25, 26], Tschebycheff polynomials [27, 28], Legendre polynomials [4], and so on. The basic requirement is that these functions themselves satisfy the applicable boundary conditions from Section II, such as leading, side, and trailing edge behavior.

#### C. SOLUTIONS BASED ON DISCRETE LOADING LINES

In steady flow, the lifting line theory of Prandtl employed a discrete vortex lifting line, with variable strength, placed at the quarter chord line. Wieghardt [29] extended this method for rectangular wings by using several lifting lines, while Rubbert [30], Dulmovits [31], and Hedman [32] assumed constant strengths of the lifting lines in subintervals in a vortex lattice approach.

The vortex lifting line in steady flow corresponds in the nonsteady case to a potential doublet strip with strength varying harmonically in the streamwise direction. The use of a discrete lifting line approach to the nonsteady case was first proposed by Jones [22] for the incompressible case, and by Runyan and Woolston [25] for general subsonic flow.





As in the steady case, this lifting line approach for nonsteady motion has been extended to the doublet lattice method by Stark [1], and by Albano and Rodden [33]. The downwash from the doublet lattice strip is closely related to the kernel function discussed previously in this section. Since the surface loading is replaced by discrete doublet strips, it is not necessary to assume the loading functions, as required in the continuous function approach to lifting surface theory, and the integral downwash equation (3.1) is replaced by a matrix equation relating downwash on the wing to doublet lattice strength. This approach then removes one of the shortcomings to general lifting surface theory, but still retains the remaining features.

#### D. NONPLANAR CONFIGURATIONS

Limited work has been done in the area of general nonplanar configurations, since interference investigations have been primarily involved with combinations of lifting planar surfaces. The kernel functions for interfering planar surfaces, as developed by Davies [34] and by Landahl [35], become more complicated but do not contain any new singularities. In the selection of suitable loading functions, the behavior at the intersection of lifting surfaces must be taken into account. The T-tail has been treated by Stark [4] and by Davies [35], while calculations for a delta wing with folded tips have been given by Vivian and Andrew [36]. Lashka [5] has analyzed the effects of wing tip pylons as well as interfering planar surfaces [37], while Rodden [38]



has included wing/body and wing/pylon effects in nonsteady wing loading in subsonic flow.



#### IV. DISCRETE POTENTIAL ELEMENT DEVELOPMENT

##### A. WING ANALYSIS

###### 1. Basic Formulation

The integral equation relating downwash to wing loading (either velocity potential or pressure) in lifting surface theory, as discussed in Section III, is

$$w(x,y,0) = \iint_S L(\xi,\eta,0)K(x-\xi,y-\eta,0)d\xi d\eta \quad (3.1)$$

where harmonic motion is assumed so that

$$\bar{w}(x,y,z,t) = w(x,y,z)e^{i\omega t}$$

$$\bar{L}(x,y,z,t) = L(x,y,z)e^{i\omega t}$$

In the subsequent development, the time dependence will be considered factored out, so that all symbols will refer to complex valued spatial variables. The downwash  $w$  is determined by the boundary condition of no flow through the wing surface as given for general motion by equation (2.7), and here for harmonic motion

$$w = U_\infty \frac{\partial z_s}{\partial x} + i\omega z_s \quad (4.1)$$

where  $z_s$  is the amplitude of the surface motion prescribed for the problem. The form of acoustic radiator used to model the wing is taken as a potential doublet, with axis in the  $z$ , or wing normal, direction. This dipole singularity is employed because of the requirement to sustain a pressure



difference across the wing in subsonic flow.  $K$  is the kernel function relating the downwash at point  $(x,y,0)$  on the wing due to a unit potential doublet located at  $(\xi,\eta,0)$ .

In normal lifting surface theory, the loading  $L$  would be represented by continuous chordwise and spanwise functions which satisfy the surface boundary conditions developed in Section II. However, in the discrete potential element approach this loading is represented by a network of Dirac delta functions formulated in terms of the perturbation velocity potential. Thus the velocity potential distribution over the wing is replaced by a series of point functions in the form of harmonically oscillating potential doublets with axes in the  $z$  direction. In addition, the wake must also contain a network of these doublets since the velocity potential is not zero there (Section II) and the integration region of equation (3.1) must include both wing and wake. A representation of this potential doublet grid is shown in Figure 2.

In the discrete formulation, the integral equation (3.1) is replaced by the matrix equation

$$\{w\} = [K] \{\phi\} \quad (4.2)$$

where  $w_i$  is the downwash at the  $i^{\text{th}}$  point on the wing, and  $\phi_j$  is the strength of the  $j^{\text{th}}$  potential doublet on the wing and wake in the grid of Figure 2. The location of the downwash control points are coincident with the potential doublet positions at the center of each wing control box. The choice of this location will be discussed in Section IV.A.4. In





CONSTANT POTENTIAL/PRESSURE  
CONTROL BOX ON WING

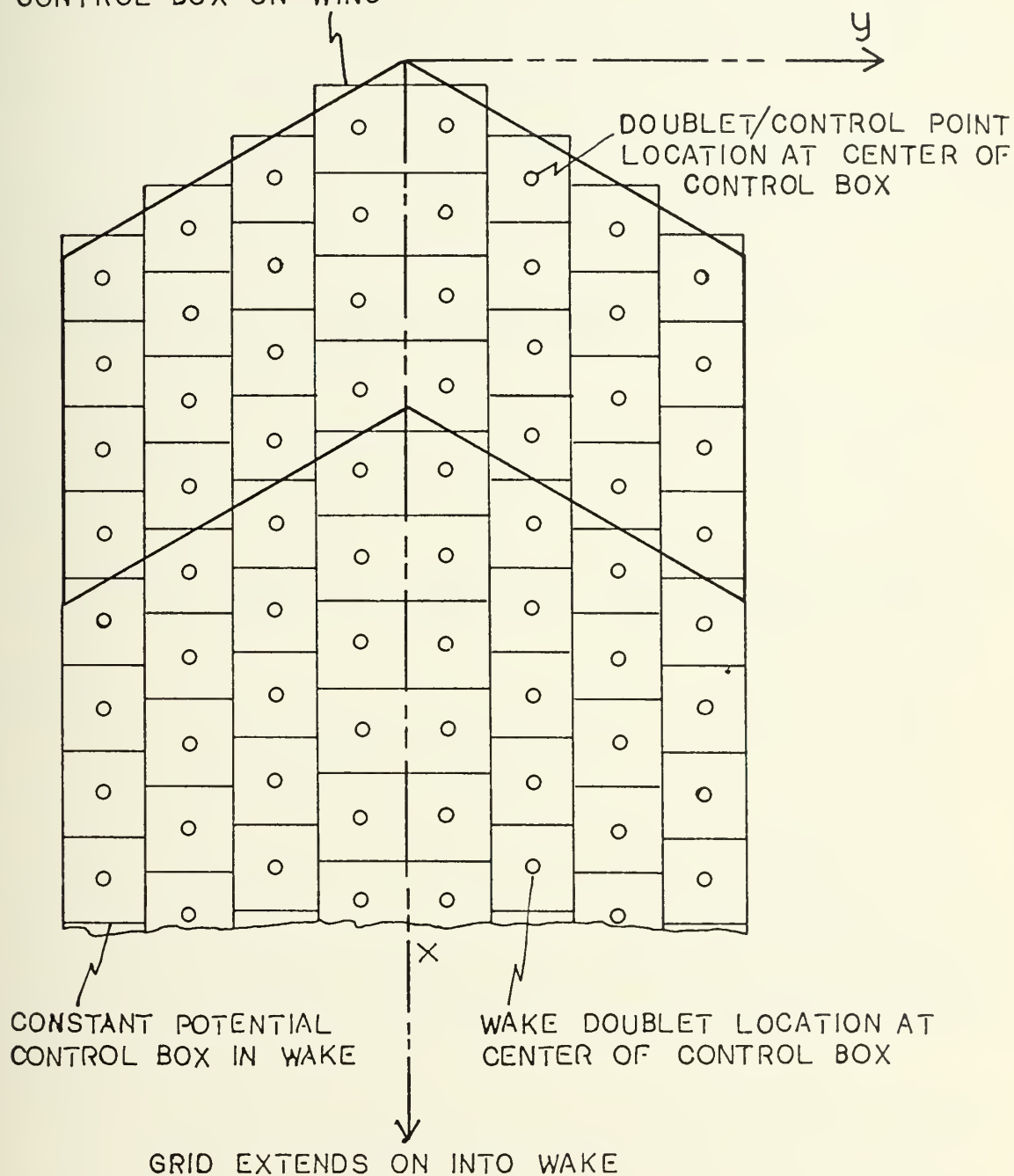


FIGURE 2  
WING/WAKE DISCRETE ELEMENT GRID



modeling the wing, the velocity potential and the pressure are considered constant over each of the control boxes, with approximations to continuous distributions given by these values at the control box midpoints.

The kernel function matrix elements represent the downwash due to potential doublets of unit strength which satisfy the governing linearized differential equation

$$\nabla^2 \phi - \frac{1}{a_\infty^2} (U_\infty \frac{\partial}{\partial x} + i\omega)^2 \phi = 0 \quad (2.12)$$

As developed in Appendix A, this kernel function has the form

$$K_{ij} = \frac{-\beta}{4\pi R^3} (1+i \frac{\omega}{a_\infty \beta^2} R) \exp\{i \frac{\omega}{a_\infty \beta^2} [M_\infty(x_i - x_j) - R]\} \quad (4.3)$$

where

$$R = \sqrt{(x_i - x_j)^2 + \beta^2 (y_i - y_j)^2}$$

In this formulation the kernel function is singular only when the downwash control point is coincident with the potential doublet location ( $i=j$ ). The handling of this singularity is vital to this development and is discussed in detail in Section IV.A.4.

The discrete loading element approach to the nonsteady wing problem requires the solution of the system of linear complex equations (4.2) to determine the velocity potential vector  $\{\phi\}$ . The downwash vector  $\{w\}$  is specified by the wing motion through equation (4.1), so that the solution has the form



$$\{\phi\} = [K]^{-1} \{w\} \quad (4.4)$$

where  $\{\phi\}$  and  $\{w\}$  cover both wing and wake regions. The resultant velocity potential distribution is used to determine the pressure loading over the wing through the relationship

$$\Delta p = -2\rho_{\infty}(U_{\infty} \frac{\partial}{\partial x} + i\omega)\phi \quad (4.5)$$

taken for the harmonic case from equation (2.18).

## 2. Wake Effect

One of the historic drawbacks to the potential approach to lifting surface theory has been the necessity of including the wake region in the solution of the integral equation (3.1). This equally complicates the discrete element approach since the matrix equation (4.2) is required to include the effect of the wake potential dipole grid. Even though the effective wake is terminated at some representative length behind the wing, as is commonly done in steady flow problems, the size of the resulting potential strength vector and kernel function matrix would severely restrict, or entirely preclude, the use of this method even on large modern computers.

Following a suggestion by Professor R. E. Ball of the Naval Postgraduate School, a careful examination of the boundary conditions governing harmonic wing motion, as depicted in Figure 3, was made. In the wake region the pressure is zero, but the velocity potential is not zero



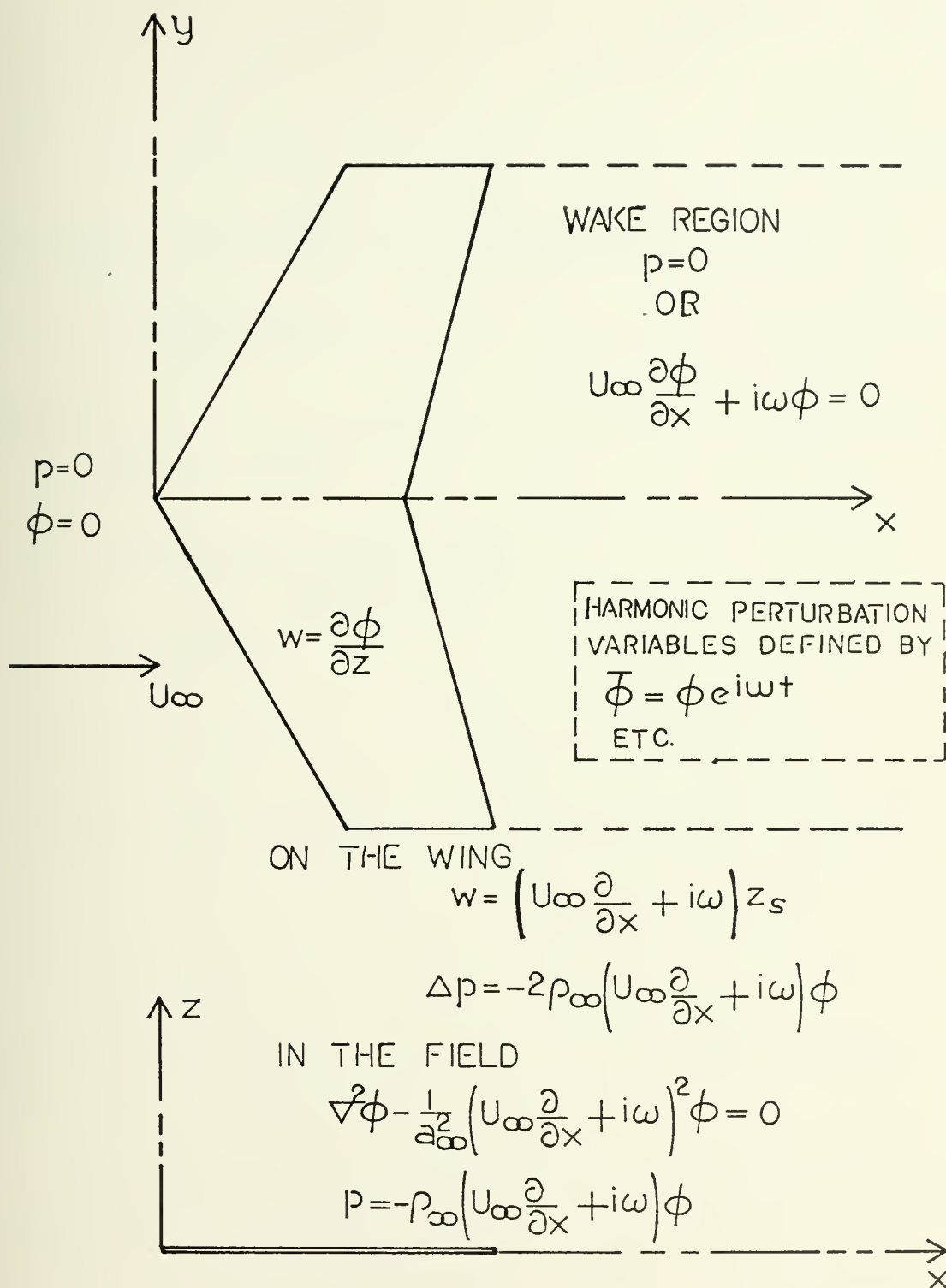


FIGURE 3  
 BOUNDARY CONDITIONS FOR  
 LINEARIZED HARMONIC MOTION





because of the discontinuity in the  $u$  component of the perturbation velocity.  $\phi$  and  $p$  are related by

$$p = -\rho_{\infty} (U_{\infty} \frac{\partial}{\partial x} + i\omega) \phi \quad (2.13)$$

In the wake, therefore, this relationship becomes

$$U_{\infty} \frac{\partial \phi}{\partial x} + i\omega \phi = 0 \quad (4.5)$$

or

$$\frac{\partial \phi}{\partial x} = -i \frac{\omega}{U_{\infty}} \phi$$

which can be integrated to give

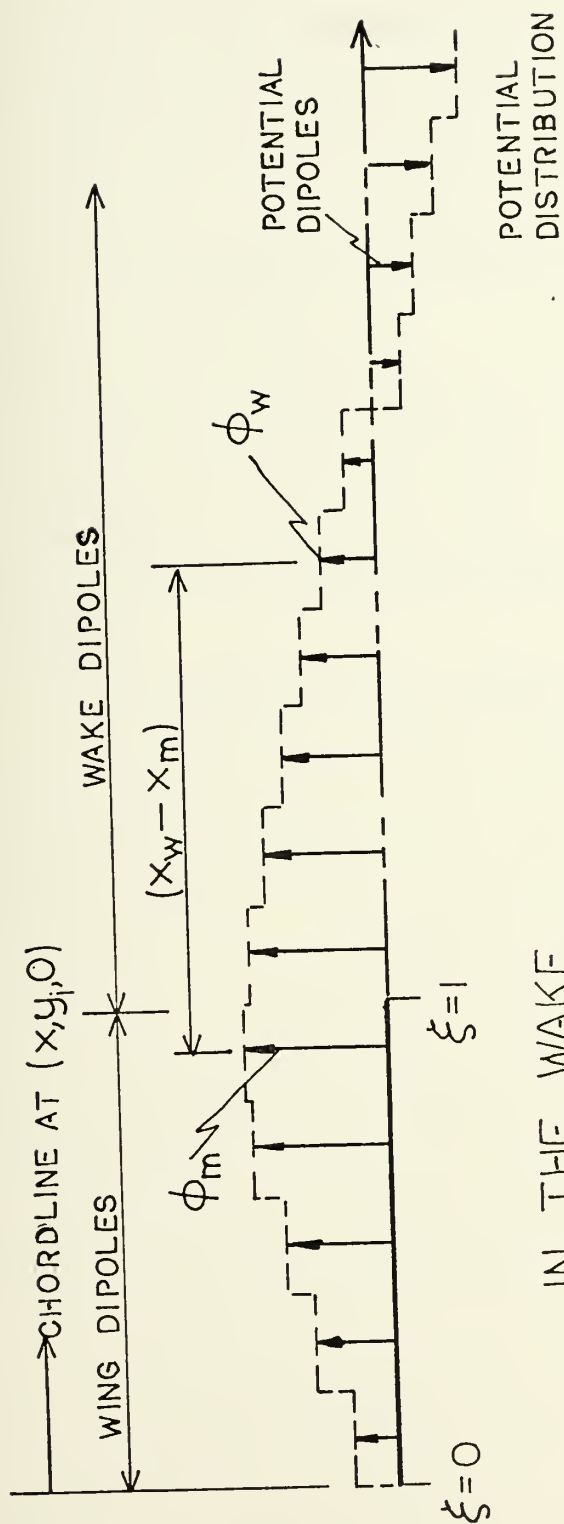
$$\phi_w = \phi_m e^{-i \frac{\omega}{U_{\infty}} (x_w - x_m)} \quad (4.6)$$

$\phi_w$  is the strength of the wake velocity potential at  $(x_w, y_i, 0)$ , and  $\phi_m$  is the strength of the velocity potential at the boundary between the wing and the wake  $(x_m, y_i, 0)$  along the line of integration  $y=y_i$ . In the discrete potential element formulation,  $\phi_m$  becomes the strength of the last wing dipole on the appropriate chord line, with  $(x_w - x_m)$  the distance between this dipole and the wake dipole  $\phi_w$ , as is shown schematically in Figure 4.

The wake potential strength distribution is therefore expressible as a function of the wing potential distribution and can be included in the wing doublet kernel functions. This relationship can be represented by

$$\{\phi_w\} = [A] \{\phi\}$$





IN THE WAKE

$$p=0 \quad \text{OR} \quad u_{\infty} \frac{\partial \phi}{\partial x} + i\omega \phi = 0$$

$$\phi_w = \phi_m \exp \left[ -i \frac{\omega}{u_{\infty}} (x_w - x_m) \right]$$

FIGURE 4  
DISCRETE POTENTIAL REPRESENTATION  
OF WAKE EFFECT



where  $\{\phi\}$  is the wing velocity potential vector and the appropriate elements of  $[A]$  express the relationship of equation (4.6) with respect to the wake potential vector  $\{\phi_w\}$ . The downwash matrix equation (4.2) therefore becomes

$$\begin{aligned}\{w\} &= [K_1] \{\phi\} + [K_2] \{\phi_w\} \\ &= [K_1] \{\phi\} + [K_2][A] \{\phi\} \\ &= [K_1 + K_2 A] \{\phi\}\end{aligned}$$

The size of this matrix equation has thus been limited to that necessary to represent only the wing grid, making the discrete potential element approach much more tractable on the computer.

### 3. Matrix Equation for Symmetric Motion

In considering a wing undergoing harmonic oscillations which are symmetric with respect to the x-z plane, the wing/wake planform can be represented as shown in Figure 5. The x-z plane, being a plane of symmetry, represents a no-flow surface, or reflection plane, for the disturbances caused by the symmetric motion of the full-span wing. Viewing the physical problem in a different, but equally valid light, the half-span wing ①, with its root along the x axis, can be considered undergoing oscillations in the presence of an infinite wall coincident with the x-z plane. Therefore, the motion of the wing need only be prescribed for wing ①, while the function of the virtual wing ③ and wake ④ is to establish the no-flow condition at the x-z plane.

The full wing/wake system is represented by the matrix equation



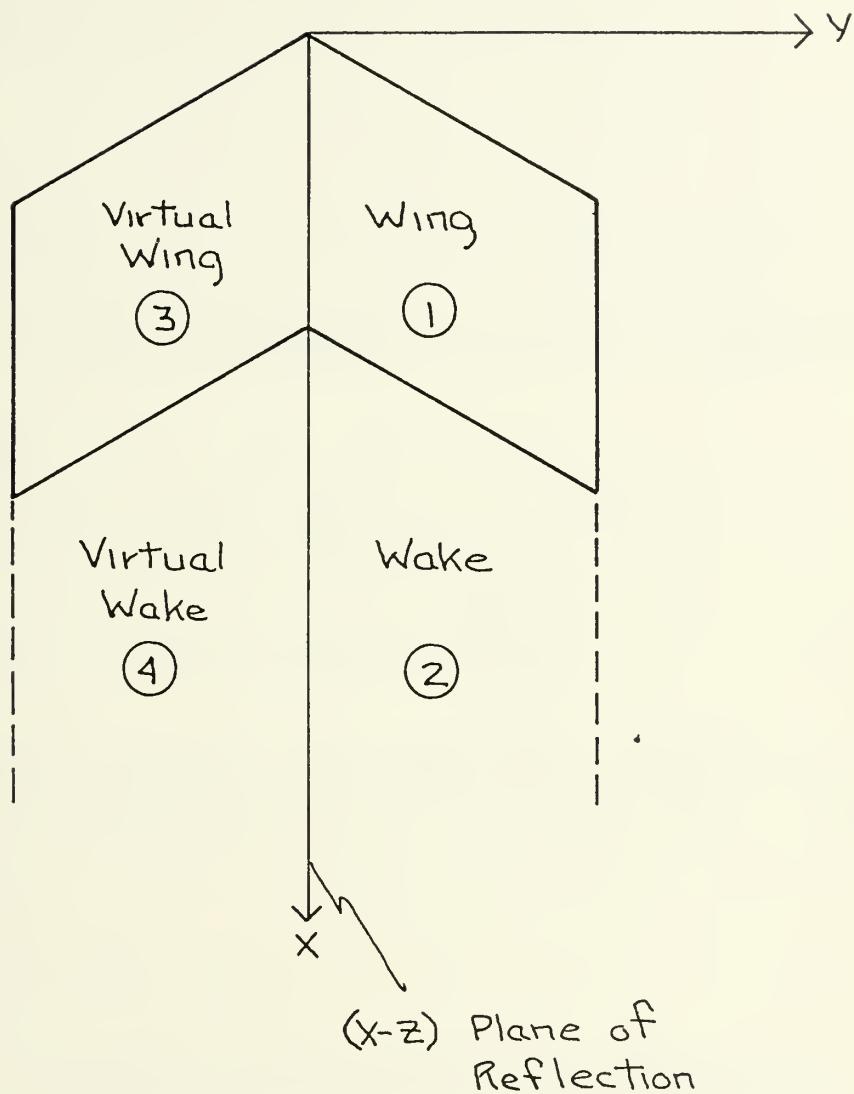


FIGURE 5

WING/WAKE PLANFORM FOR ANALYSIS  
OF SYMMETRIC WING MOTION





$$\begin{Bmatrix} w_1 \\ w_3 \end{Bmatrix} = \begin{bmatrix} K_{11} & K_{12} & K_{13} & K_{14} \\ K_{31} & K_{32} & K_{33} & K_{34} \end{bmatrix} \begin{Bmatrix} \phi_1 \\ \phi_2 \\ \phi_3 \\ \phi_4 \end{Bmatrix}$$

where subscripts denote the areas of Figure 5 and  $K_{ij}$  is the kernel function matrix for downwash at points in area (i) due to doublets located in area (j). For symmetric motion

$$\{\phi_3\} = \{\phi_1\} \quad \text{and} \quad \{\phi_4\} = \{\phi_2\}$$

so the required downwash equation is reduced to

$$\{w_1\} = [K_{11}+K_{13} \quad K_{12}+K_{14}] \begin{Bmatrix} \phi_1 \\ \phi_2 \end{Bmatrix}$$

In the previous section, the relationship between wing and wake potential distributions was developed, and can here be expressed as

$$\{\phi_2\} = [A] \{\phi_1\}$$

Therefore, the final wing downwash matrix equation has the form of equation (4.2)

$$\{w_1\} = [K] \{\phi_1\} \quad (4.7)$$

but the kernel function matrix is here formed from the following expression

$$[K] = [K_{11}] + [K_{13}] + [K_{12}+K_{14}][A] \quad (4.8)$$

Thus, through use of motion symmetry and the boundary condition in the wake, the effective integration of equation (4.7)



need only be carried out over the half-span wing surface ①. Acknowledgement of the full physical problem is obtained through formation of the kernel function matrix via equation (4.8), which incorporates effects of the potential dipole grids in all four areas of the wing and wake depicted in Figure 5.

It should be noted that antisymmetric motion of the wing about the x-z plane requires that

$$\{\phi_3\} = -\{\phi_1\} \quad \text{and} \quad \{\phi_4\} = -\{\phi_2\}$$

The final kernel function matrix is therefore formed by

$$[K] = [K_{11}] - [K_{13}] + [K_{12} - K_{14}][A]$$

Since any general harmonic motion of the wing can be expressed as a combination of symmetric and antisymmetric modes, this approach has general application and need not be restricted to the symmetric case considered in detail here.

#### 4. Doublet Singularity

The location of the collocation points required to satisfy the no-flow condition in lifting surface theory is historically based on two-dimensional steady flow theory, Vortex lattice methods such as Rodden's [38] arrange the vortex strip on the local quarter chord of the control box, with the downwash collocation point centered on the local three-quarter chord line as in two-dimensional thin airfoil theory. Houbolt [6] proposes using this local quarter chord, three-quarter chord control box grid in conjunction with



concentrated pressure loads. This type of grid network was tried by the author in an early form of the wing analysis computer program with unsatisfactory results. The approach was found not to converge, but to be very sensitive to grid size; that is, to the distance between the potential dipole and its associated control point. This is much like the sensitivity that a continuous loading method experiences when a control point is located too close to a wing edge [11].

The control or collocation points were subsequently placed at the center of the wing control boxes (Figure 2) coincident with the potential doublet locations. In this way, the above mentioned sensitivity to grid spacing was removed, but the value of the upwash of a doublet at its own control point had to be determined. As can be seen from equation (4.3), the kernel function ( $K_{ij}$ ) is singular at the doublet location ( $i=j$ ). This singularity in the upwash from a doublet is pictured in Figure 6a, where the doublet produces an infinite upwash at its location, but finite and decreasing downwash in the plane of the wing as the distance from the doublet is increased.

If the dipole is considered within the framework of the discrete element grid where dipole strengths and downwash velocities are held constant, or averaged, over each control box, a cross-section of the dipole flow pattern would appear as in Figure 6b, where the infinite upwash at the doublet has been replaced by a finite value  $w_0$ . To determine a



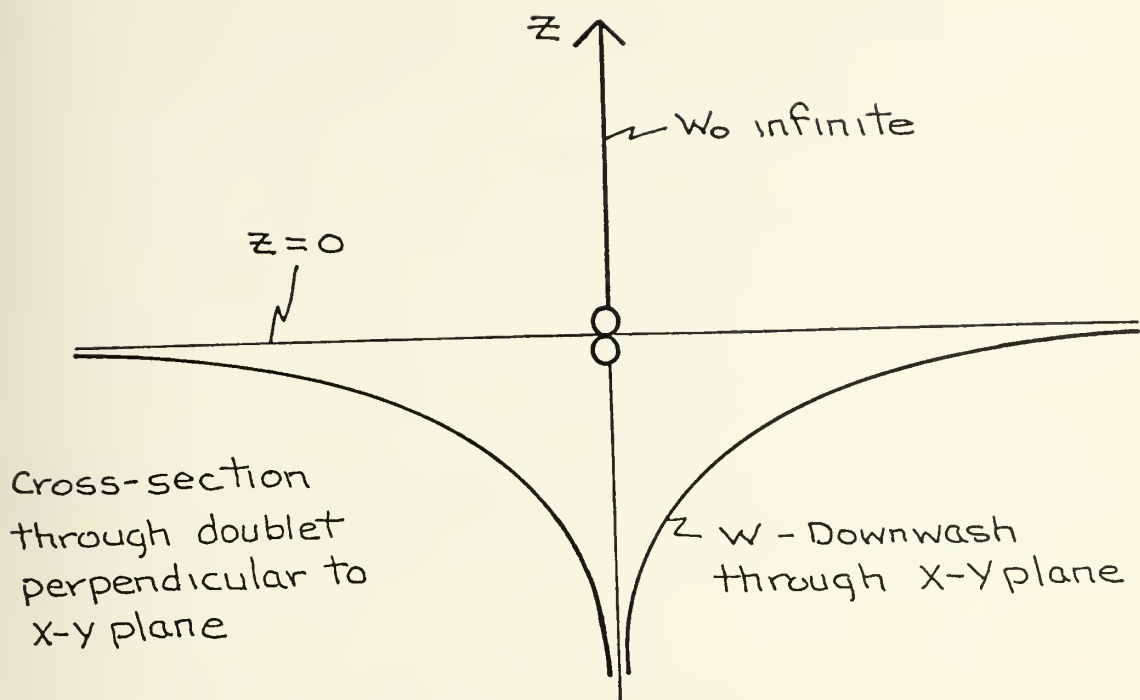


FIGURE 6a  
SINGULARITY IN DOUBLET UPWASH

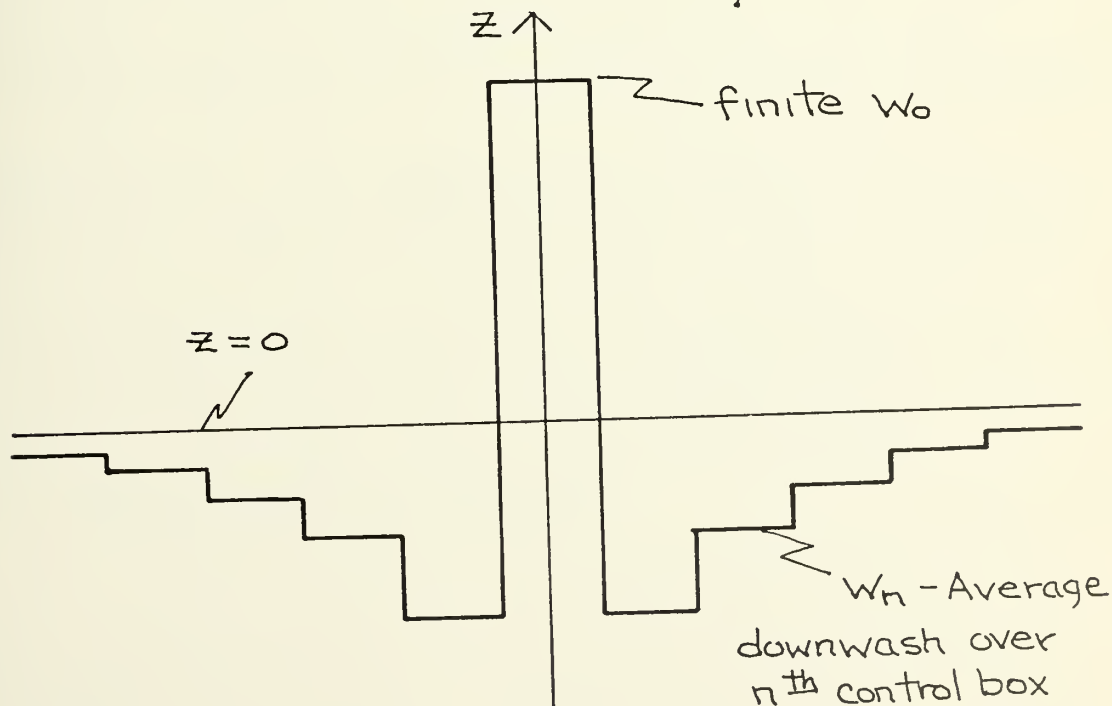


FIGURE 6b  
DISCRETE ELEMENT REPRESENTATION  
OF DOUBLET SINGULARITY





value for  $w_o$  which adequately represents the singularity strength within the framework of the discrete element approximation, the law of continuity was employed. The total fluid outflow in the discrete representation is  $w_o A_o$ , where  $A_o$  is the area of the doublet control box. Modeling the entire x-y plane with control boxes without regard to wing/wake geometry, the total amount of fluid passing back through the x-y plane is  $\sum_{n=1}^{\infty} w_n A_n$ , where  $w_n$  is the average velocity over the control box with area  $A_n$ . Therefore, continuity requires

$$w_o A_o + \sum_{n=1}^{\infty} w_n A_n = 0$$

and if the  $A_n$ 's are chosen so that  $A_o = A_n$ , the upwash velocity is determined by

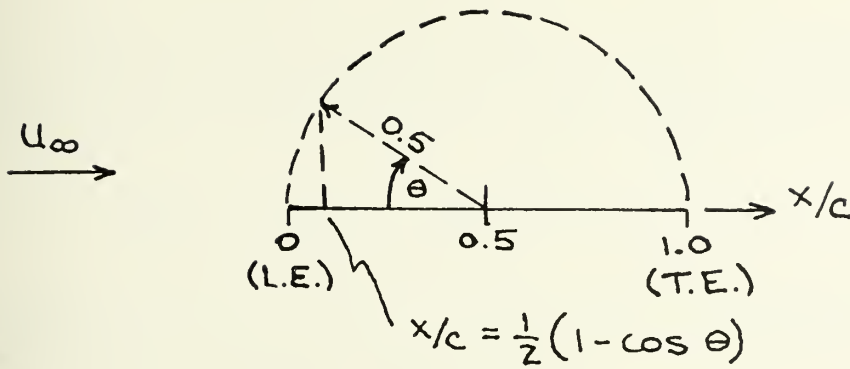
$$w_o = - \sum_{n=1}^{\infty} w_n \quad (4.9)$$

In actual practice, the summation of the downwash velocities through the x-y plane is necessary only to some finite radius from the doublet, since the inverse proportionality of the kernel function with distance from the doublet causes the value of  $w_o$  to converge within a reasonable summation.

## 5. Section and Wing Coefficients

To obtain section lift and moment coefficients, the chordwise pressure distribution at each spanwise station was integrated in the manner employed in thin airfoil theory. First a coordinate transformation of the chordwise variable is made as follows





The pressure coefficient is then expressed in terms of a Fourier expansion of the new variable

$$c_p(\theta) = c_{p_0} \cot \frac{\theta}{2} + \sum_{n=1}^{\infty} c_{p_n} \sin n\theta \quad (4.9)$$

where the first term accounts for the leading edge singularity, while the trailing edge slope singularity is acknowledged by the infinite series. The section lift is obtained from

$$c_l = \int_0^1 c_p d\left(\frac{x}{c}\right) \quad (4.10)$$

Substituting the Fourier expansion for  $c_p$  and performing the coordinate transformation, equation (4.10) becomes

$$c_l = \frac{c_{p_0}}{2} \int_0^{\pi} (1 + \cos \theta) d\theta + \sum_{n=1}^{\infty} \frac{c_{p_n}}{2} \int_0^{\pi} \sin n\theta \sin \theta d\theta \quad (4.11)$$

Due to the orthogonality of the sine function, this integration yields

$$c_l = \frac{\pi}{2} (c_{p_0} + \frac{1}{2} c_{p_1}) \quad (4.12)$$

The section moment about the leading edge is defined by



$$c_{m_o} = - \int_0^1 c_p \frac{x}{c} d\left(\frac{x}{c}\right) \quad (4.13)$$

Performing the same transformation and integration as for the section lift coefficient, the following results

$$c_{m_o} = - \frac{\pi}{8} (c_{p_o} + c_{p_1} - \frac{1}{2} c_{p_2}) \quad (4.14)$$

Transferring this moment coefficient to the mid-chord point requires the further calculation

$$c_{m_{\frac{1}{2}}} = c_{m_o} + \frac{1}{2} c_\ell \quad (4.15)$$

The integration of section lift and moment values to wing coefficients is performed in a similar manner. Here the coordinate transformation is made to the spanwise variable, such that

$$y/b = \frac{1}{2} (1 - \cos \theta)$$

The product of the section chord and the section lift coefficient is then expressed as the Fourier series.

$$cc_\ell = c_{\ell_o} \cos \frac{\theta}{2} + \sum_{n=1}^{\infty} c_{\ell_n} \sin n\theta \quad (4.16)$$

Performing the integration

$$C_L = \frac{b}{s} \int_0^1 cc_\ell d\left(\frac{y}{b}\right) \quad (4.17)$$

of the Fourier expansion of the section lift in the transformed coordinate system, the following results

$$C_L = \frac{b}{s} \left( \frac{2}{3} c_{\ell_o} + \frac{\pi}{4} c_{\ell_1} \right) \quad (4.18)$$



The same relationship is obtained for the wing moment coefficient when the sectional moment is expressed as in the Fourier expansion of equation (4.16). For swept wings, the sectional moments were transferred to an axis extending from the half-root-chord point, prior to developing the Fourier series.

The infinite series of equations (4.9) and (4.16) are of course terminated at the number of chordwise and spanwise points respectively of the wing discrete element grid. This places a minimum limit on the number of chordwise and spanwise control points which are required to achieve valid sectional and wing coefficient values, a factor which will be discussed in Section VI.

## B. WING/BODY ANALYSIS

### 1. Basic Formulation

Inclusion of a finite radius body in the nonsteady lifting surface analysis is equivalent to adding one more boundary condition to the problem formulation: the requirement for no flow through the body surface. For the analysis pursued here, the body will be stationary with regard to the perturbation motion, and will be idealized as an infinitely long cylindrical surface with axis coincident with the undisturbed flow. The cantilevered, midmounted wing is harmonically oscillating within the limitations of small disturbance theory previously developed.

In steady flow analysis, the body effects have been traditionally handled by singularities, matching the wing





singularity distribution, at image points within the body in the wing plane [39]. This method will satisfy the nonsteady boundary conditions only in a quasi-steady sense, because of phase differences between disturbances at the body surface caused by a wing singularity and its corresponding image. Therefore, to model the body in the nonsteady problem, a system of singularities are placed on the body surface establishing a grid similar to that for the wing. These curvilinear panels each have an harmonically oscillating singularity at its center, coincident with a normalwash control point. Thus, in effect the wing grid is merely extended over the body surface as shown in Figure 7.

In order to handle the more complex geometry of the wing/body problem, a coordinate transformation from the rectangular  $(x,y,z)$  system of the wing analysis is made to a cylindrical  $(r,\theta,x)$  system, where the undisturbed flow direction ( $x$  axis) is common. Thus the transformation is defined by

$$\begin{aligned} x &= x \\ y &= r \cos \theta \\ z &= r \sin \theta \end{aligned} \tag{4.19}$$

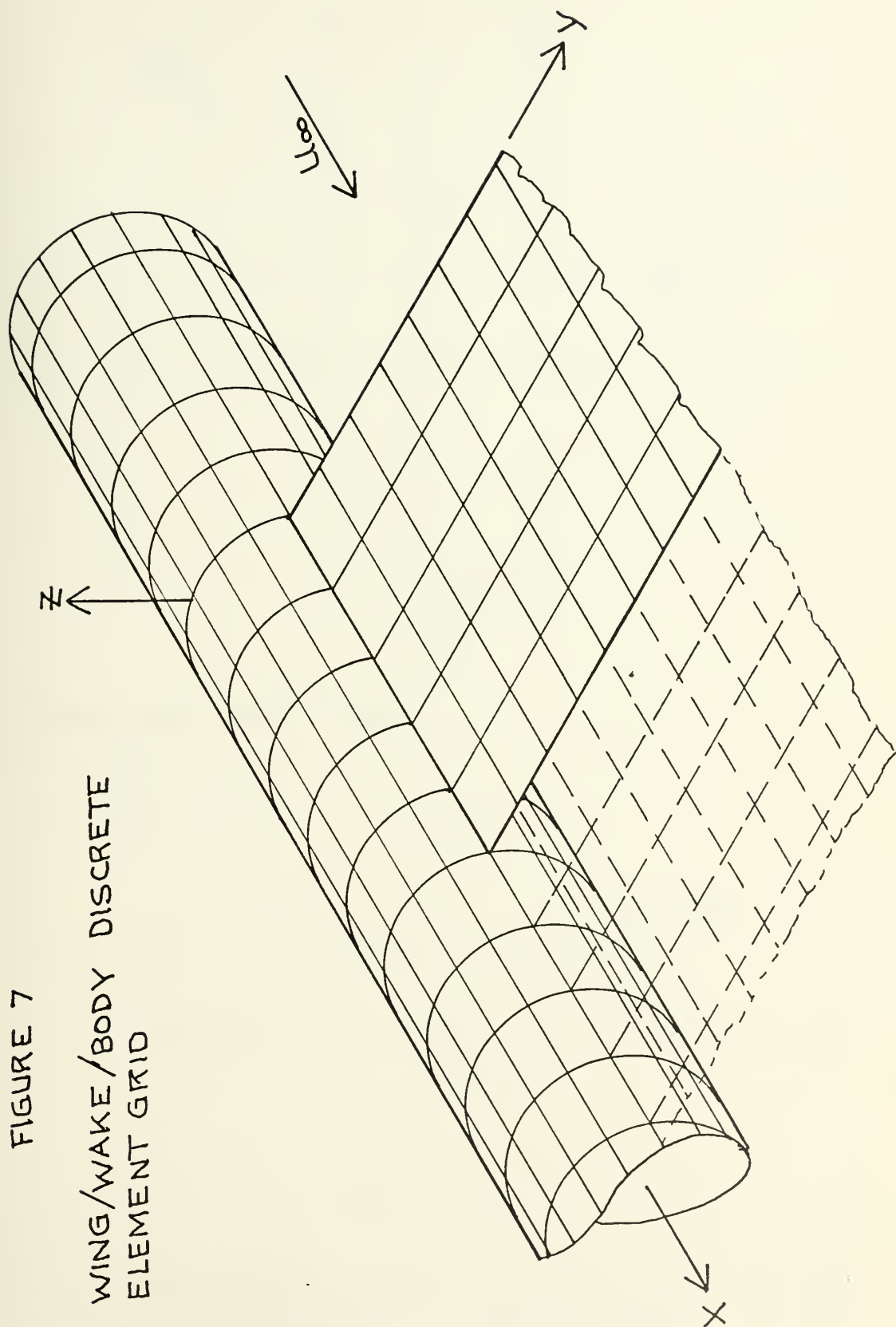
Figure 8 shows the wing/body configuration with the boundary conditions in the cylindrical coordinate system. The downwash velocity over the wing is now related to the velocity potential distribution by

$$u_{\theta} = \frac{1}{r} \frac{\partial \phi}{\partial \theta} \bigg|_{\theta=0 \text{ or } \pi} \tag{4.20}$$

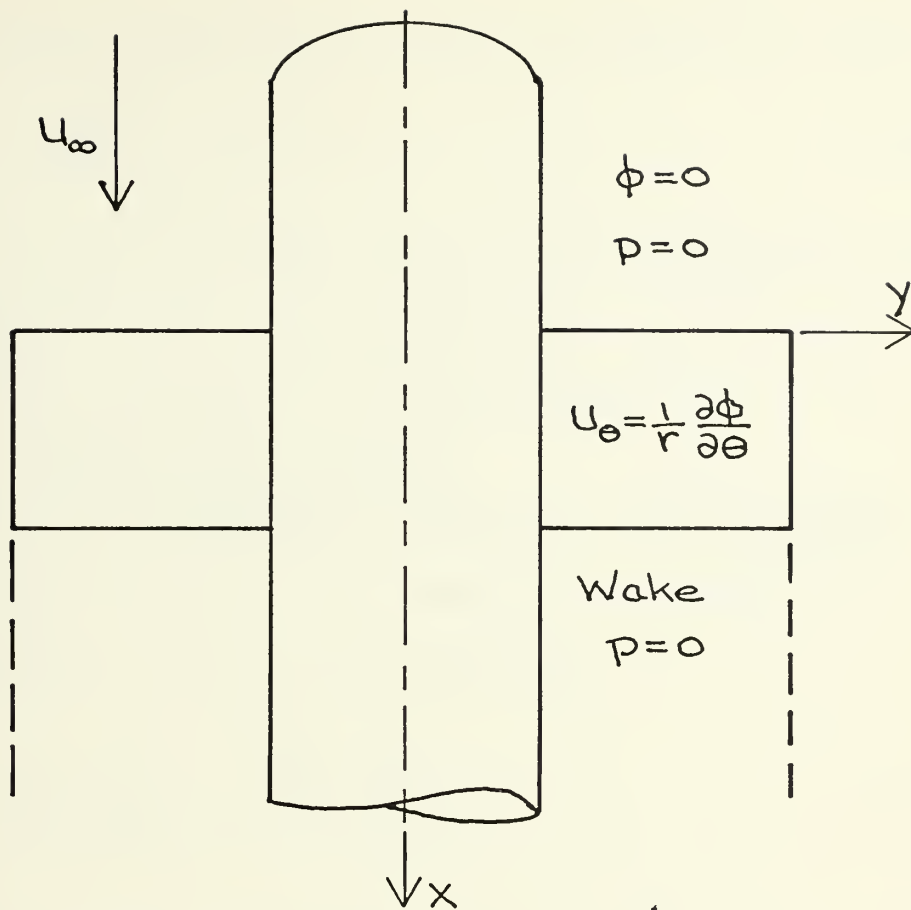


FIGURE 7

WING/WAKE/BODY DISCRETE  
ELEMENT GRID







Coordinate Transformation

$$x = x$$

$$y = r \cos \theta$$

$$z = r \sin \theta$$

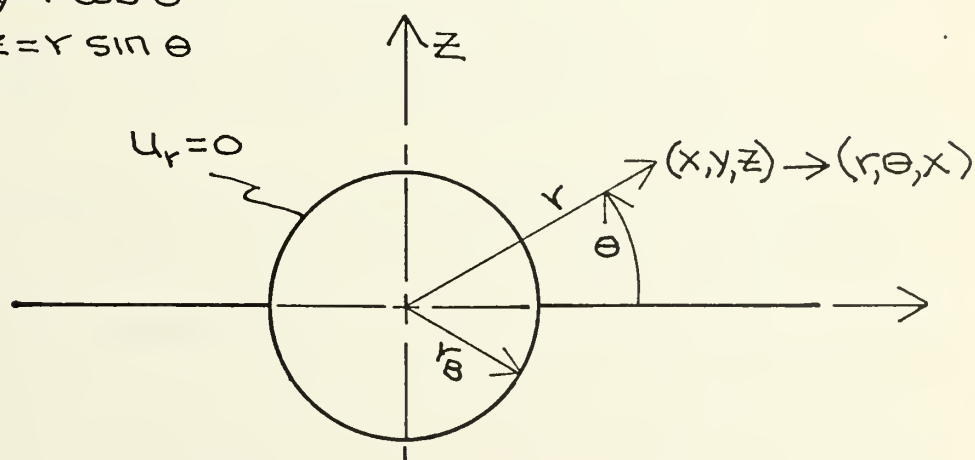


FIGURE 8

WING/BODY CONFIGURATION IN  
CYLINDRICAL COORDINATES



and the no-flow condition for the body surface is stated as

$$u_r = \left. \frac{\partial \phi}{\partial r} \right|_{r=r_B} = 0 \quad (4.21)$$

where  $r_B$  is the body radius. As in the wing analysis, the wing downwash velocity  $u_\theta$  is determined from the type of surface motion prescribed for the problem.

## 2. Governing Matrix Equation

The governing matrix equation for the wing/body problem takes on a much more formidable appearance than the basic equation (4.2) for the wing along

$$\begin{Bmatrix} u_\theta \\ u_r \end{Bmatrix} = \begin{bmatrix} K_W & | & K_{WB} \\ \hline K_{BW} & | & K_B \end{bmatrix} \begin{Bmatrix} \phi_W \\ \phi_B \end{Bmatrix} \quad (4.22)$$

where  $\{u_\theta\} \equiv$  wing downwash vector

$\{u_r\} \equiv$  body normalwash vector

$\{\phi_W\} \equiv$  wing singularity potential vector

$\{\phi_B\} \equiv$  body singularity potential vector

The kernel function matrices are defined as follows

$K_W \equiv$  downwash on wing due to wing singularities

$K_{WB} \equiv$  downwash on wing due to body singularities

$K_{BW} \equiv$  normalwash on body due to wing singularities

$K_B \equiv$  normalwash on body due to body singularities

Direct solution of equation (4.22) for the velocity potential distribution would be limited due to the computer storage requirements of the large complex kernel function matrix .





However this approach is not feasible at any rate, since the kernel function matrix is ill conditioned in this form and does not lend itself to efficient inversion.

To attack the problem, equation (4.22) is separated into two matrix equations

$$\{u_\theta\} = [K_W]\{\phi_W\} + [K_{WB}]\{\phi_B\}$$

$$\{u_r\} = [K_{BW}]\{\phi_W\} + [K_B]\{\phi_B\}$$

The second of these can be solved for the body potential distribution

$$\{\phi_B\} = [K_B]^{-1} [u_r - K_{BW}\phi_W] \quad (4.23)$$

which is then substituted into the first equation.

$$\{u_\theta\} = [K_W]\{\phi_W\} + [K_{WB}][K_B]^{-1}\{u_r\} - [K_{WB}][K_B]^{-1}[K_{BW}]\{\phi_W\}$$

This may be rewritten in the following form

$$\{u_\theta - K_{WB}K_B^{-1} u_r\} = [K_W - K_{WB}K_B^{-1} K_{BW}]\{\phi_W\} \quad (4.24)$$

The left hand matrix is a modified wing downwash vector incorporating body effects, as does the modified kernel function matrix on the right hand side of equation (4.24).

In the analysis considered here the body is steady at zero angle of attack to the main stream, while the wing is undergoing nonsteady motion, so that

$$\{u_r\} = \{0\}$$

Therefore, equation (4.24) becomes



$$\{u_\theta\} = \begin{bmatrix} K_W - K_{WB}K_B^{-1} & K_{BW} \end{bmatrix} \{\phi_W\} \quad (4.25)$$

which is in the same form as equation (4.2), but in which the modified kernel function matrix incorporates the body boundary condition.

### 3. Symmetry

The individual kernel function matrices of equation (4.25) incorporating body effects can be quite large when control points are placed around the entire circumference of the body, severely limiting the utility of this method. However these matrices may be reduced appreciably in size through use of symmetry. Considering the representation of Figure 9a, it can be seen that for wing motion symmetric about the x-z plane

$$\{\phi_{W_2}\} = \{\phi_{W_1}\}; \quad \{\phi_{B_2}\} = \{\phi_{B_1}\}; \quad \{\phi_{B_3}\} = \{\phi_{B_4}\} \quad (4.26)$$

where  $\{\phi_{W_i}\}$  stands for the doublet strength distribution on the respective wing, and  $\{\phi_{B_i}\}$  stands for the singularity strength distribution on the body in the respective quadrant. It can also be seen that due to the antisymmetric nature of the wing doublet flow with respect to the x-y plane

$$\{\phi_{B_4}\} = -\{\phi_{B_1}\}; \quad \{\phi_{B_3}\} = -\{\phi_{B_2}\} \quad (4.27)$$

since the purpose of the body singularities is to counter the flow of the wing doublets through the body surface.

Considering first the body kernel function matrix ( $K_B$ ), which is defined by the relation



$$\{u_r\} = [K_B]\{\phi_B\}$$

or

$$\{u_r\} = [K_{B_1}]\{\phi_{B_1}\} + [K_{B_2}]\{\phi_{B_2}\} + [K_{B_3}]\{\phi_{B_3}\} + [K_{B_4}]\{\phi_{B_4}\}$$

Symmetry allows this formulation to be reduced to

$$\{u_r\} = [K_{B_1} + K_{B_2} - K_{B_3} - K_{B_4}]\{\phi_{B_1}\} \quad (4.28)$$

In the case of the wing-body kernel function matrix ( $K_{WB}$ ), this same consideration produces

$$\{u_\theta\} = [K_{WB_1} + K_{WB_2} - K_{WB_3} - K_{WB_4}]\{\phi_{B_1}\} \quad (4.29)$$

Control points need only be placed, therefore, over the first quadrant of the body surface, reducing the size of the body effect kernel function matrices of equation (4.25) by one-fourth. The surface over which the flow conditions are specifically satisfied are indicated by the solid line of Figure 9b, which then satisfies the boundary conditions on the whole wing/body surface through symmetry. The body-wing kernel function matrix ( $K_{BW}$ ) follows the same development as in Section IV.A.3 for the wing alone and has the same form as  $K_W$  given by equation (4.8).

It should also be noted that for antisymmetric wing motion the kernel functions of equations (4.28) and (4.29) would have the form

$$[K] = [K_1 - K_2 + K_3 - K_4]$$



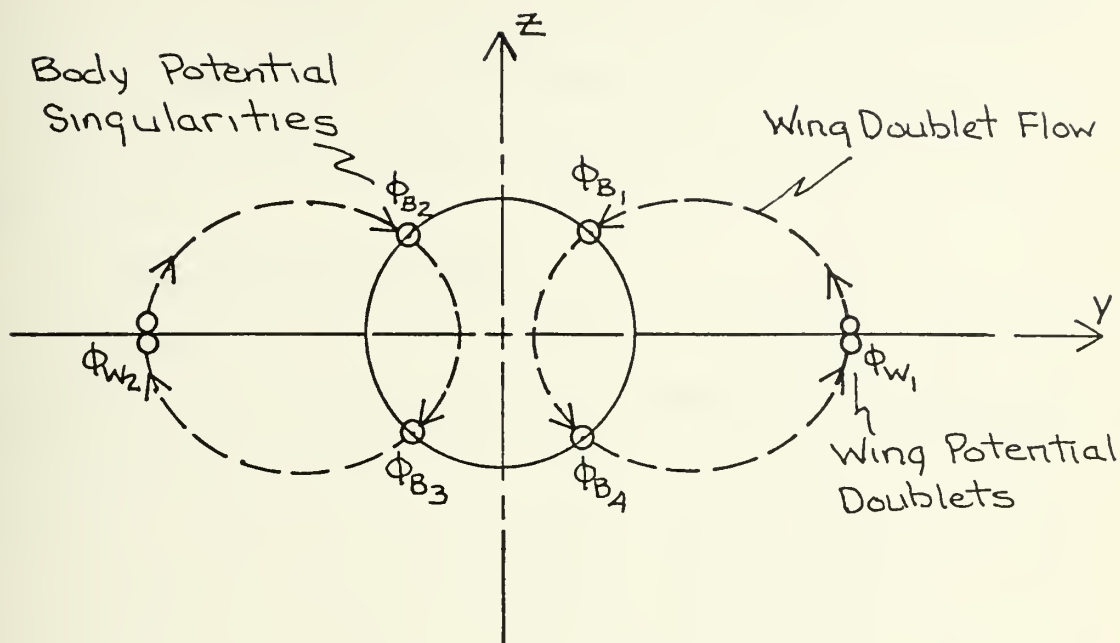


FIGURE 9a  
REPRESENTATION OF WING/BODY POTENTIAL  
SINGULARITIES .

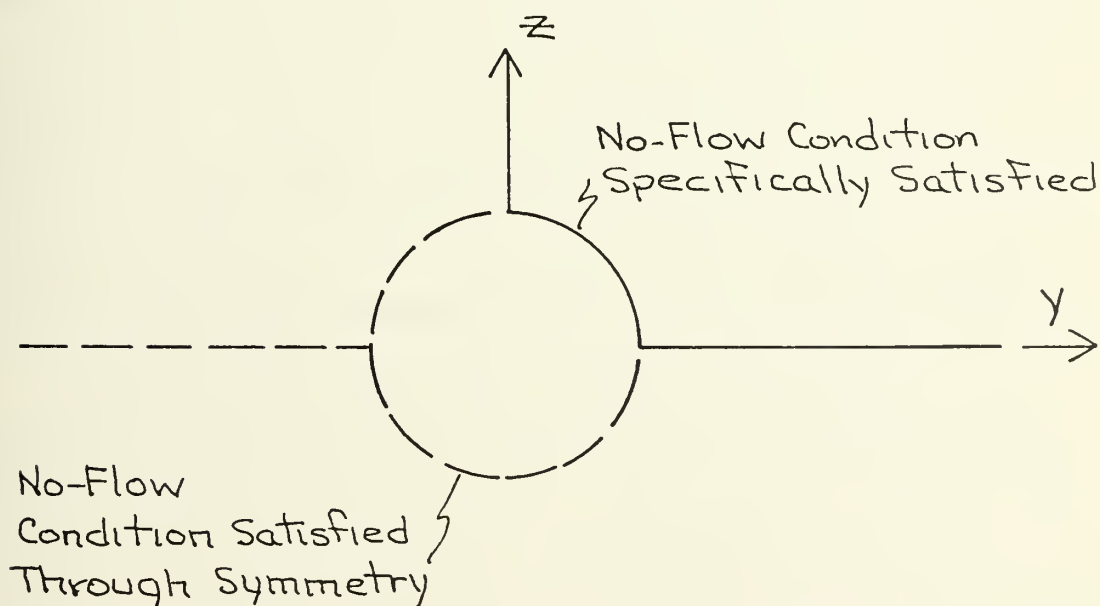


FIGURE 9b  
WING/BODY NO-FLOW BOUNDARY CONDITION





Since any general harmonic motion of the wing can be expressed as a combination of symmetric and antisymmetric motion, this method, as in the wing alone case, need not be restricted to the symmetric motion case considered in detail here.

#### 4. Effective Body Length

The body considered in this analysis is idealized as an infinitely long cylinder with axis aligned with the undisturbed free stream flow. This is not an unrealistic limitation, since in most practical cases, the center part of a fuselage is nearly cylindrical and the fineness ratio of the fuselage is large enough so that the flow at the center part is nearly the same as for an infinitely long cylindrical body. Experiments in steady flow have proved that beyond an effective body length, the lift distribution of the wing/body combination is independent of the body length [40]. Steady flow analyses, such as Woodward's [41], employ a "wing-body interference region," where the body no-flow boundary condition is explicitly applied a finite distance upstream and downstream from the wing root section.

A similar effective body length is modeled in this approach, where the body singularity grid extends from a finite distance upstream of the wing root to a point downstream of the effective wake. The actual body length which must be modeled in order to include all interference effects is discussed in Section VI. Since the kernel function velocities decrease approximately as the distance from the



singularity cubed, it is not unreasonable to assume that interference effects are concentrated close to the wing/wake area.

## 5. Body Singularities

The acoustic singularity used to model the wing was a potential doublet, due to the requirement for a pressure differential across the wing surface. No such requirement exists for the body singularities, so that an harmonically oscillating source could be employed as well as the dipole. However, in the development of the wing computer program, it became apparent that the solution to the matrix equation (4.4) was very sensitive to the value placed on the kernel function upwash singularity. Approximate methods used to obtain an average value of the upwash did not produce acceptable loading distributions over the wing. Only when this upwash was determined numerically, as indicated in Section IV.A.4 were good results obtained. Unfortunately a source singularity, while having a somewhat simpler form of kernel function, can not be analyzed by this same type of numerical development.

The body was therefore modeled by a network of harmonically oscillating potential doublets, as on the wing, with axes oriented in the radial direction. Each doublet is at the center of its control panel, coincident with a normalwash control point. Determination of the normalwash (radial velocity  $u_{r_0}$ ) at the doublet location is obtained, as with the wing singularity, from a consideration of continuity.



The total fluid outflow from the doublet is  $u_{r_0} A_0$ , where  $A_0$  is the area of the doublet control panel on the body. The amount of fluid passing back through the body at a control panel away from the doublet is  $(u_r)_{nm} A_{nm}$  where  $n$  indicates the axial location and  $m$  the circumferential location of this control panel. Continuity is then expressed for this discrete element representation as

$$u_{r_0} A_0 + \sum_{n=1}^{\infty} \sum_{m=1}^M (u_r)_{nm} A_{nm} = 0$$

where  $M$  equals the number of panels located around the circumference of the body. If the  $A_{nm}$ 's are chosen so that  $A_{nm} = A_0$  the value of the doublet singularity is given by

$$u_{r_0} = - \sum_{n=1}^{\infty} \sum_{m=1}^M (u_r)_{nm} \quad (4.30)$$

This continuity equation states, in effect, that all the fluid which leaves the doublet in the radial direction must pass back through the body surface prior to returning to the doublet. As in the wing singularity case, the summation of normalwash in the axial direction can be terminated after a reasonable distance in both the upstream and downstream directions.

## 6. Kernel Functions

The elements of each of the kernel function matrices defined in Section IV.B.2 represent the normalwash on either wing or body surface due to a harmonically oscillating doublet of unit strength which satisfies the governing linearized differential equation (2.12). Doublets on the



wing are of course oriented in the  $\theta$  (or  $z$ ) direction, while those on the body have their axes in the radial direction.

The formulation of these kernel functions is developed in Appendix A. They are summarized below with control point at  $(r, \theta, x)$  and doublet located at  $(r_o, \theta_o, x_o)$ . The body radius is  $r_B$ .

- (i)  $K_W$  - Downwash on wing due to unit wing/wake singularity.

$$u_\theta = \frac{-\beta^2}{4\pi R^3} (1 + i \frac{\omega}{a_\infty \beta^2} R) \exp \{ i \frac{\omega}{a_\infty \beta^2} [M_\infty (x - x_o) - R] \} \quad (4.31)$$

where

$$R = \sqrt{(x - x_o)^2 + \beta^2 (r^2 + r_o^2 + 2rr_o)}$$

- (ii)  $K_{BW}$  - Normalwash on body due to unit wing/wake singularity.

$$u_r = \frac{-\beta^2}{4\pi R^3} \sin \theta (1 - \frac{3r_B}{R} \frac{\partial R}{\partial r}) (1 + i \frac{\omega}{a_\infty \beta^2} R) + (\frac{\omega}{a_\infty \beta^2})^2 [r_B R \frac{\partial R}{\partial r}] \exp \{ i \frac{\omega}{a_\infty \beta^2} [M_\infty (x - x_o) - R] \} \quad (4.32)$$

where

$$R = \sqrt{(x - x_o)^2 + \beta^2 (r_B^2 + r_o^2 + 2r_o r_B \cos \theta)}$$

$$\frac{\partial R}{\partial r} = \frac{\beta^2}{R} (r_B + r_o \cos \theta)$$





In both the above formulations, the minus sign represents a singularity on the  $\theta=0$  wing/wake, and the plus sign a singularity on the  $\theta=\pi$  virtual wing/wake.

(iii)  $K_B$  - Normalwash on body due to unit body singularity.

$$u_r = \frac{-\beta^2}{4\pi R^3} \left\{ \left[ \cos(\theta-\theta_o) + \frac{3}{R} r_B (1 - \cos\langle\theta-\theta_o\rangle) \frac{\partial R}{\partial r} \right] \right. \\ \left. \left[ 1 + i \frac{\omega}{a_\infty \beta^2} R \right] - \left( \frac{\omega}{a_\infty \beta^2} \right)^2 R r_B (1 - \cos\langle\theta-\theta_o\rangle) \frac{\partial R}{\partial r} \right\} \\ \exp \left\{ i \frac{\omega}{a_\infty \beta^2} [M_\infty(x-x_o) - R] \right\} \quad (4.33)$$

where

$$R = \sqrt{(x-x_o)^2 + 2\beta^2 r_B^2 (1 - \cos\langle\theta-\theta_o\rangle)}$$

$$\frac{\partial R}{\partial r} = \frac{\beta^2}{R} r_B (1 - \cos\langle\theta-\theta_o\rangle)$$

(iv)  $K_{WB}$  - Downwash on wing due to unit body singularity.

$$u_\theta = \frac{-\beta^2}{4\pi R^3} \left\{ \left[ r \sin \theta_o + \frac{3}{R} (r_B - r \cos \theta_o) \frac{\partial R}{\partial \theta} \right] \right. \\ \left[ 1 + i \frac{\omega}{a_\infty \beta^2} R \right] - \left( \frac{\omega}{a_\infty \beta^2} \right)^2 R (r_B - r \cos \theta_o) \frac{\partial R}{\partial \theta} \right\} \\ \exp \left\{ i \frac{\omega}{a_\infty \beta^2} [M(x-x_o) - R] \right\} \quad (4.34)$$

where

$$R = \sqrt{(x-x_o)^2 + \beta^2 (r^2 + r_B^2 - 2rr_B \cos \theta_o)}$$

$$\frac{\partial R}{\partial \theta} = - \frac{\beta^2}{R} r r_B \sin \theta_o$$



## V. DESCRIPTION OF COMPUTER PROGRAMS

### A. GENERAL DESCRIPTION

Listings of the two computer programs developed and used in this investigation are reproduced in Appendices D and E. The programs are written in standard FORTRAN IV language. Calculations were performed on the I.B.M. 360/67 computer at the W. R. Church Computer Center of the Naval Postgraduate School. Object codes were obtained with the I.B.M. G-level compiler.

Both the wing and the wing/body programs are arranged in the same general format. The MAIN program reads the input data and establishes the wing or wing/body control grid. One or more subroutines are called which establish the kernel function matrix elements. MAIN calculates the wing downwash velocity vector and calls subroutine COMAT to solve the matrix downwash equation (4.2) for the wing velocity potential distribution. MAIN finally calls subroutine PRES which calculates the perturbation pressure distribution over the wing by applying finite difference approximations to equation (4.5). PRES then calls subroutines SECLM and WINGLM to integrate this distribution to obtain sectional and wing forces and moments. These results are printed by PRES and control is returned to MAIN for the reading of data cards for the next problem.



## B. WING PROGRAM

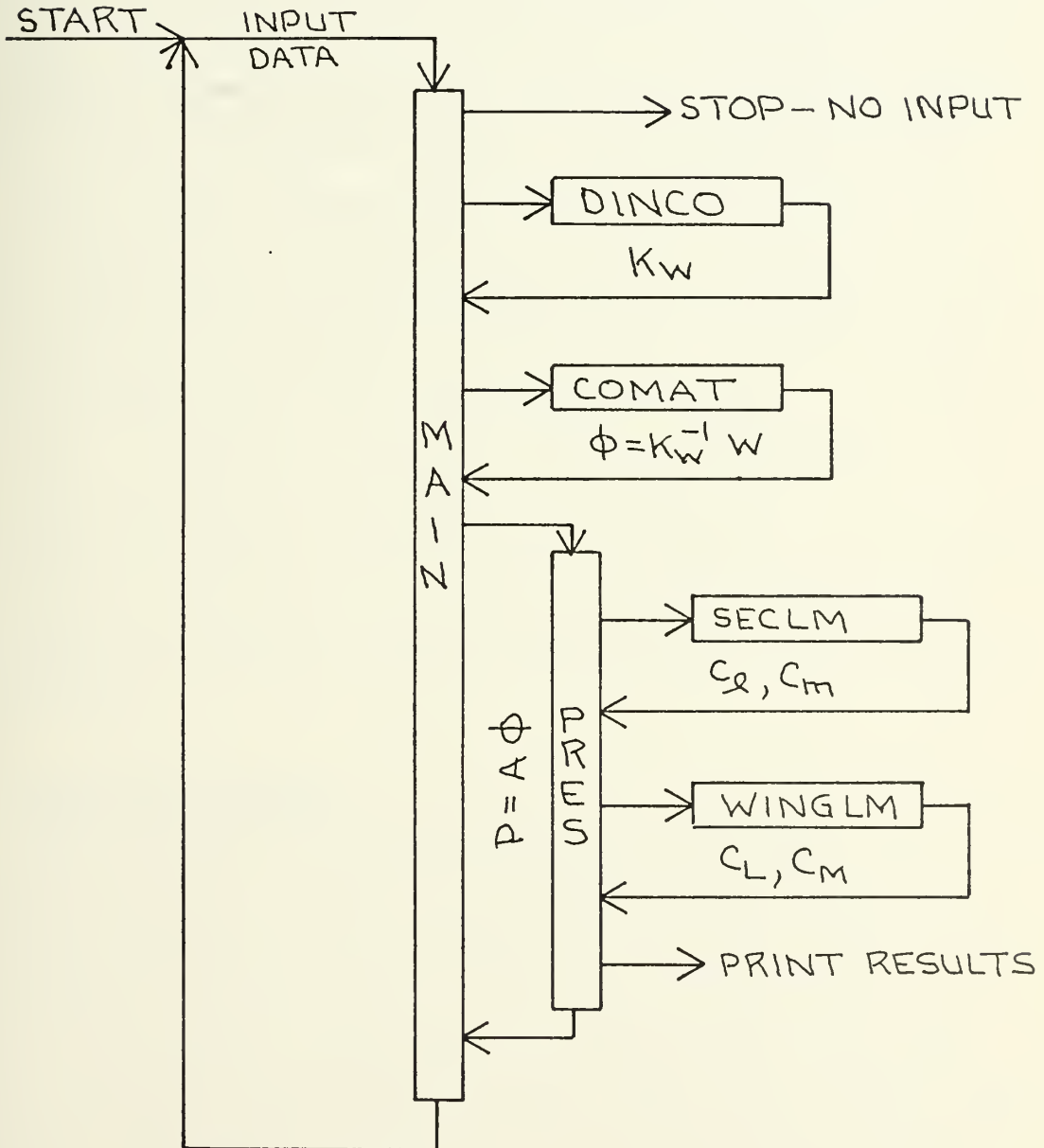
The wing program computes potential and pressure loadings due to harmonic motion on general planar wing configurations from rectangular to arbitrary sweep angles for both the leading and trailing edges. The program is restricted, however, to constant sweep angles, and to a finite tip chord with minimum taper ratio of about one-fifth. Thus delta wing configurations are excluded. This restriction is caused by the method used to integrate the chordwise pressure distribution to obtain sectional lift and pitching moment, discussed in Section IV.A.5. The program provides for a maximum of 100 control points on the wing and ten control points in either the chordwise or spanwise directions. Storage requirements are the equivalent of 18,000 single precision complex words, or 144,000 bytes on the I.B.M. 360, with a maximum run time of approximately twelve minutes for one problem. Provision is made for the running of successive problems for as many sets of input data cards as are provided.

Figure 10 is a diagram of the wing program, while subroutine flow diagrams are presented in Appendix C. Subroutine DINCO forms the kernel function matrix from equation (4.8), with the matrix elements defined by equation (4.3). The COMAT subroutine solves the linear complex matrix equation (4.2) by the Gauss-Jordan method with total pivoting. This subroutine was written for systems of real equations by Mrs. Sharon Good, David Taylor Model Basin, as published in Ref. 42, and modified to include the complex



FIGURE 10

WING PROGRAM DIAGRAM







capability by Mr. Hellmut Golde, Department of Electrical Engineering, University of Washington. COMAT was further modified by the author for particular application to the wing and wing/body programs.

Input instructions are presented in Appendix B. Any number of spanwise and chordwise control points, up to the maximum of ten each, may be specified for a semi-span wing. The wing is modeled by an equal number of chordwise control points at each spanwise station. The program is limited by theory to the subsonic flow regime, within which any mode, amplitude, or frequency of harmonic wing motion may be specified, including the steady case. Results printed by the program for each spanwise station are:

- (i) Potential doublet strength distribution
- (ii) Pressure coefficient distribution
- (iii) Section lift and pitching moment coefficients

In addition, wing lift and pitching moment coefficients are presented.

#### C. WING/BODY PROGRAM

The wing/body program incorporates the body surface boundary condition into the harmonic motion analysis of a rectangular wing planform. As in the wing program, a maximum of 100 control points may be used to model the wing, while up to 130 points are allowed in the body control panel network. Storage requirements are the equivalent of 43,500 single precision complex words, or 348,000 bytes on the



I.B.M. 360. A maximum run time of about 20 minutes for the wing/body problem is required, while a wing only solution (body radius equals zero) is obtained in less than seven minutes. As in the wing program, successive problems for different wing, body, and flow geometries may be run.

Figure 11 diagrams the wing/body program, with individual subroutine flow charts presented in Appendix C. The influence coefficient matrices defined in Section IV.B.2 are formed in the following subroutines:

- (i) DINCO -  $D_W$  from equation (4.31)
- (ii) UTHETA -  $K_{WB}$  from equation (4.34)
- (iii) URAD1 -  $K_{BW}$  from equation (4.32)
- (iv) URAD2 -  $K_B$  from equation (4.33)

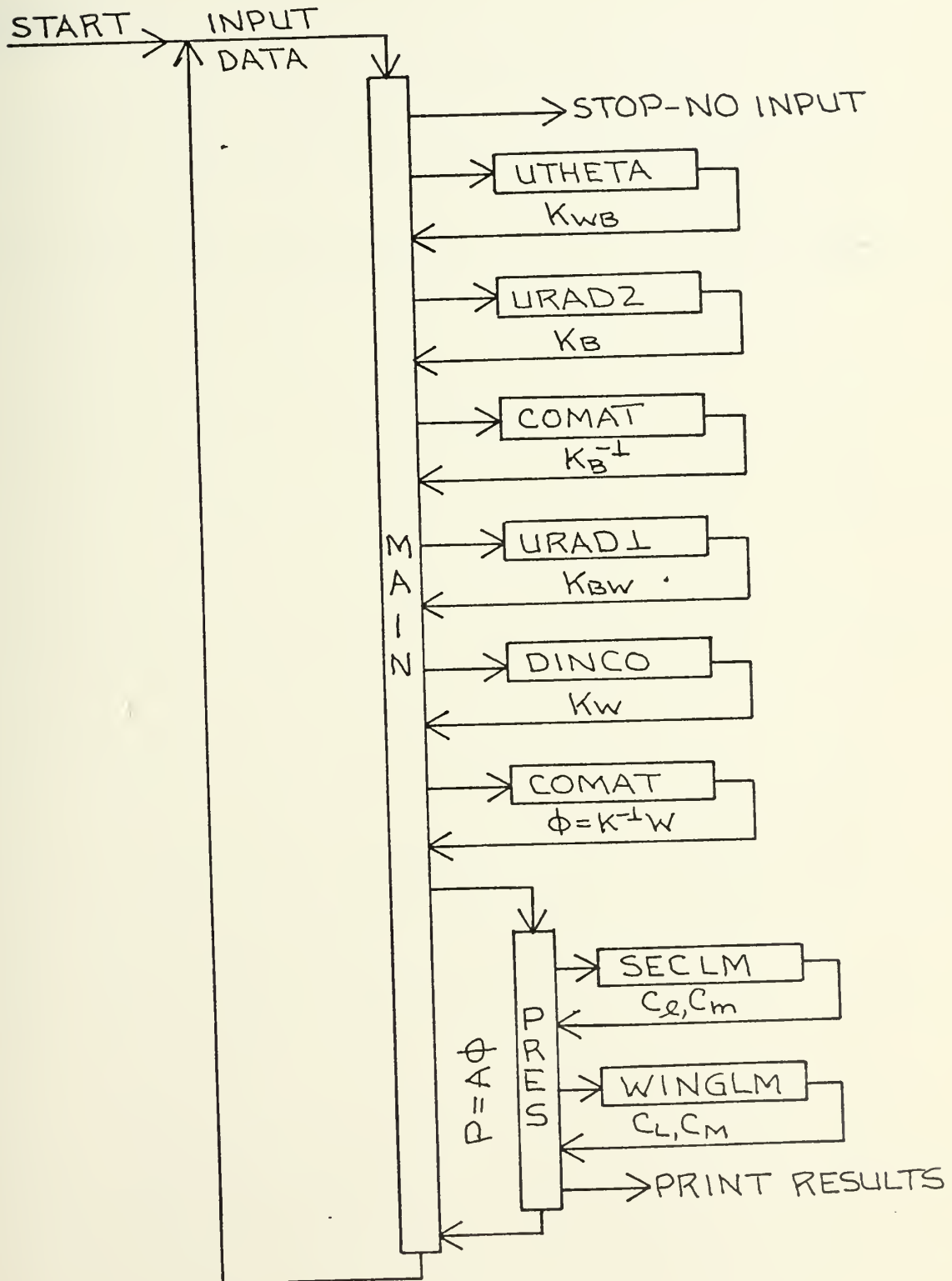
The matrix  $K_B$  is inverted by subroutine COMAT and the modified kernel function matrix of equation (4.25) is formed in MAIN. COMAT is again called to solve the resulting matrix equation and PRES performs the same function with the same data printouts as in the wing program. Subroutine DINCO, while performing the same function as in the wing program, is here in a more simplified form because of the restricted wing geometry of the wing/body program. This accounts for the reduced running time of wing only problems in this program as compared to the general wing program.

The wing/body program uses the same wing grid and flow geometry parameters as the wing program. Any number of body control points may be specified up to the maximum of 130. An effective body length of one wing chord upstream



FIGURE 11

# WING/BODY PROGRAM DIAGRAM





from the wing leading edge to one wing chord downstream from the termination of the effective wake is modeled by the program. Input data instructions are presented in Appendix B.





## VI. RESULTS AND DISCUSSION

### A. WING ANALYSIS

#### 1. Comparison with Lifting Surface Theory

In order to investigate the validity of the discrete potential element approach to lifting surface theory, the wing program was run for a wide variety of wing/flow geometries and types of oscillatory motion. Examples were picked which could be checked against previous work reported in the literature, representing a variety of lifting surface theory approaches, as well as the relatively limited amount of experimental results which have been obtained in the unsteady field.

The figures presented in this section are a representative summary of this investigation. The subsonic flow regime was covered from the incompressible  $M_\infty=0$  to the high subsonic  $M_\infty=0.9$ , while the range of frequencies varied from the steady case to the relatively high reduced frequency of  $k=1.2$ . The wing planforms considered had a range of aspect ratios from one to six, sweep angles from zero to 45 degrees, and taper ratios from one to one-half. The types of symmetric harmonic motion considered were:

- (i) Pitching - rigid body oscillations of the wing about a spanwise axis perpendicular to the flow direction;
- (ii) Bending - oscillations of the wing as a beam cantilevered at the root chord in the first natural mode of bending.



(iii) Plunging - rigid body oscillations of the wing in the z direction at a mean angle of attack of zero;

(iv) Flapping - rigid body roll oscillation of the wing simply supported from a chordwise axis inboard of the root. Steady data were obtained with the wing analyzed as a rigid body at a fixed angle of attack. The results have been presented as chordwise pressure distributions, spanwise lift and pitching moment distributions, and wing coefficients plotted with respect to reduced frequency.

In each of the figures, the coefficient amplitudes are normalized with respect to the motion as follows:

- (i) Pitching - angle of attack amplitude;
- (ii) Bending - wing tip angle of attack amplitude;
- (iii) Plunging - vertical motion amplitude;
- (iv) Flapping - amplitude of flapping angle.

These represent the conventions used in the applicable references, however the phase angle relationship were converted to the coordinate convention used in this paper where differences occurred.

Correlation of the wing program results with existing lifting surface theory was in general quite good. Deviations appeared to come from the different methods employed to handle the wing edge singularities in the pressure distribution. The lifting surface approaches assume the form of these singularities a priori in the choice of their loading functions, as discussed in Section III.B. The discrete element approach, on the other hand, assumes no



loading profile, but obtains proper potential and pressure distributions through inclusion of the boundary conditions in the problem formulation. As discussed in Ref. 1, much effort has been devoted in lifting surface theory to developing the most numerically efficient and accurate loading functions, as well as to improve the numerical methods of handling the singular kernel functions.

The first four figures compare wing program results with one of the most recent lifting surface theories. This advanced kernel function method, based on the acceleration potential, was presented by Laschka in 1963 [5] and further developed by Laschka and Schmid for interfering planar surfaces in a 1967 paper [43]. Figure 12 compares chordwise pressure distributions on a swept, tapered wing undergoing pitching oscillations in low subsonic flow with Laschka's results [46]. Good correlation is evident at each spanwise station, with the only variance being a small difference in the shape of the pressure distribution near the leading edge, as previously discussed.

Figures 13 and 14 present spanwise loading on a 45 degree swept constant chord wing in both the pitching and plunging modes. Results are compared with Lashka's work [5] for both low subsonic ( $M_\infty \approx 0$ ) and  $M_\infty = 0.8$  flows. Correlation is again good. The discrete potential element approach appears to overestimate the amplitude of the lift and pitching moment slightly, especially near the wing tip. In fact this latter trend appears in almost all the results of the present



method. The explanation again would appear to lie in the method of handling the wing tip pressure slope singularity, which is included implicitly in the boundary conditions. Further development of the discrete potential element approach would definitely have to include investigation of the adequate recognition of this wing tip condition in the problem formulation.

In Ref. 37 Laschka compares his results, for the wing configurations of Figures 13 and 14, with the work of Pao Tan Hsu [44]. It should be noted that the wing program results agree more closely with Laschka's data, while falling between Laschka's and Hsu's results except for amplitudes at the wing tip. The theory here is further compared with experimental results obtained by Laidlaw [45] with fair correlation.

Figure 15 compares wing program spanwise loading with Laschka's results from Ref. 37 for a steady swept, tapered wing in low subsonic flow. The lift and pitching moment coefficients are presented on an expanded scale, with the same type of comparisons already noted.

The results presented in Figures 16 through 18 are noteworthy for the Mach number range considered ( $M_\infty = 0.24$  to  $0.9$ ) and for the consistent experimental data presented from the work of Lessing, Troutman, and Menees [47]. Spanwise and chordwise loadings are plotted for an aspect ratio three rectangular wing in the bending mode. Theoretical comparison is made to the lifting surface results developed by Lessing





et al in 1960 from the original kernel function methods of Refs. 25 and 48.

At a Mach number of 0.24, the chordwise pressure loadings obtained from the two theories are almost identical. The spanwise lift and moment curves show a somewhat heavier loading concentration near the wing tip for the discrete potential element method, as in the preceding figures. This trend also appears at Mach numbers of 0.7 and 0.9. The  $M_\infty = 0.7$  chordwise pressure distributions show a difference in the representations of the leading edge pressure distributions outboard of  $\eta = 0.5$ . These deviations can probably again be laid to the different methods employed to handle the wing pressure singularities. However, the wing program results agree more closely to the experimental data of Ref. 47, than does the kernel function approach. No explanation can be found for the deviation of the pressure phase angles in the wing trailing edge area for both the 0.24 and 0.7 Mach number cases. It should be noted, however, that the experimental points again correlate more closely with the wing program results in this area. In fact, the close correlation of these experimental data with the results of the present method is quite gratifying.

It is interesting to observe that a shock wave may have started to form on the wing in the 0.7 Mach number flow downstream of the 60% chord line, as indicated by the drastic jump in the pressure phase angle measurements at this location in Figure 17b. The theoretical analyses would not, of course, reflect the existence of the shock wave.



The closeness of the two theoretical approaches at  $M_\infty = 0.9$  is also noteworthy. As discussed in Section II.C, the linearization of the basic problem for perturbation analysis would appear somewhat questionable this close to the speed of sound. However, the consistency of the results would seem to indicate that the linearized subsonic theory is still valid at this high subsonic Mach number.

Figure 19 analyzes the pitching motion of an aspect ratio two rectangular wing. Chordwise and spanwise loadings are compared with the experimental and theoretical results of Laidlaw [45]. The latter represents a numerical treatment of the rectangular wing aspect ratio theory of Reissner [49, 50] developed in 1947. Considering the fact that Reissner's approach basically involves applying correction factors to two-dimensional results in order to account for finite aspect ratio, this theory agrees quite well with the discrete potential element approach. The experimental data, although not as consistent as that of Lessing [47], agrees reasonably well with the Wing Program results. Figure 20 presents spanwise loading for the same wing in plunging motion. Correlation of pressure distributions between theories and experimental data for this mode of nonsteady motion is the same as for the pitching case.

The frequency response of a rectangular wing in the flapping mode is presented in Figure 21. Comparison is made to experimental and theoretical data by Woolston, Clevenson, and Leadbetter [51], who employed a basic kernel function



approach. Correlation of the wing program results with the experimental data is reasonably good, although there is some difference in the phase angle values. However, the variations of both lift and pitching moment with reduced frequency compares very well. Woolston's theoretical points coincide essentially with the wing program curves except for the pitching moment phase angle. No explanation can be found for this difference. Laschka [5], in comparing his results with those of Woolston, produced virtually the same curves as the discrete potential element program.



# FIGURE 12

## CHORDWISE PRESSURE DISTRIBUTION

### PITCHING

$$k=1.19$$

$$M_{\infty}=0.1$$

$$AR=1.45$$

$$\Lambda=39^{\circ}$$

$$\lambda=0.54$$

WING PROGRAM

○ Re  $C_{pa}$

△ Im  $C_{pa}$

— THEORY LASCHKA

REF. 46

$$C_{pa} = \text{Re } C_{pa} + i \text{Im } C_{pa}$$

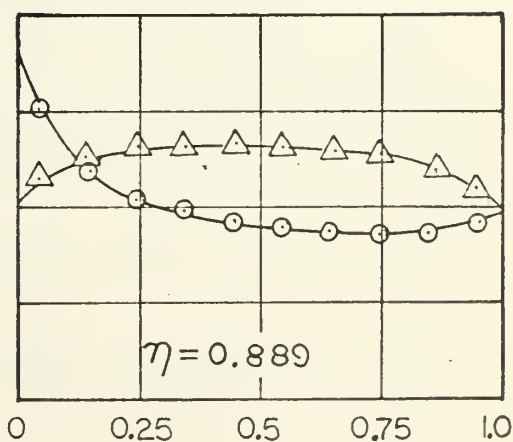
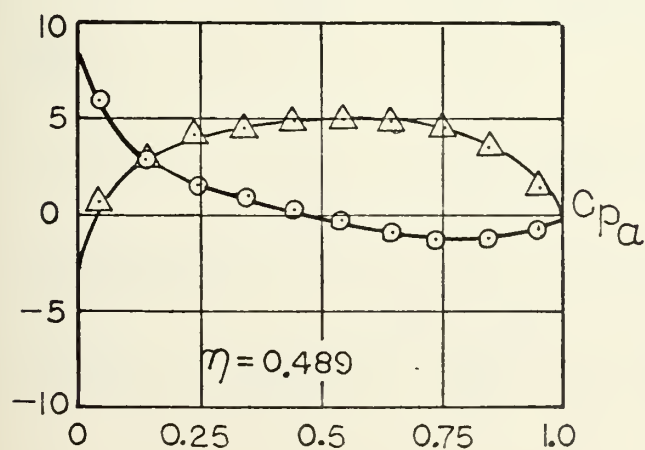
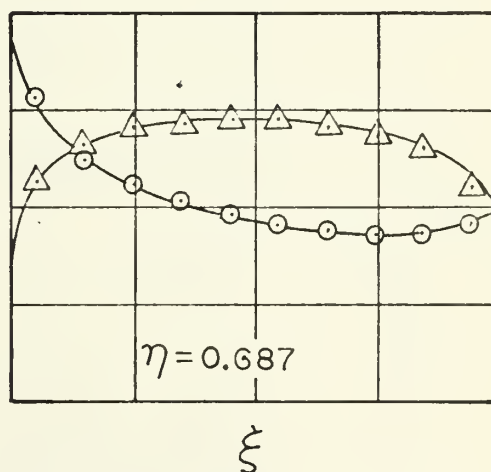
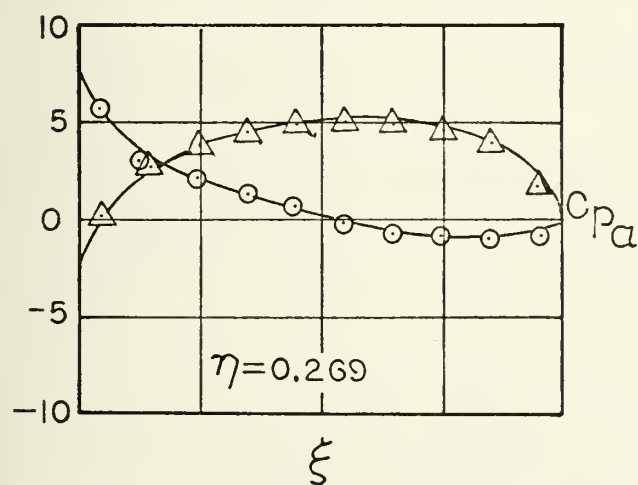
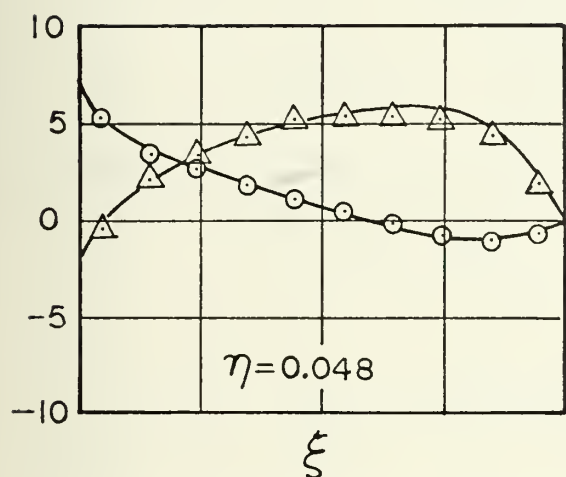






FIGURE 13<sub>a</sub>

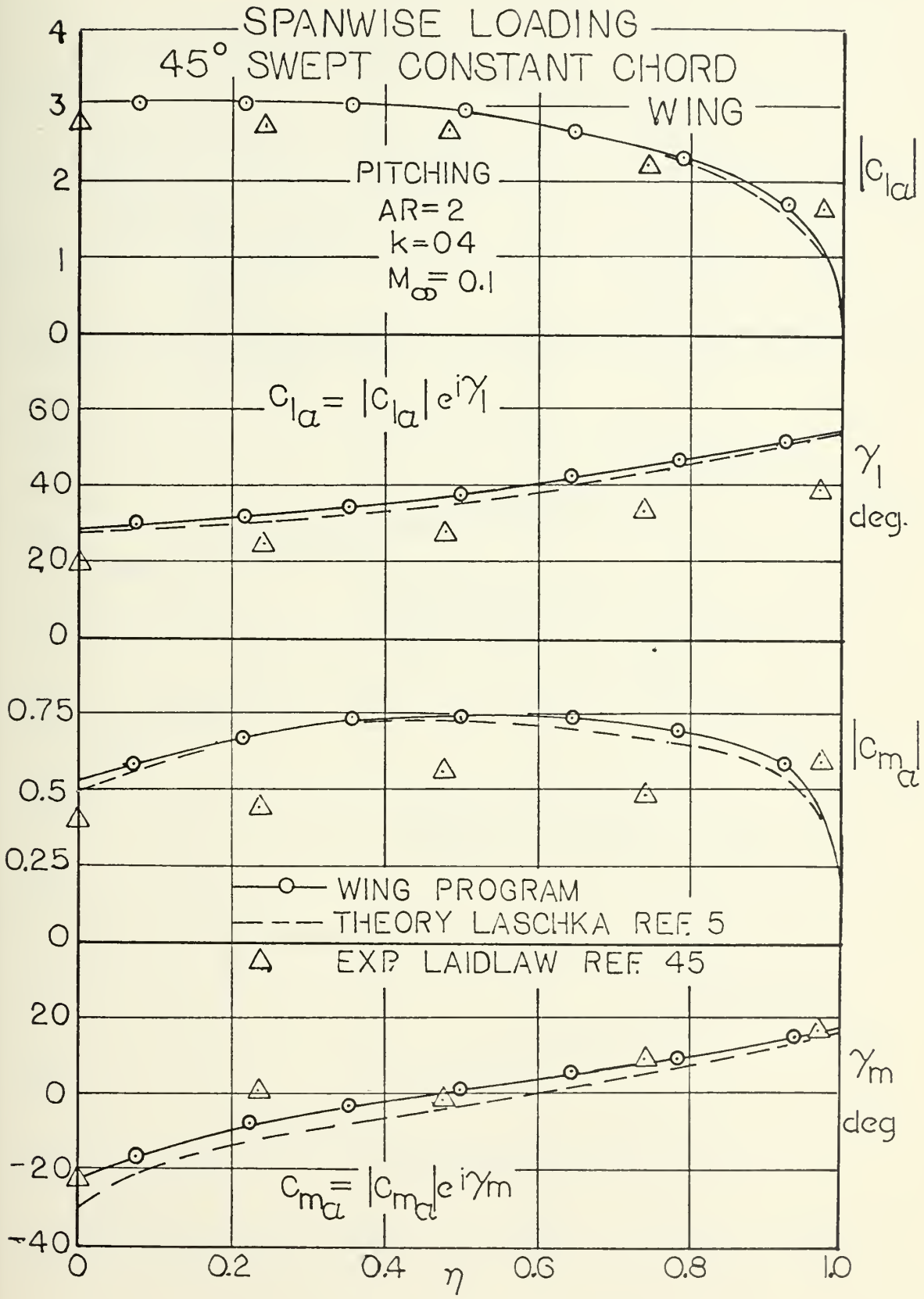




FIGURE 13b

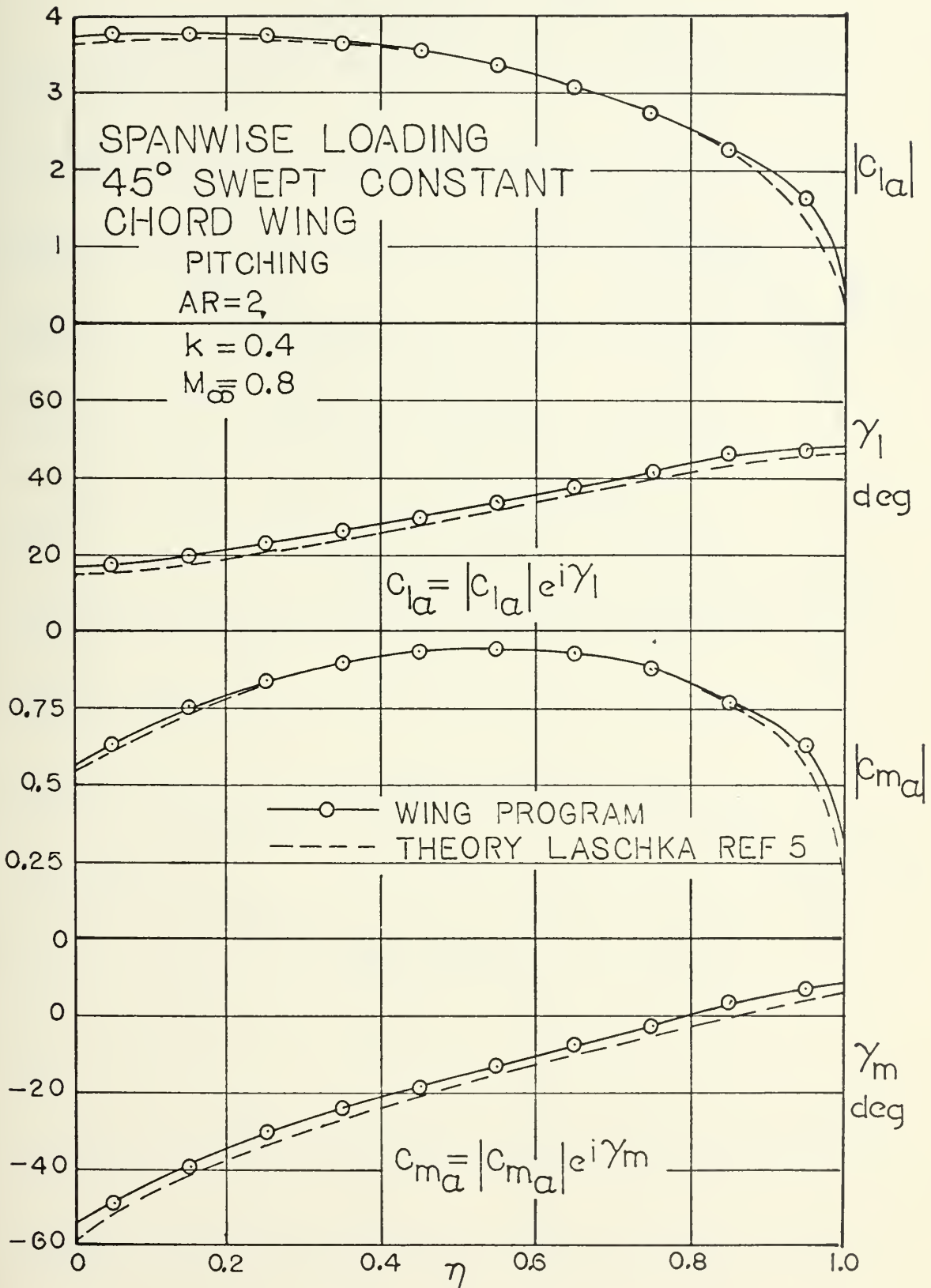




FIGURE 14<sub>a</sub>  
SPANWISE LOADING  
45° SWEEP CONSTANT CHORD WING

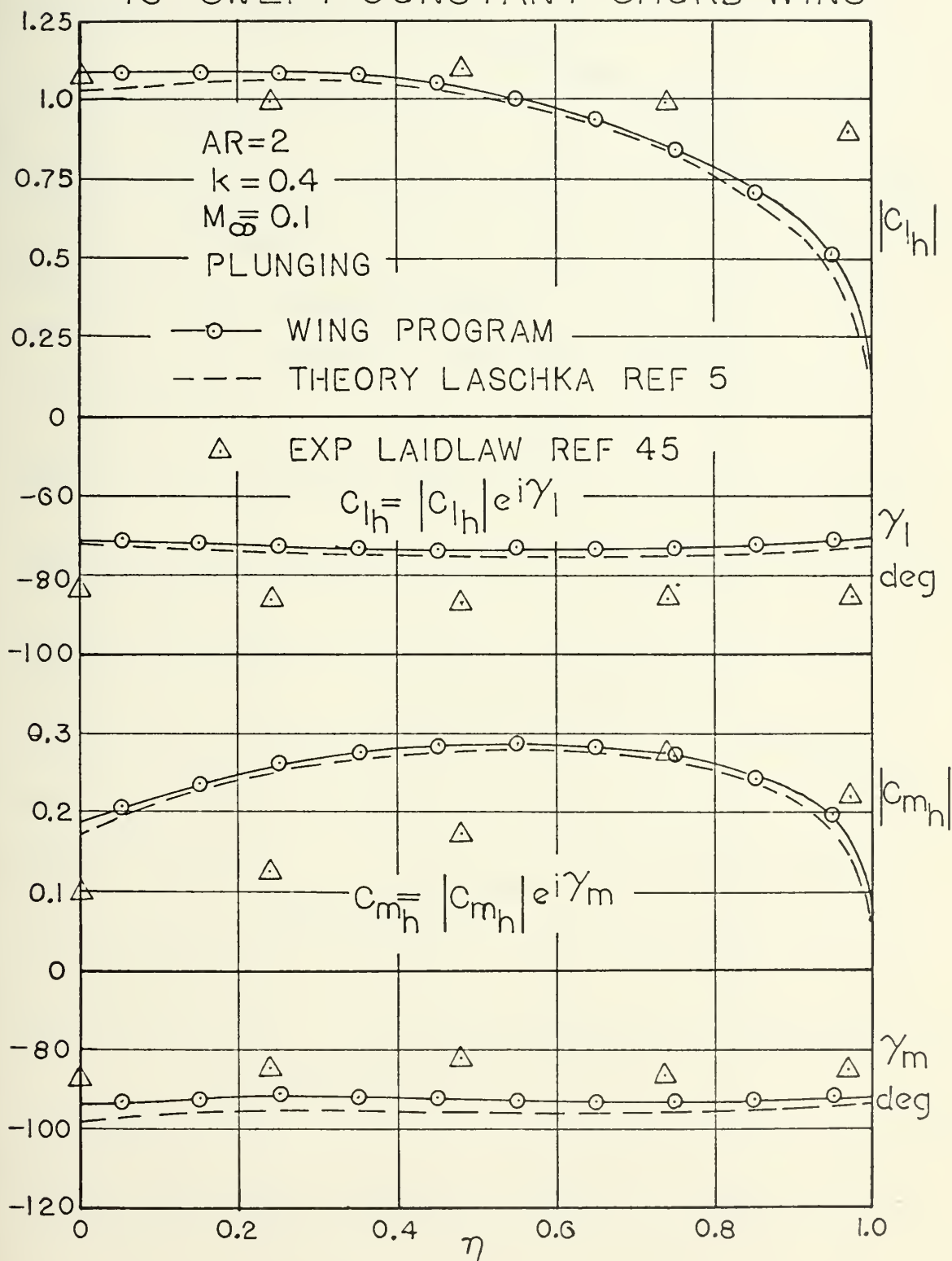




FIGURE 14b

SPANWISE LOADING

45° SWEEPED CONSTANT CHORD WING

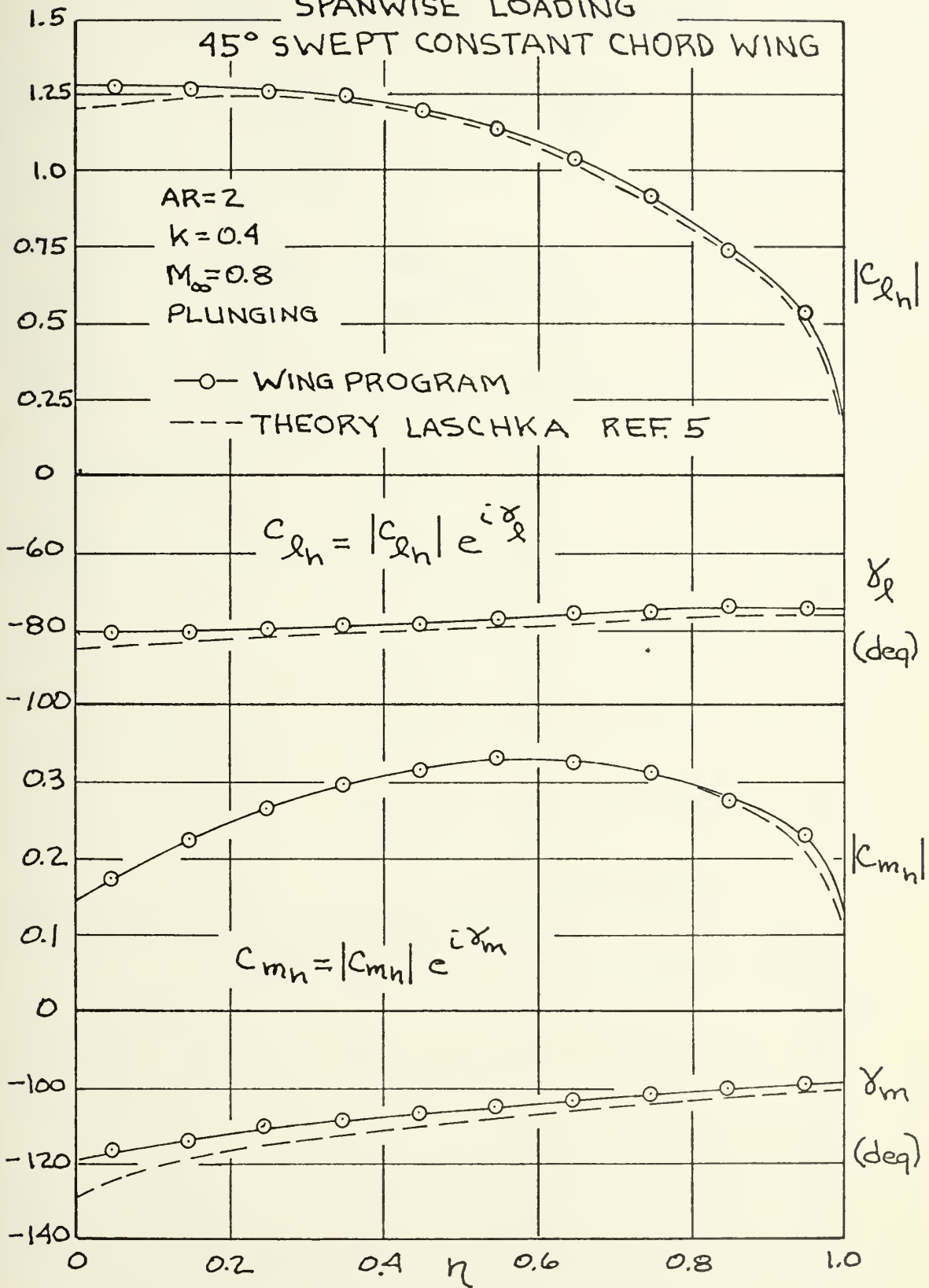






FIGURE 15  
STEADY SPANWISE LOADING

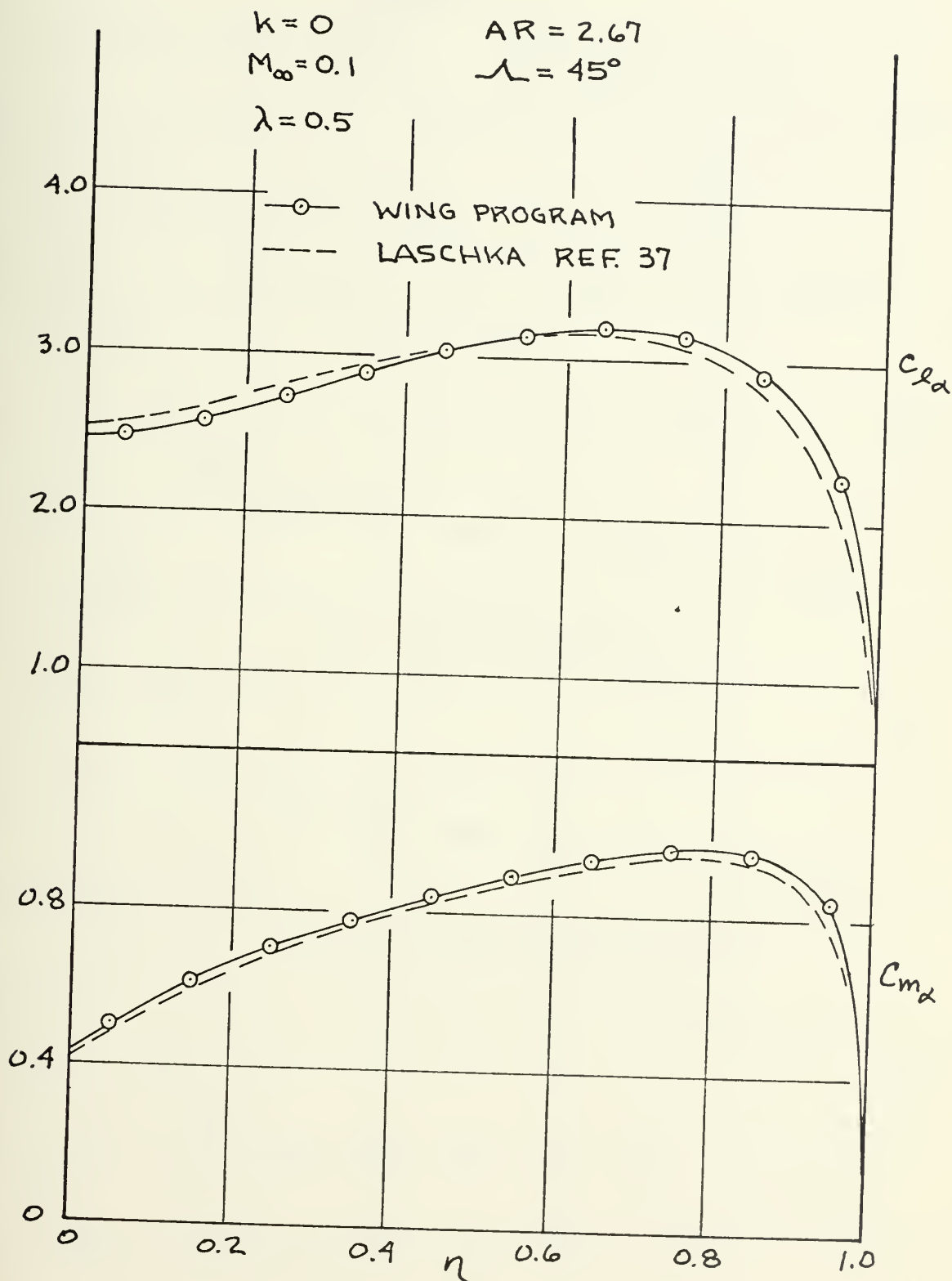




FIGURE 16a

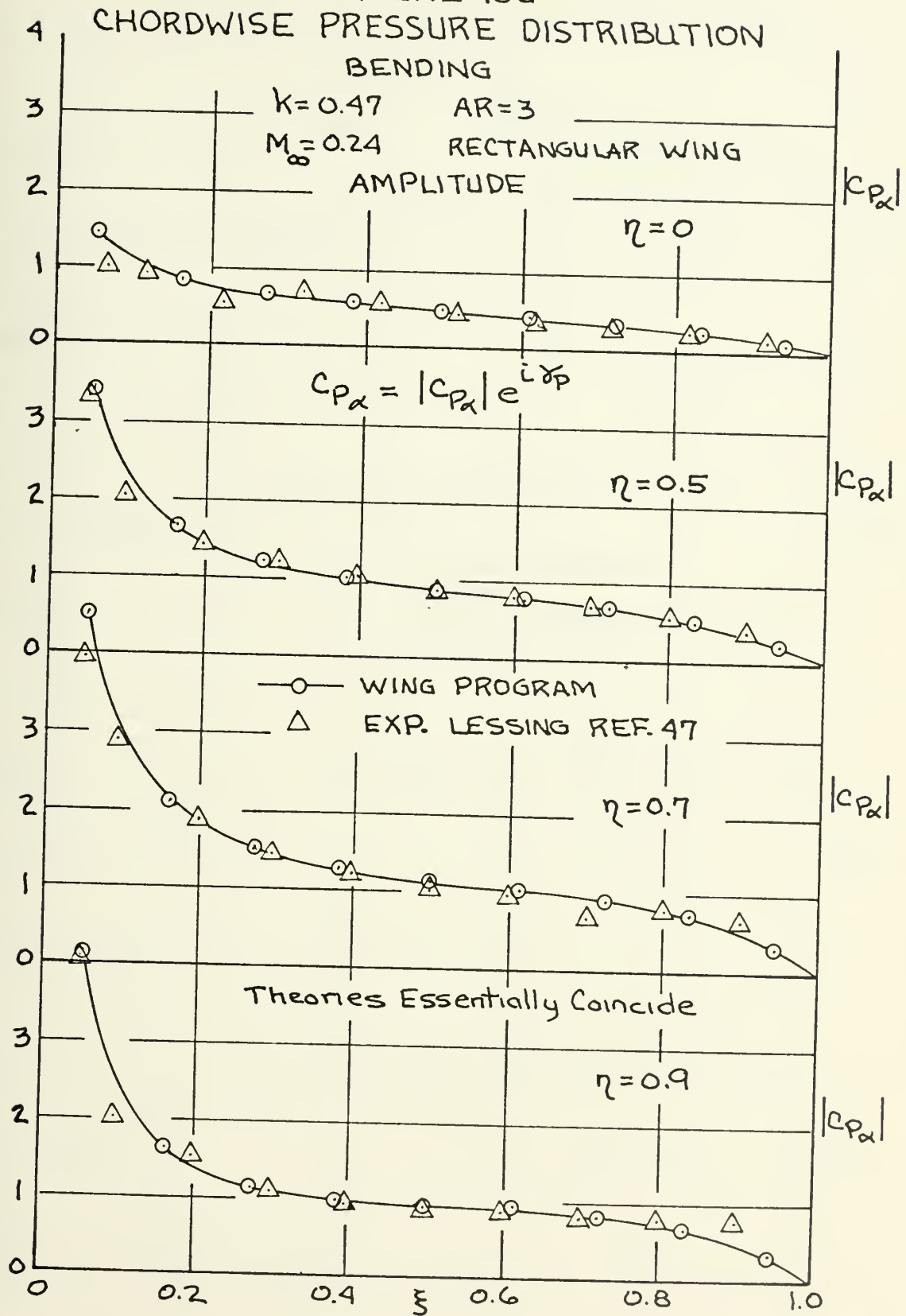




FIGURE 16b  
CHORDWISE PRESSURE DISTRIBUTION  
BENDING

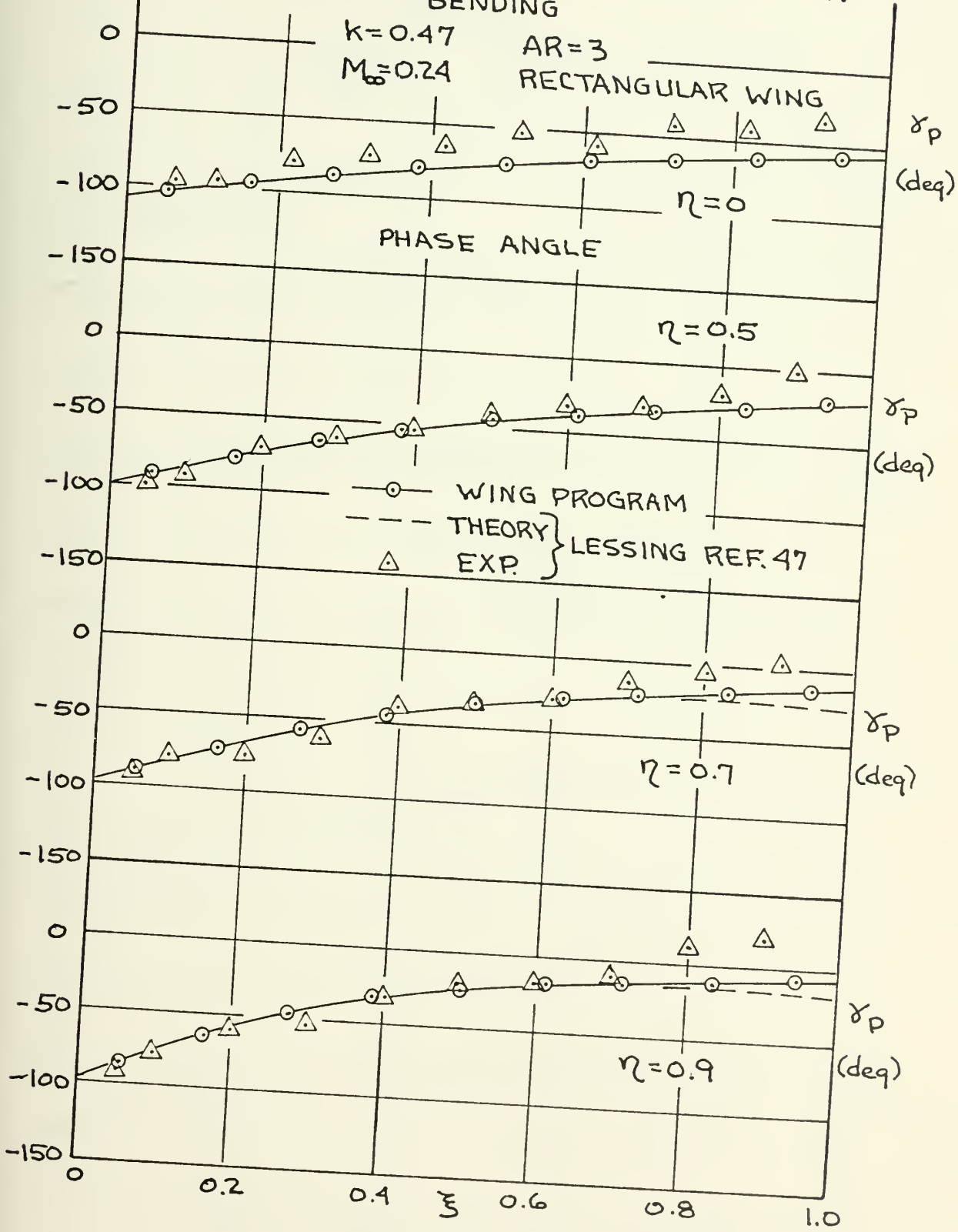




FIGURE 16c  
SPANWISE LOADING  
BENDING

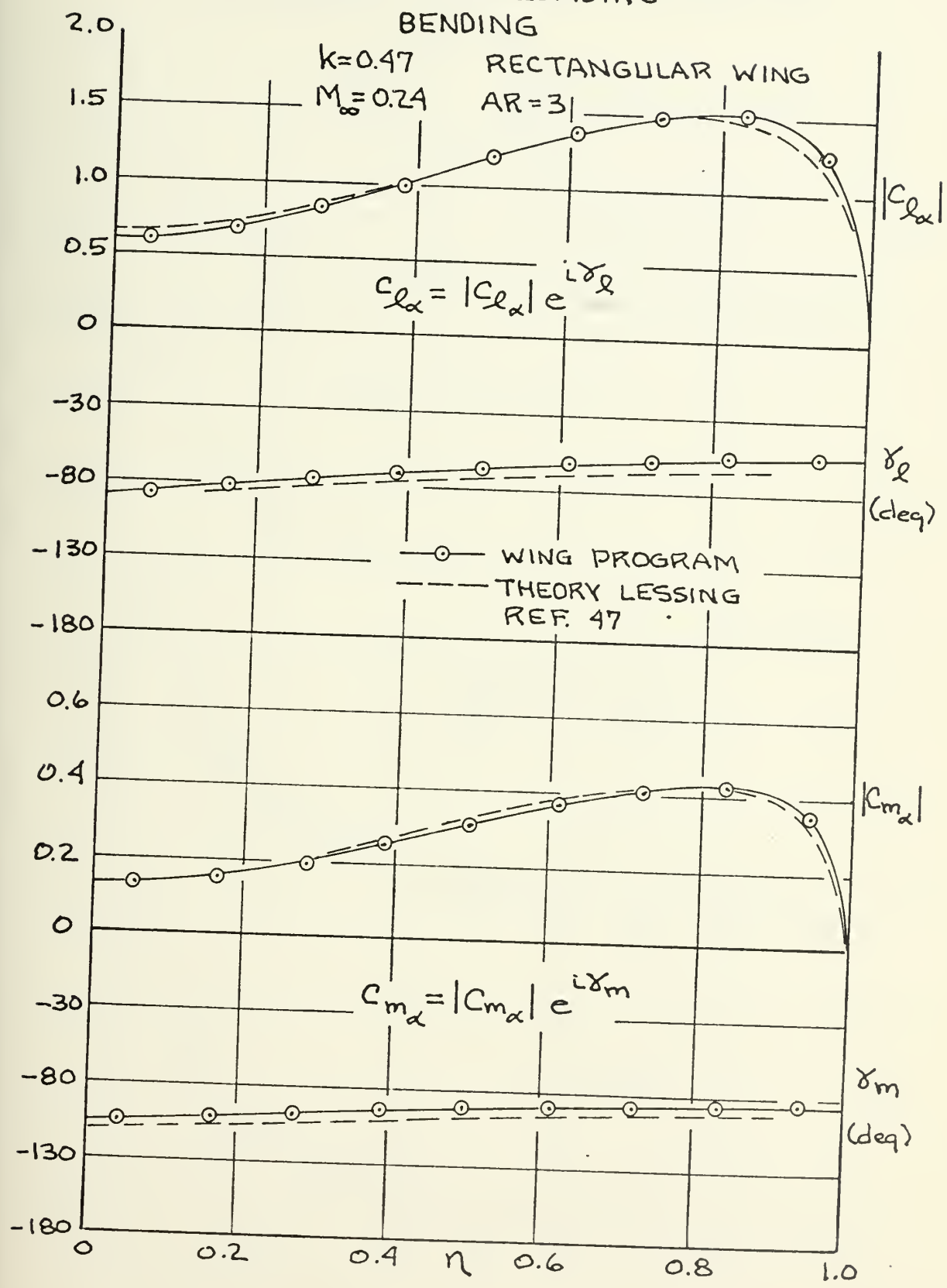






FIGURE 17a  
CHORDWISE PRESSURE DISTRIBUTION

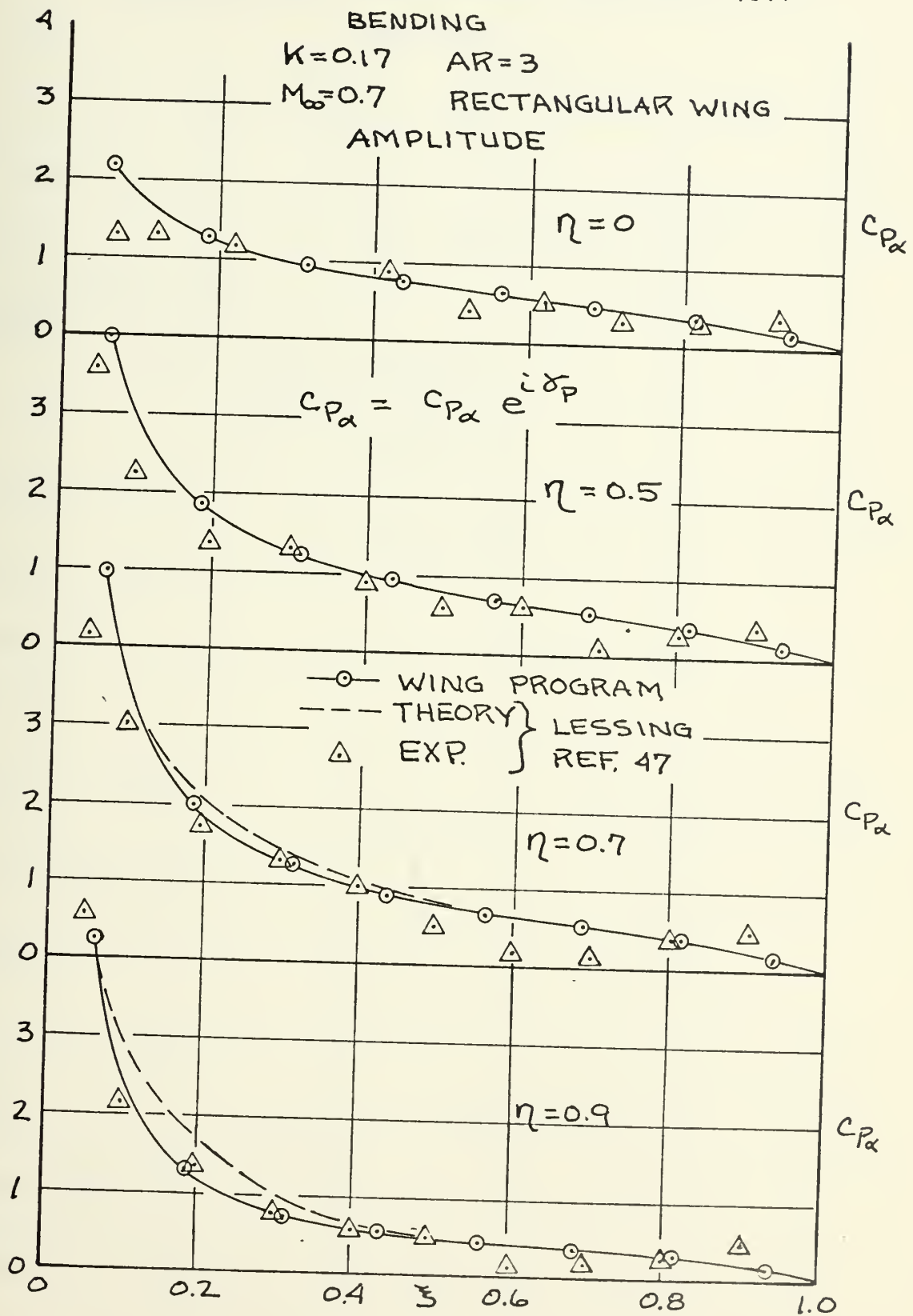




FIGURE 17b  
CHORDWISE PRESSURE DISTRIBUTION

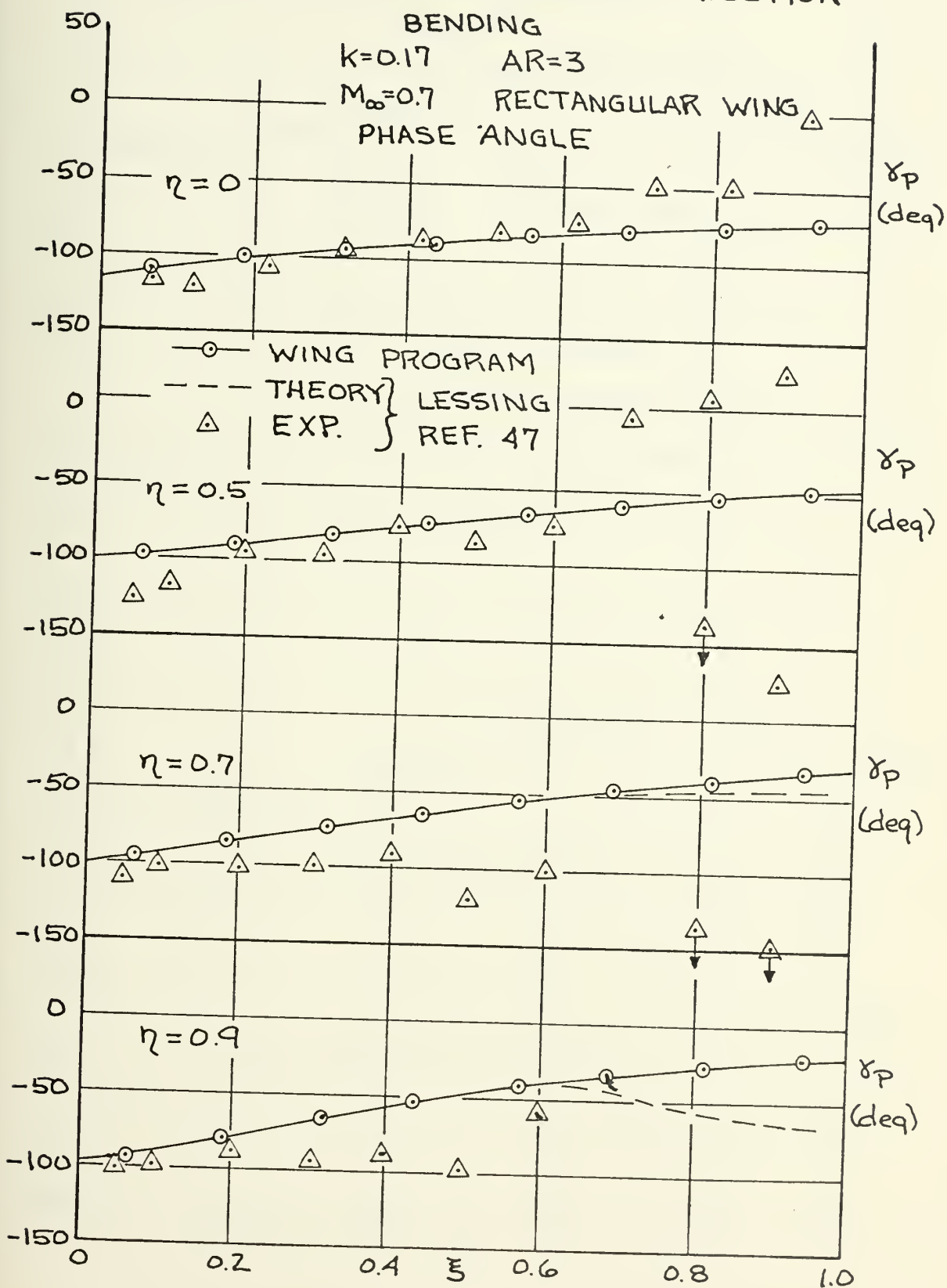




FIGURE 17c  
SPANWISE LOADING  
BENDING

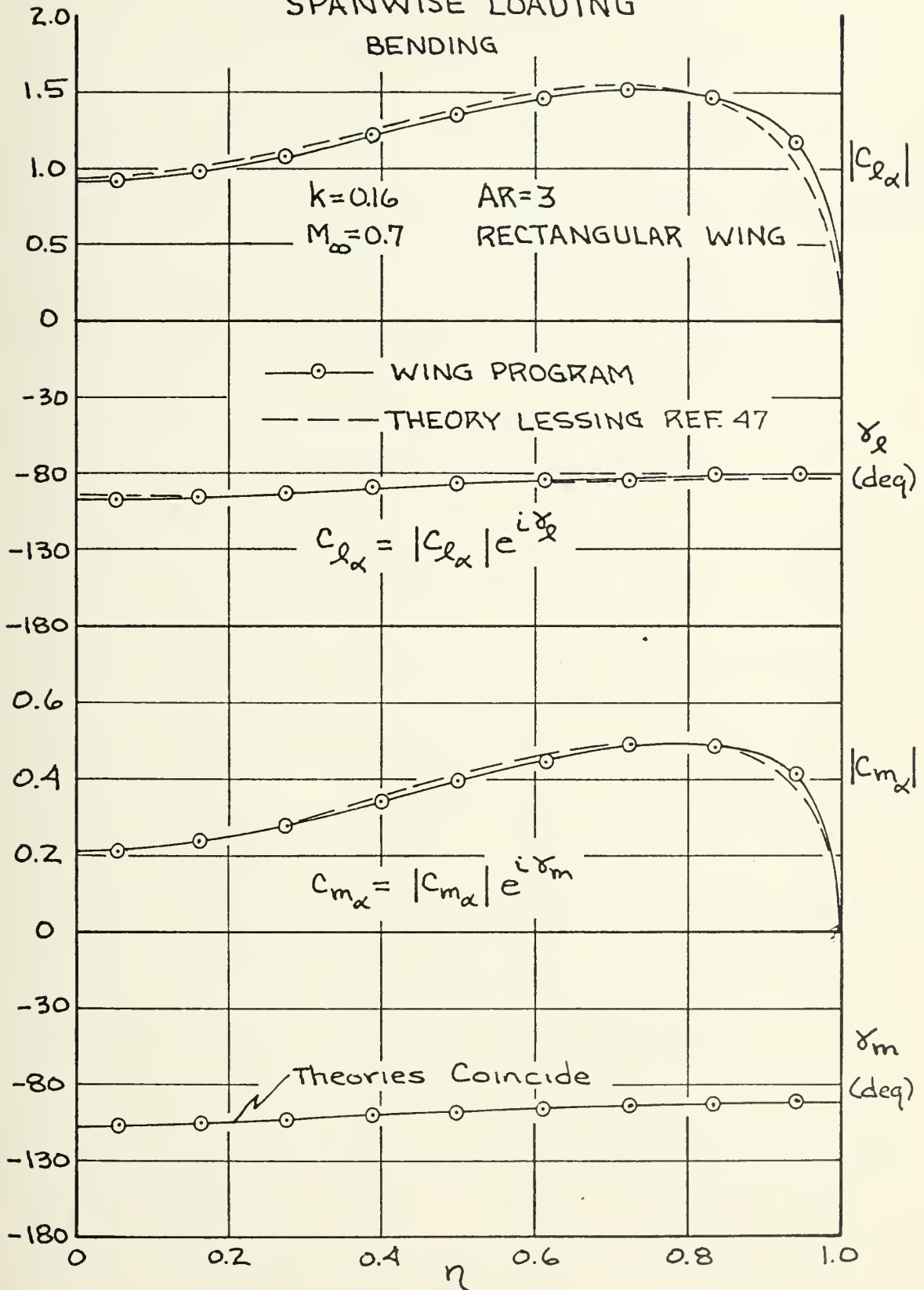




FIGURE 18  
SPANWISE LOADING

BENDING

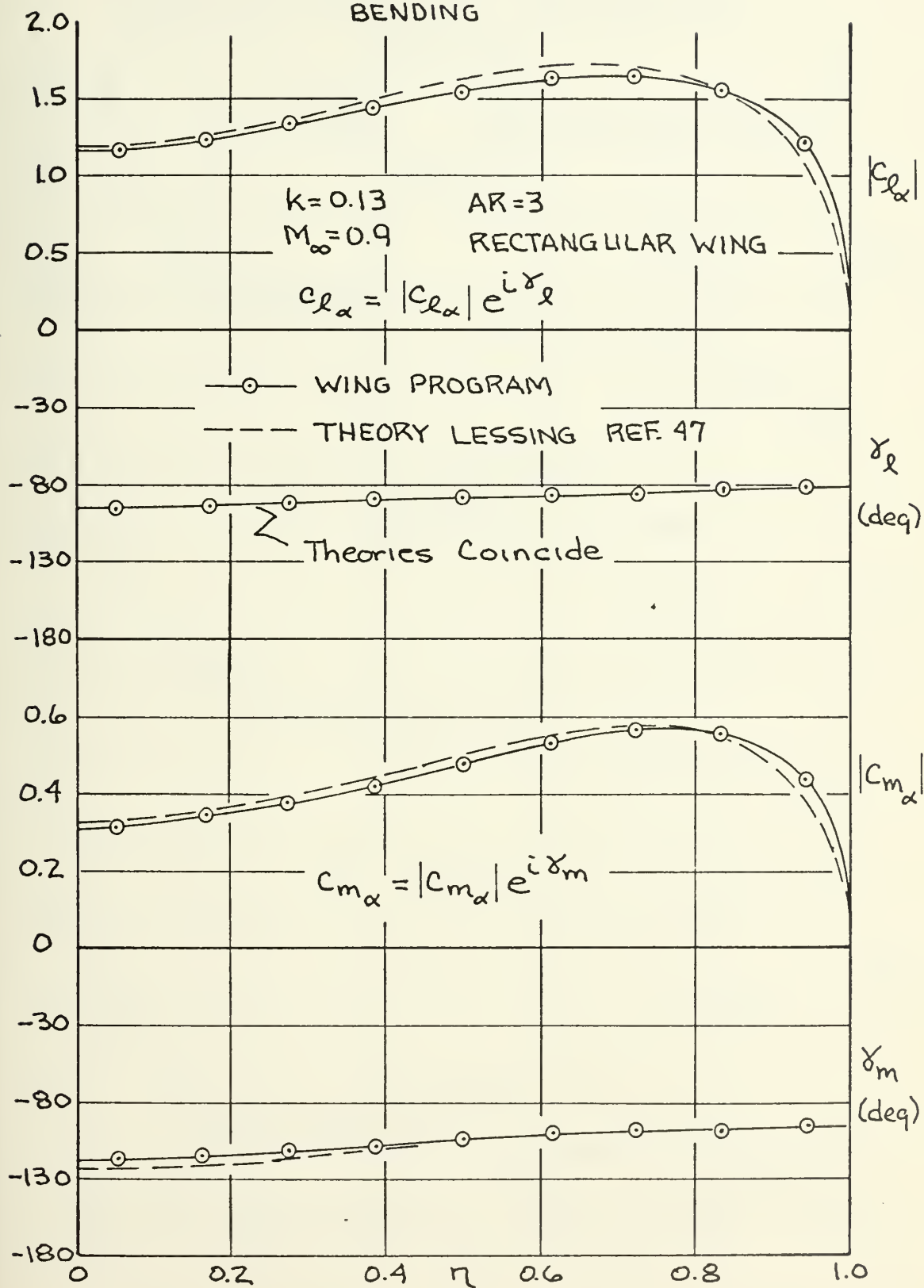






FIGURE 19a  
CHORDWISE PRESSURE DISTRIBUTION  
PITCHING

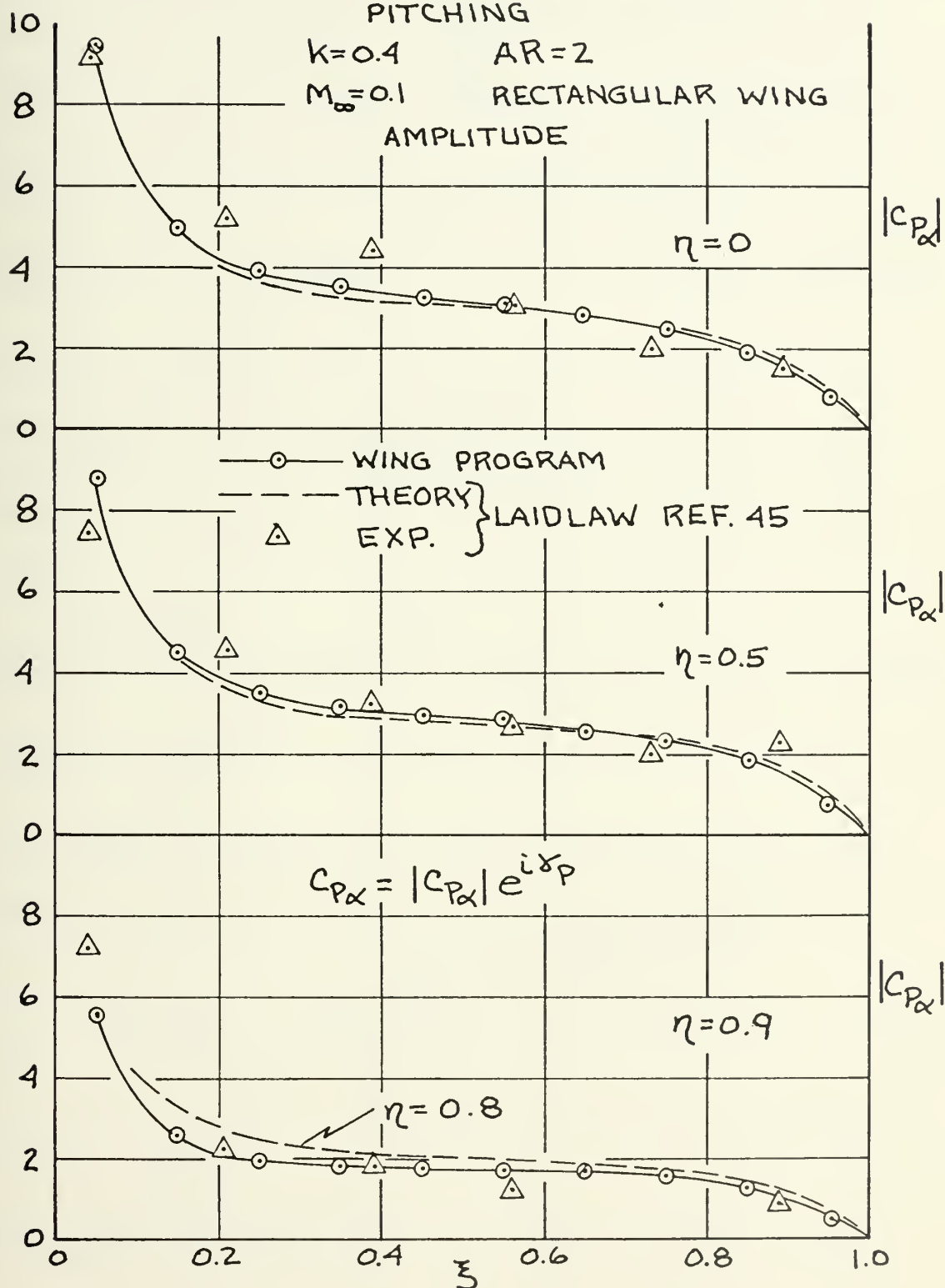




FIGURE 19b  
CHORDWISE PRESSURE DISTRIBUTION  
PITCHING

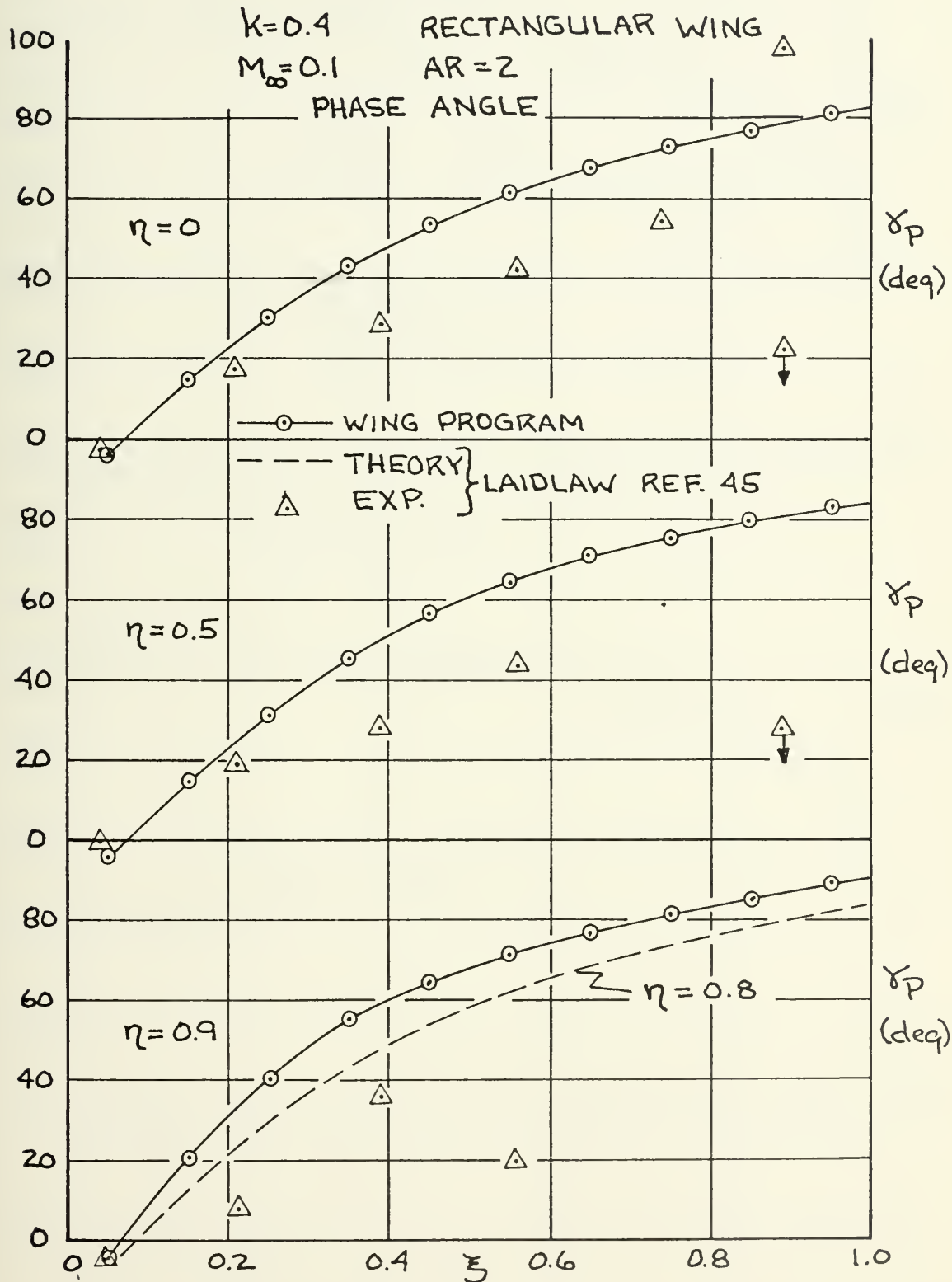




FIGURE 19c  
SPANWISE LOADING  
PITCHING

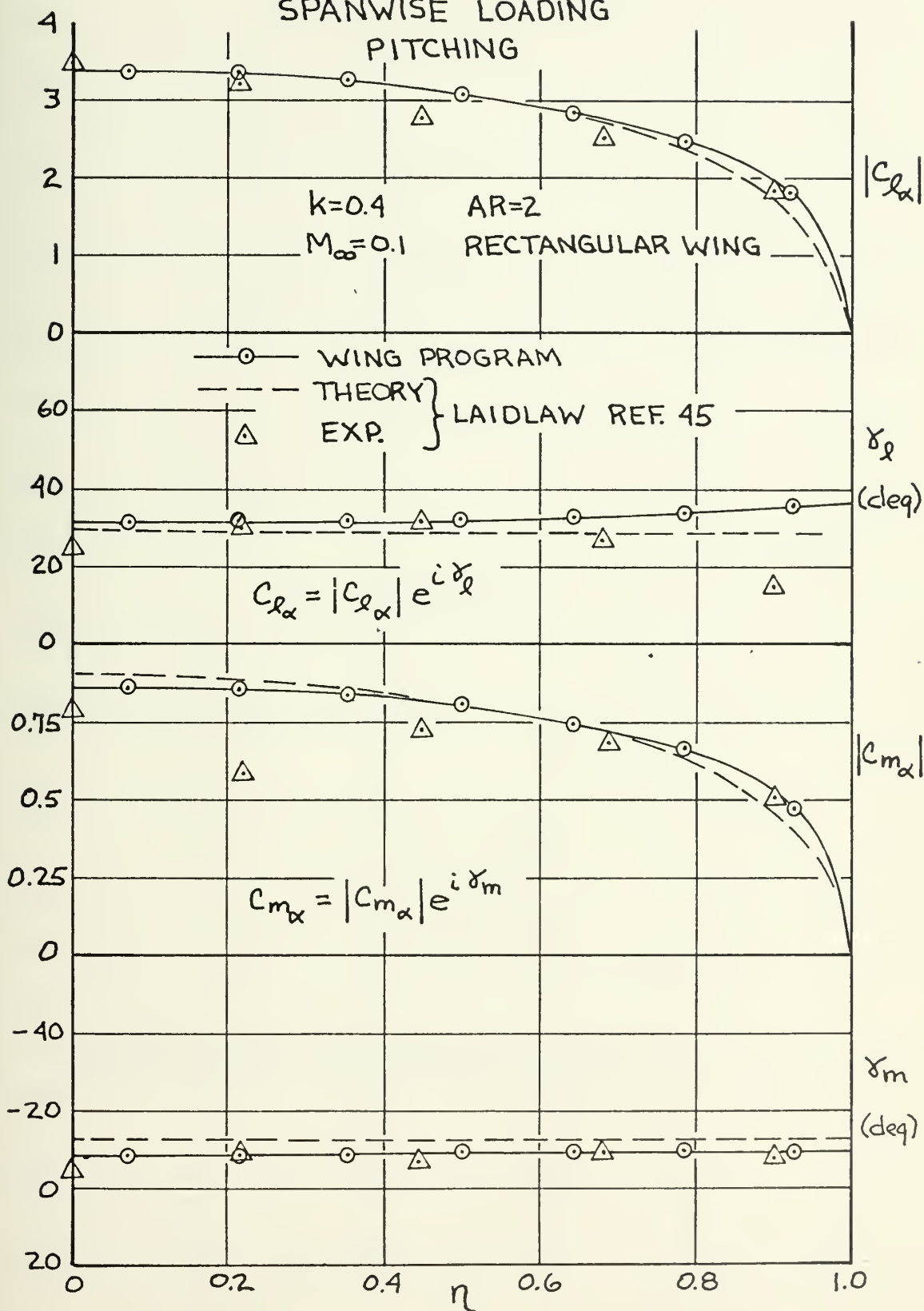




FIGURE 20  
SPANWISE LOADING

PLUNGING

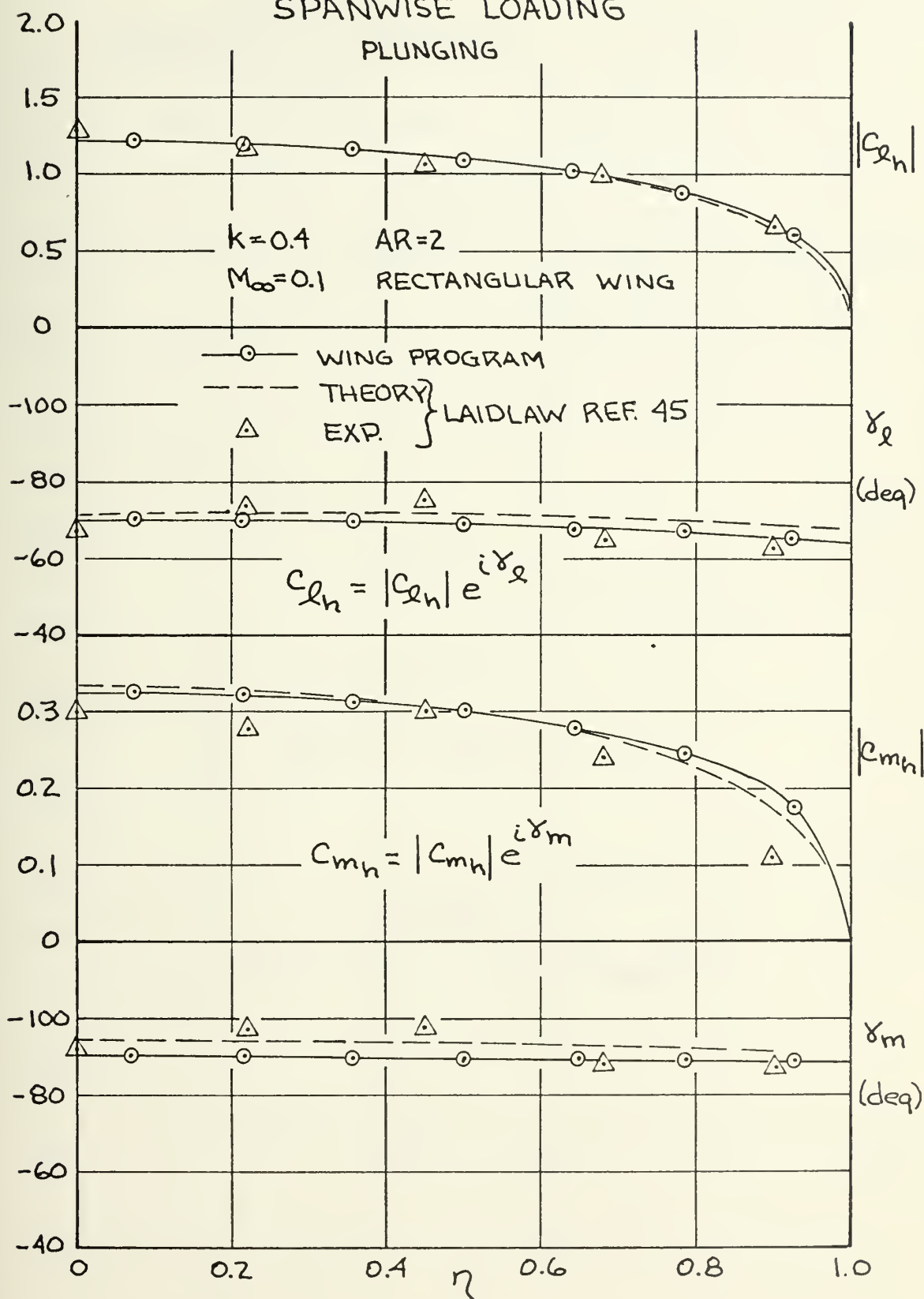
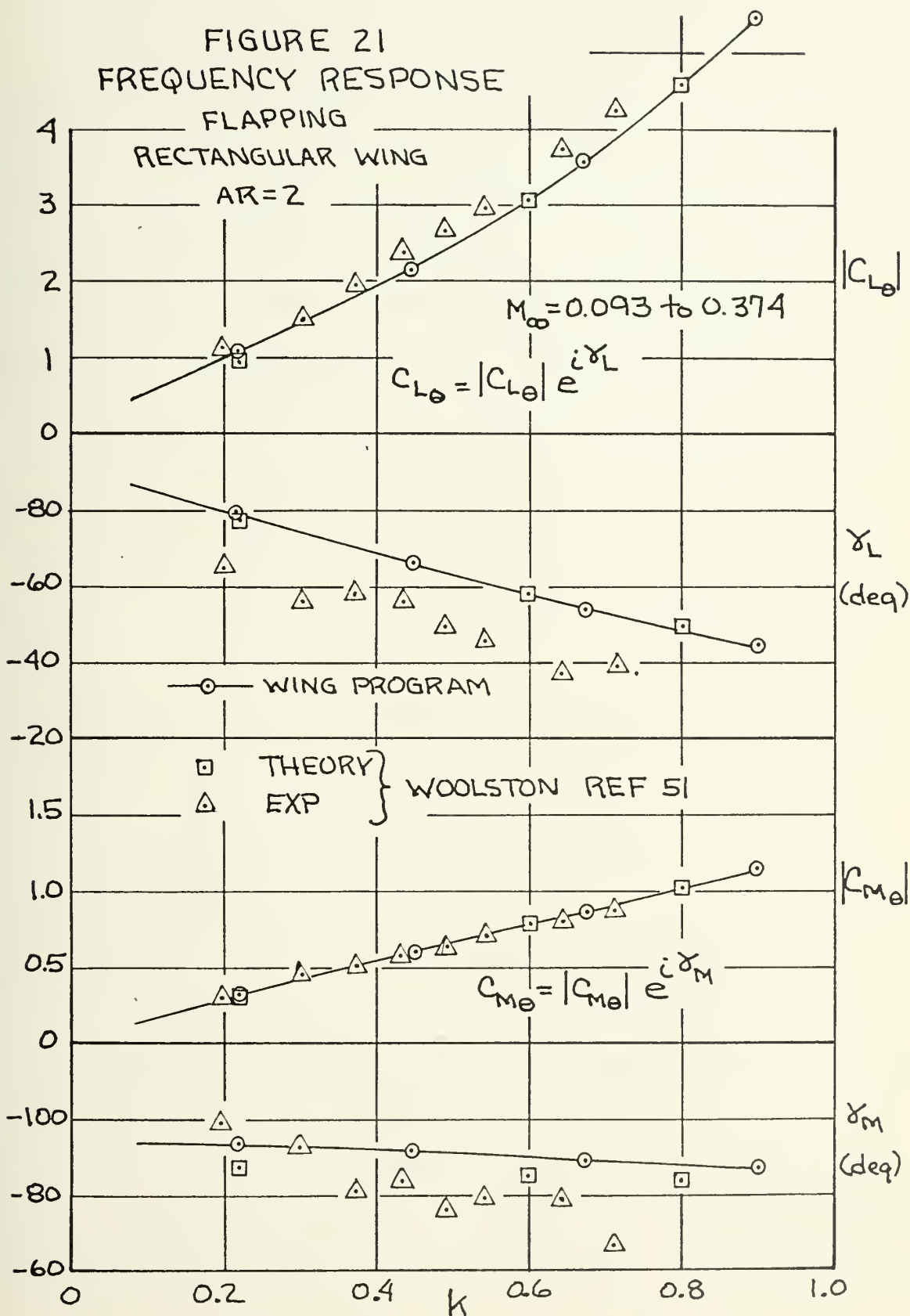






FIGURE 21  
FREQUENCY RESPONSE





## 2. Convergence

Figures 22 through 24 present spanwise loading for three different wing planforms as a function of the singularity grid density in order to show convergence of the wing program. Three types of motion are considered, with wing grids numbering from 25 to 100 points. Figure 25 shows convergence of the wing program for the steady case on an aspect ratio six rectangular wing. This wing planform is used in the basic reference for the wing/body analysis in steady flow. The ordinate of these graphs has been greatly expanded to permit a good evaluation of convergence.

All of the examples are seen to converge at about the same rate. At 50 control points on the wing the maximum deviation is less than four per cent. At 60 or more points the results are virtually coincident. The shape of the control box would appear not to be a factor, since varying the grids on the individual wings of Figures 22 through 25 also varies the shape of the individual boxes. However, it would seem prudent to maintain the control boxes at reasonable aspect ratios (less than about ten) to assure valid results. Another restriction on the wing grid size is the requirement to integrate the pressure loading to obtain section and wing coefficients. A minimum of six points in either the chordwise or spanwise directions was found necessary to adequately define the loading distribution for the integration subroutines. However, the basic requirement for



60 or more points in the wing grid makes this latter restriction a factor only for higher aspect ratio wings.

A second type of restriction on the wing grid size is caused by the accuracy of the inversion method of subroutine COMAT. Solution of the downwash matrix equation is accomplished by the Gauss-Jordan method employing total pivoting. With the relative magnitudes of the kernel function matrix elements occurring in this type of analysis, the inversion process starts to lose accuracy with a system of equations or order greater than about 110. Computational accuracy was verified by substituting the velocity potential vector solution into the downwash matrix equation, and obtaining a downwash vector to compare with the original input. Checks of the solution for grid densities up to 150 points were made, for various wing/flow conditions, with consistent loss of accuracy. Thus, the program has been limited to wing grids of 100 control points or less to ensure accuracy. This also limits the aspect ratio of the wings that may be analyzed; however, for the purposes of this report, aspect ratios of six or less were well within the capability of the program. If added capability were required, a more sophisticated inversion routine would have to be developed.



FIGURE 22a  
CONVERGENCE - PITCHING

$k=0.4$

$AR=2$

$M_\infty=0.1$

RECTANGULAR WING

AMPLITUDE

$$c_{l_\alpha} = |c_{l_\alpha}| e^{i\gamma_l}$$

$|c_{l_\alpha}|$

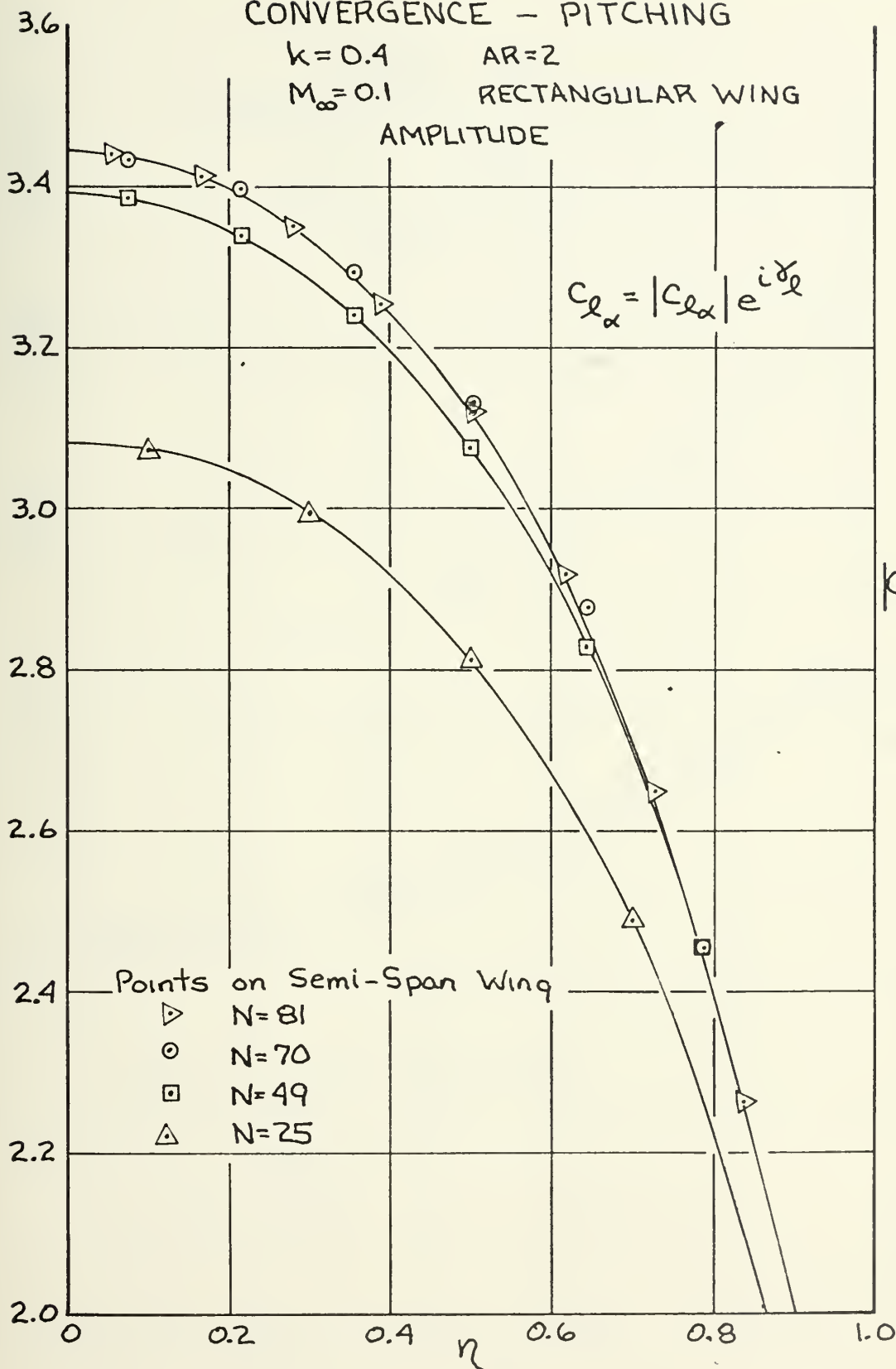






FIGURE 22b  
CONVERGENCE - PITCHING

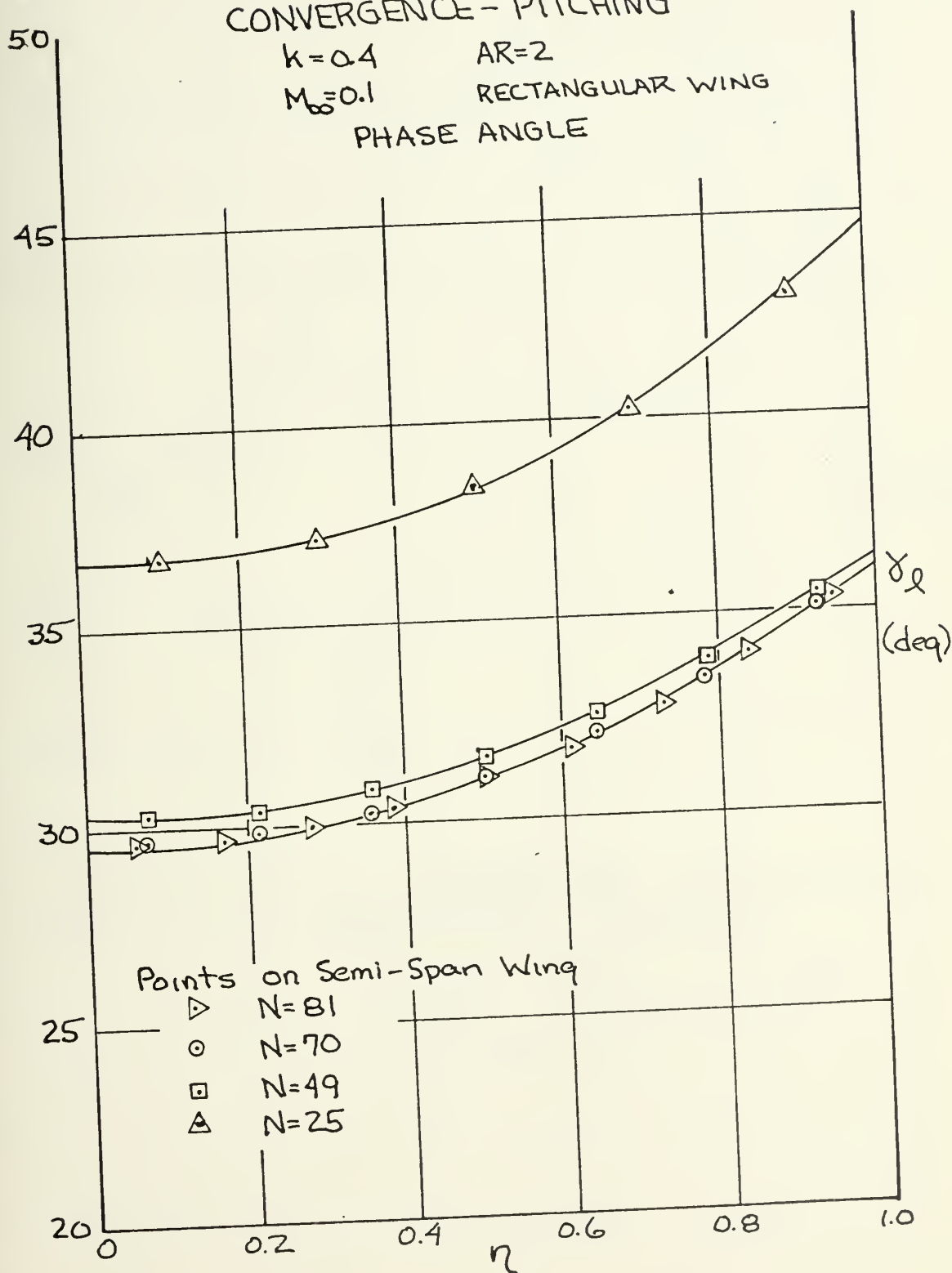
$k=0.4$

$AR=2$

$M_\infty=0.1$

RECTANGULAR WING

PHASE ANGLE





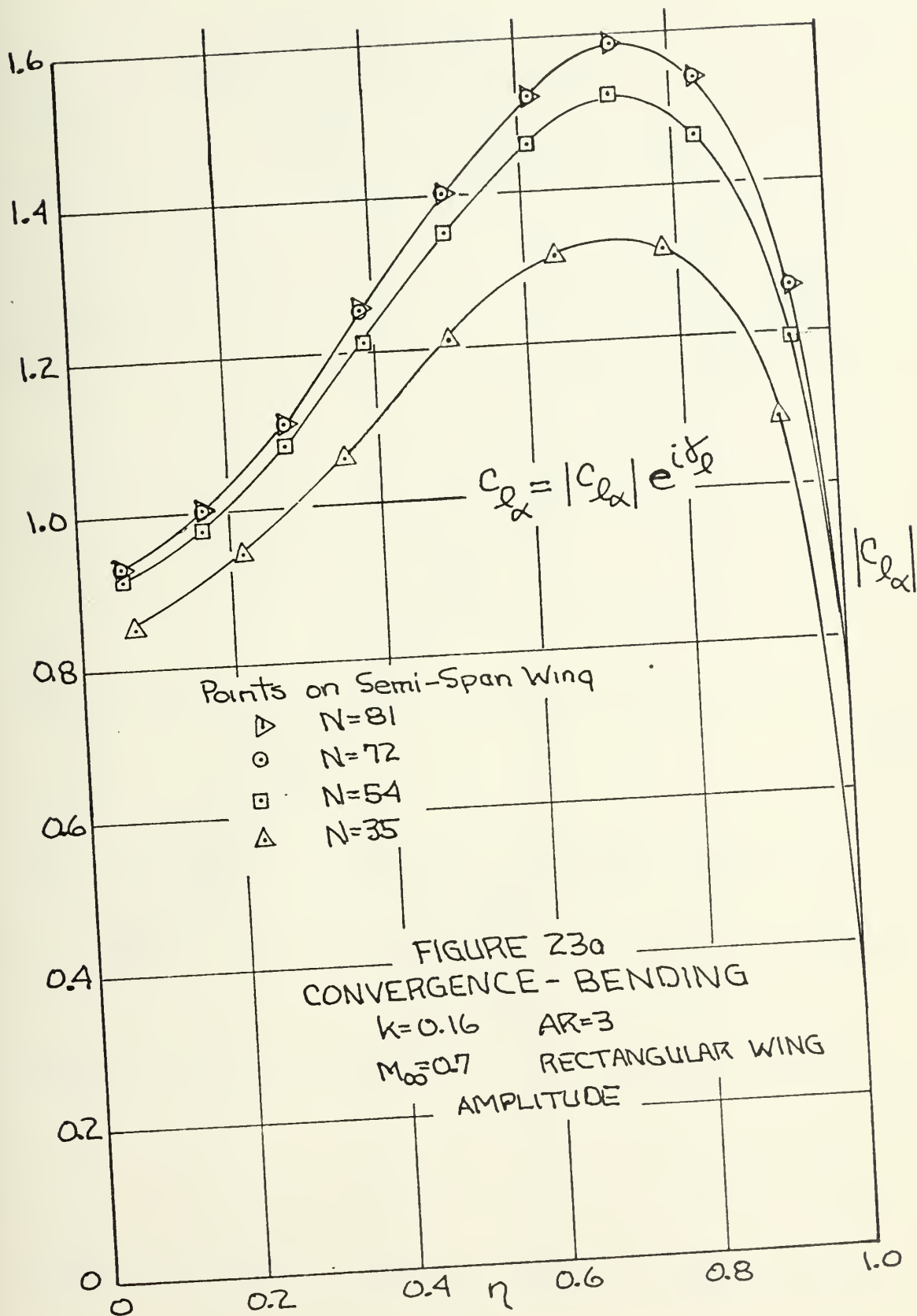




FIGURE 23b  
CONVERGENCE-BENDING

$k=0.16$   $AR=3$   
 $M_\infty=0.7$  RECTANGULAR WING  
PHASE ANGLE

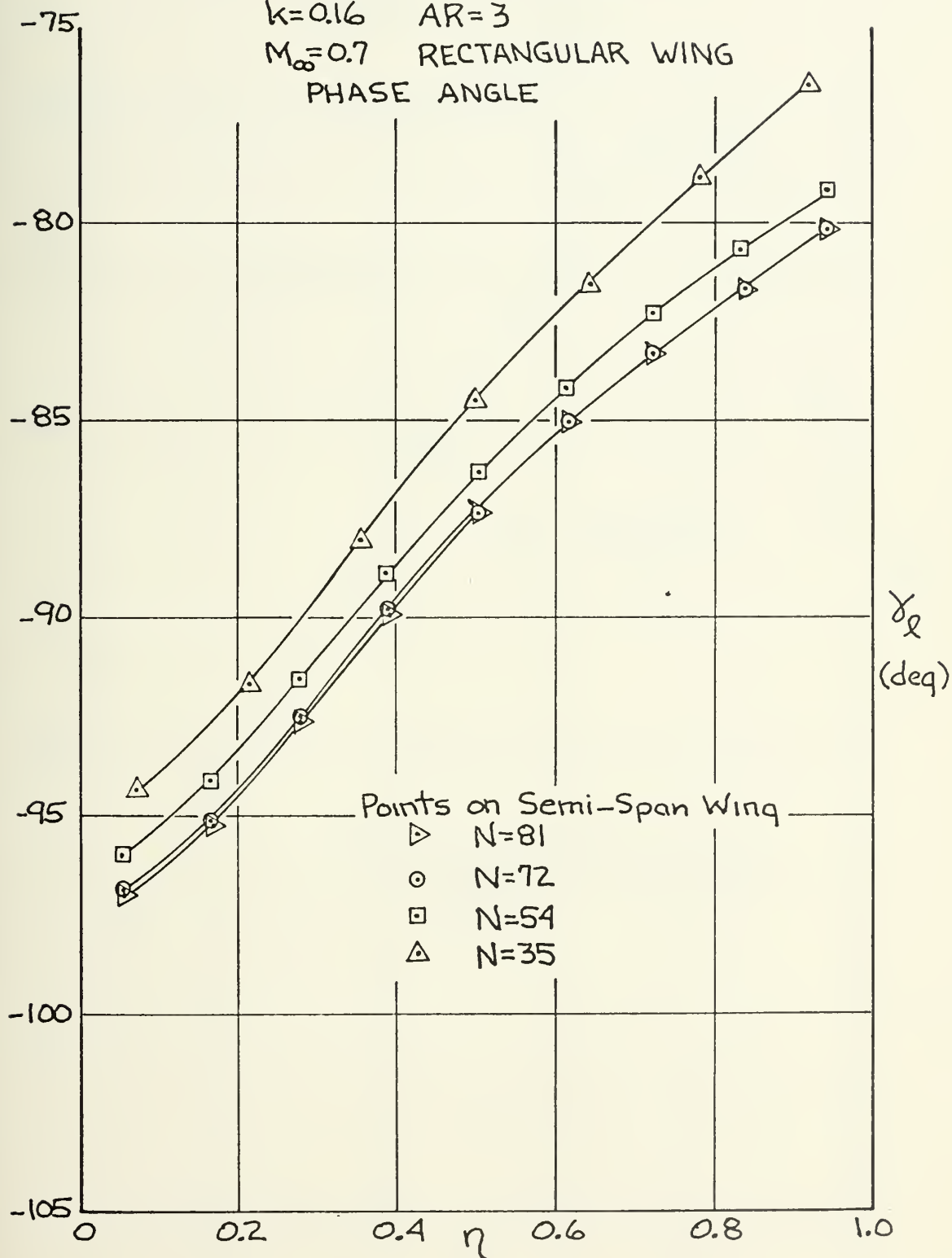




FIGURE 24a  
CONVERGENCE - FLAPPING

$k=0.4$      $AR=3$   
 $M_\infty=0.2$      $\alpha=45^\circ$   
 $\lambda=0.5$

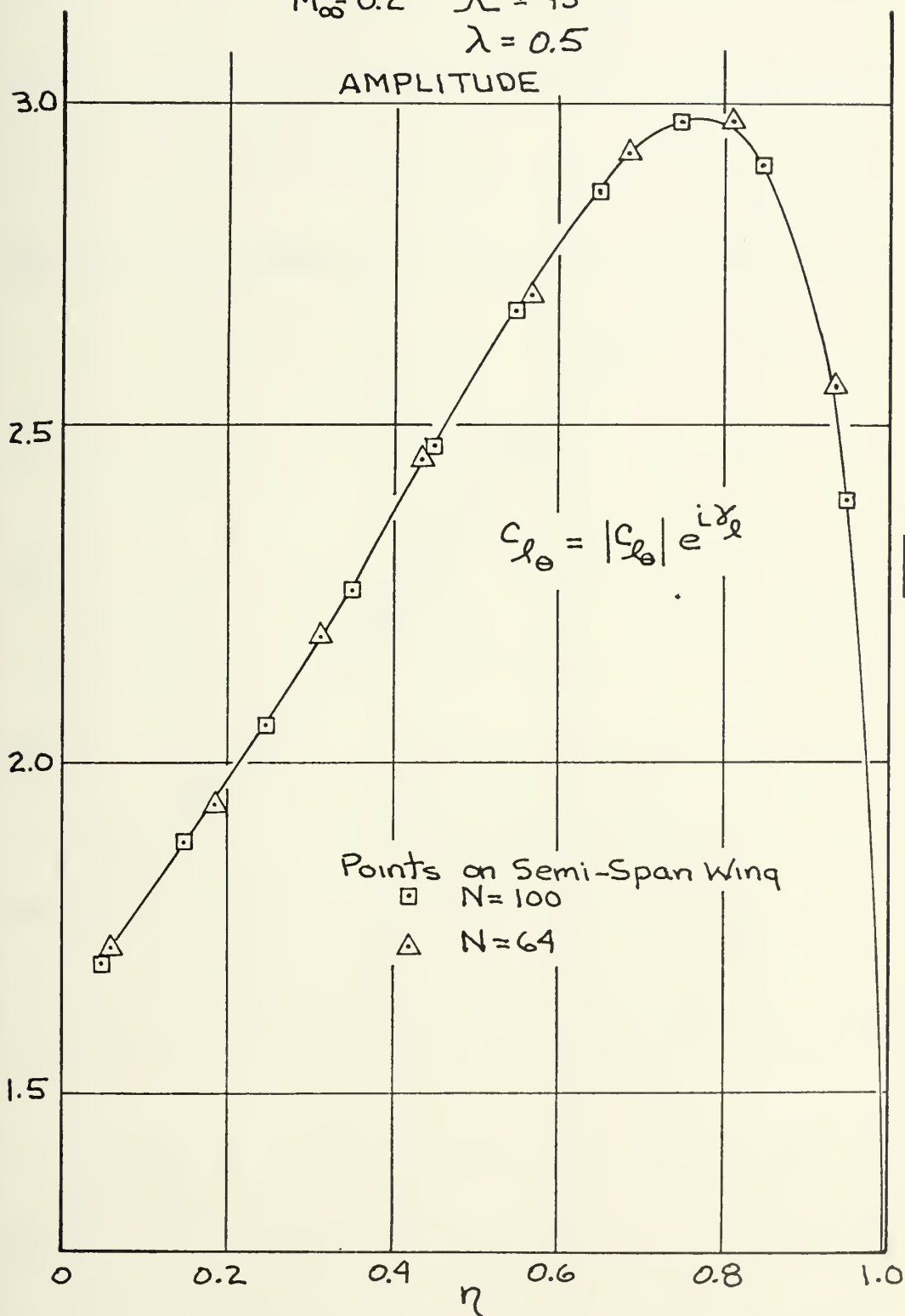






FIGURE 24b  
CONVERGENCE-FLAPPING

$k=0.4$      $AR=3$   
 $M_\infty=0.2$      $\angle=45^\circ$   
 $\lambda=0.5$

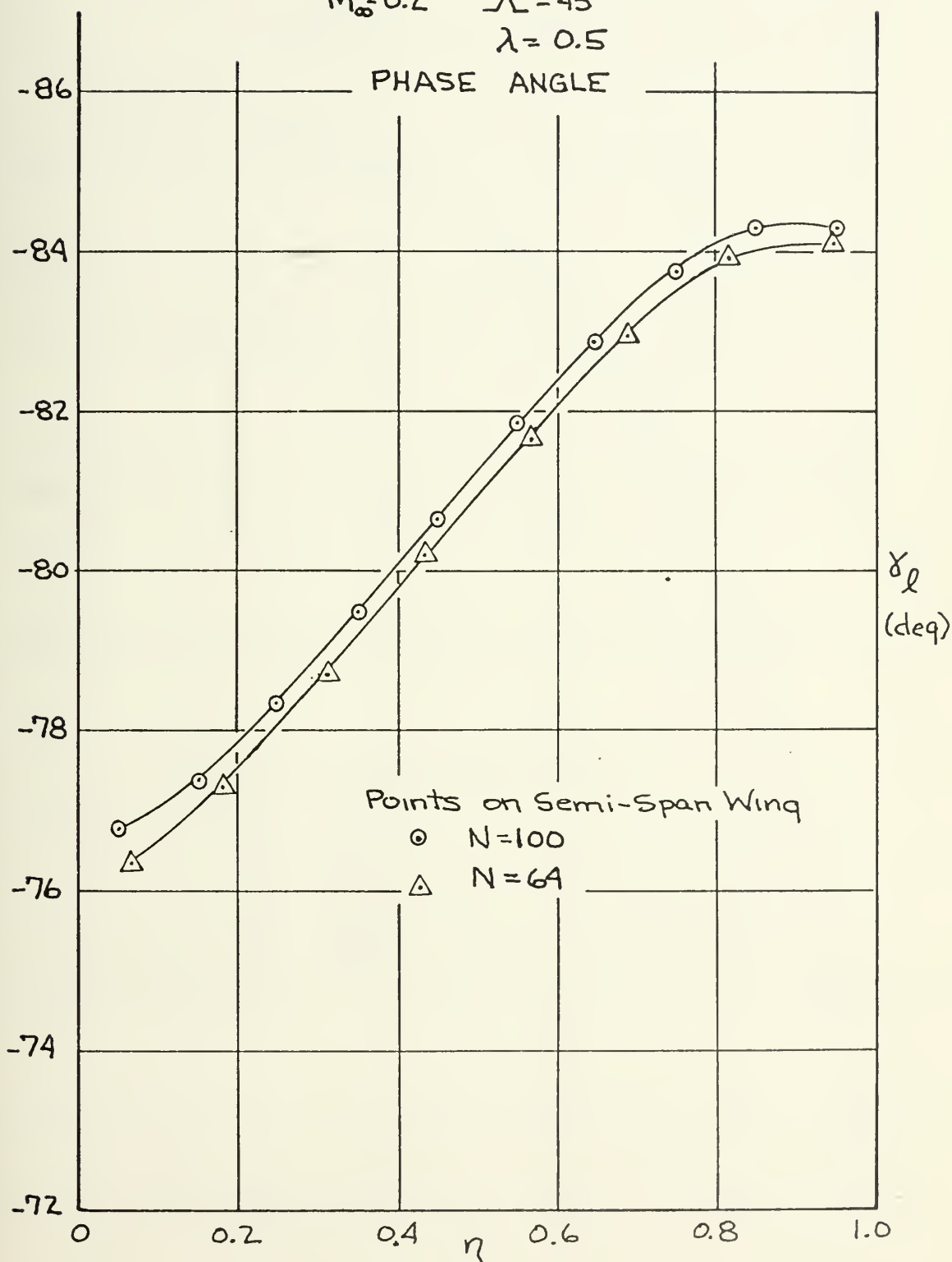


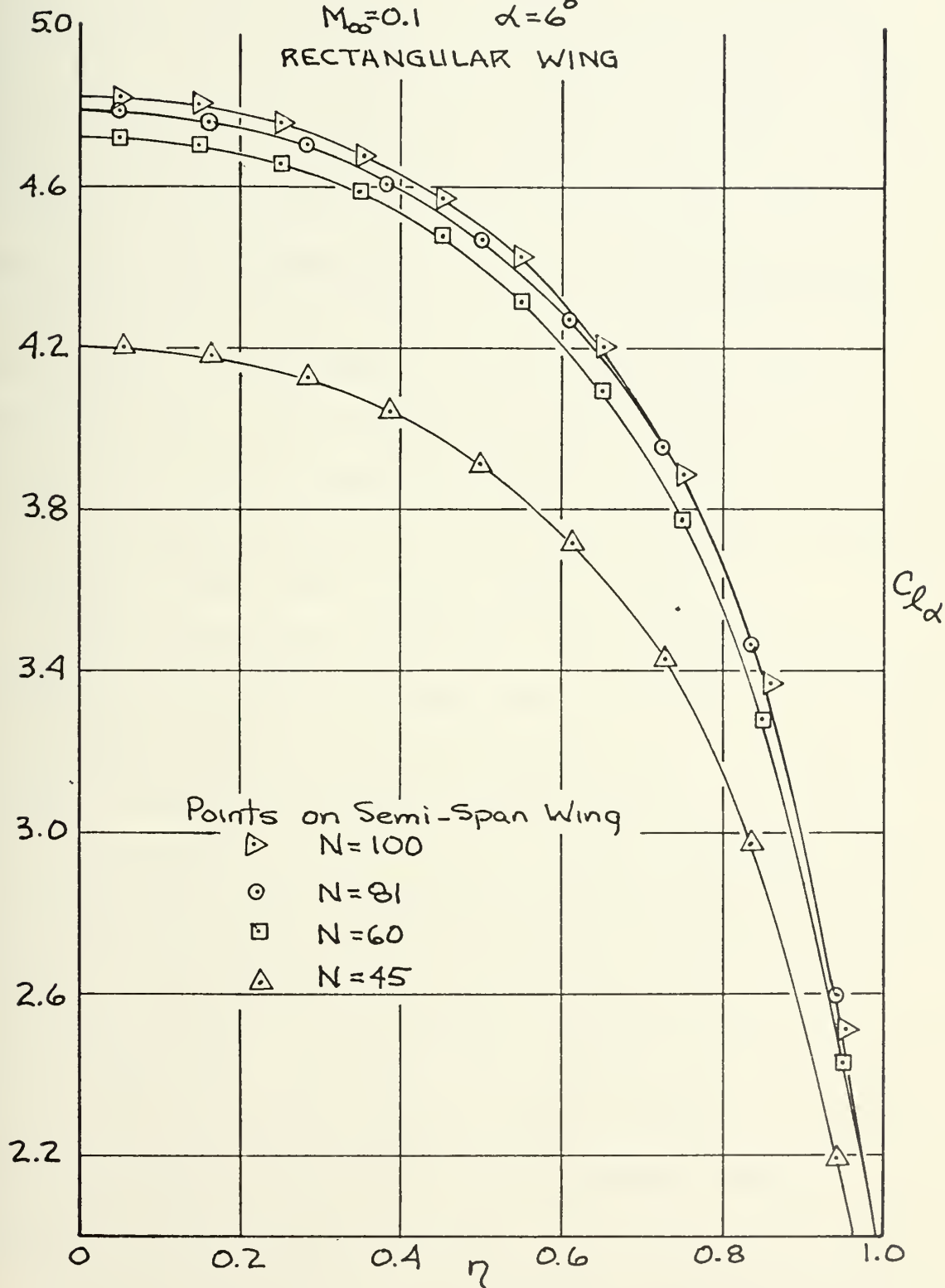


FIGURE 25  
CONVERGENCE - STEADY ANGLE OF ATTACK

$k=0$   $AR=6$

$M_\infty=0.1$   $\alpha=6^\circ$

RECTANGULAR WING





### 3. Wake Effect

Figures 26 and 27 summarize the effect of the finite wake length considered in the singularity grid network as discussed in Section IV.A.2. Seven configurations of wing/flow geometries were analyzed, covering the range of conditions considered in this paper. Wake effects were included to a maximum distance of ten root chord lengths downstream from the wing trailing edge. In all cases, wing loading had converged to within one per cent of amplitude and one-half degree of phase angle by four root chord lengths of effective wake. This correlates with Haviland's work [8], in which he reported that the effect of the wake on the wing, for a rectangular planform in the steady case, was determined to within one per cent in five chord lengths.

Figure 26 presents a specific case of wing coefficient variation with effective wake length. The maximum deviation of the wing coefficients, with respect to an effective wake length of four root chords, is shown in Figure 27. From the latter figure, it can be seen that the near wake (within one root chord length of the trailing edge) has a very great effect on the wing loading. The wake influence then dies out quite rapidly as the effective termination point is moved downstream. Therefore, the finite wake, taken into account in determining the aerodynamic loading on the wing, need only extend a relatively short distance downstream in order to obtain accurate results.

In the wing analysis of this paper, an effective wake of four root chord lengths was used. The wing program will,



however, incorporate any effective wake length desired by varying an input parameter (Appendix B). With a wing grid of 100 control points, four root chord lengths of effective wake requires a wake grid which varies from 400 singularities for a rectangular wing, to approximately 1100 singularities for a wing with a taper ratio of one-fourth. The increased number of wake singularities are required for a tapered wing because of the decreasing chordwise dimension of the control boxes towards the wing tip. Thus a greater number of singularities are required, at a spanwise station outboard of the root, to extend four root chord lengths into the wake, than are required for a rectangular wing. The large number of wake singularities pose no computational problem, since the effect of the wake is incorporated prior to the solution of the kernel function matrix equation, as discussed in Section IV.A.2.





FIGURE 26  
WAKE EFFECT - EXAMPLE  
BENDING

$K=0.16$

$AR=3$

$M_\infty=0.7$

RECTANGULAR WING

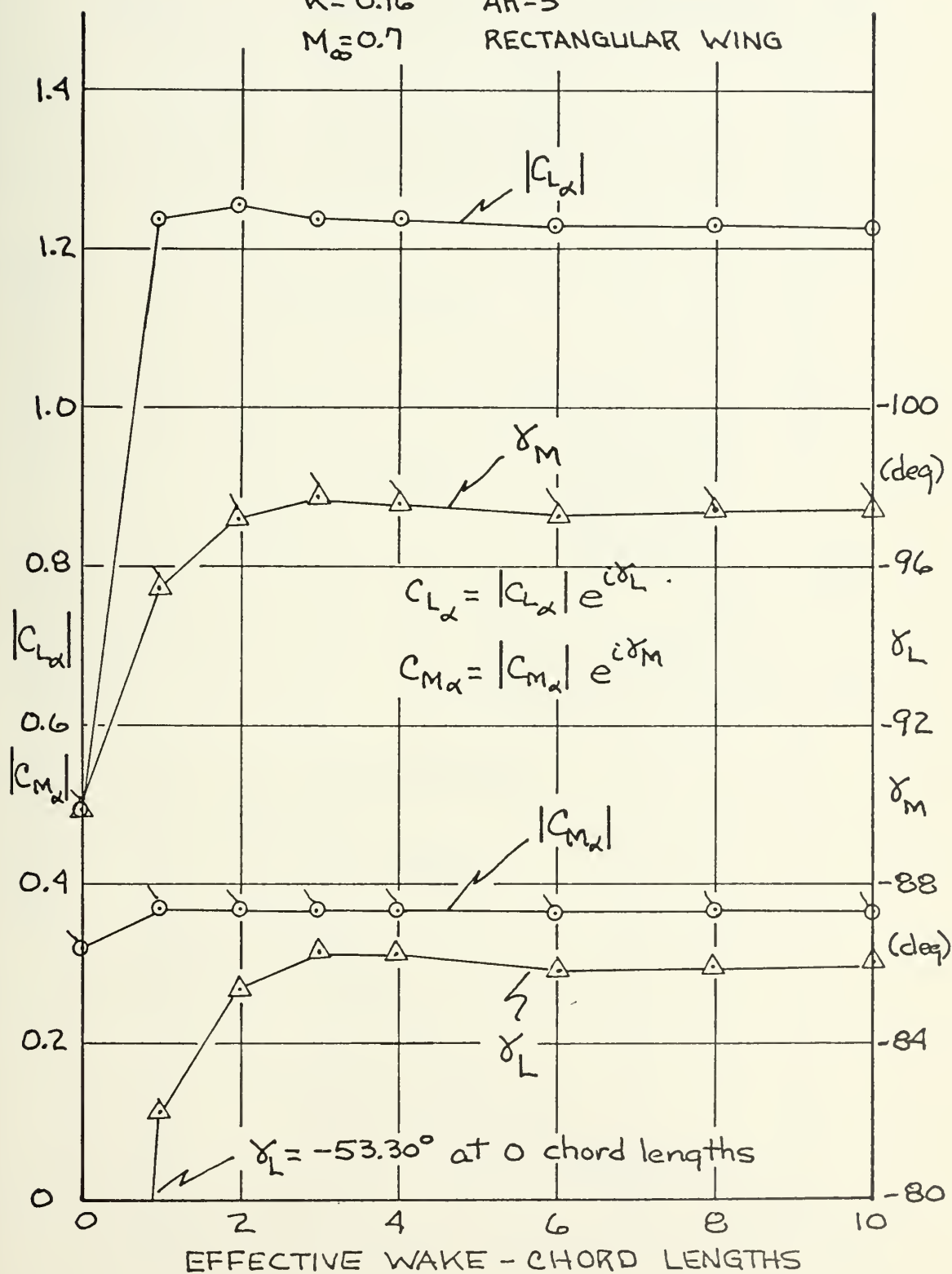
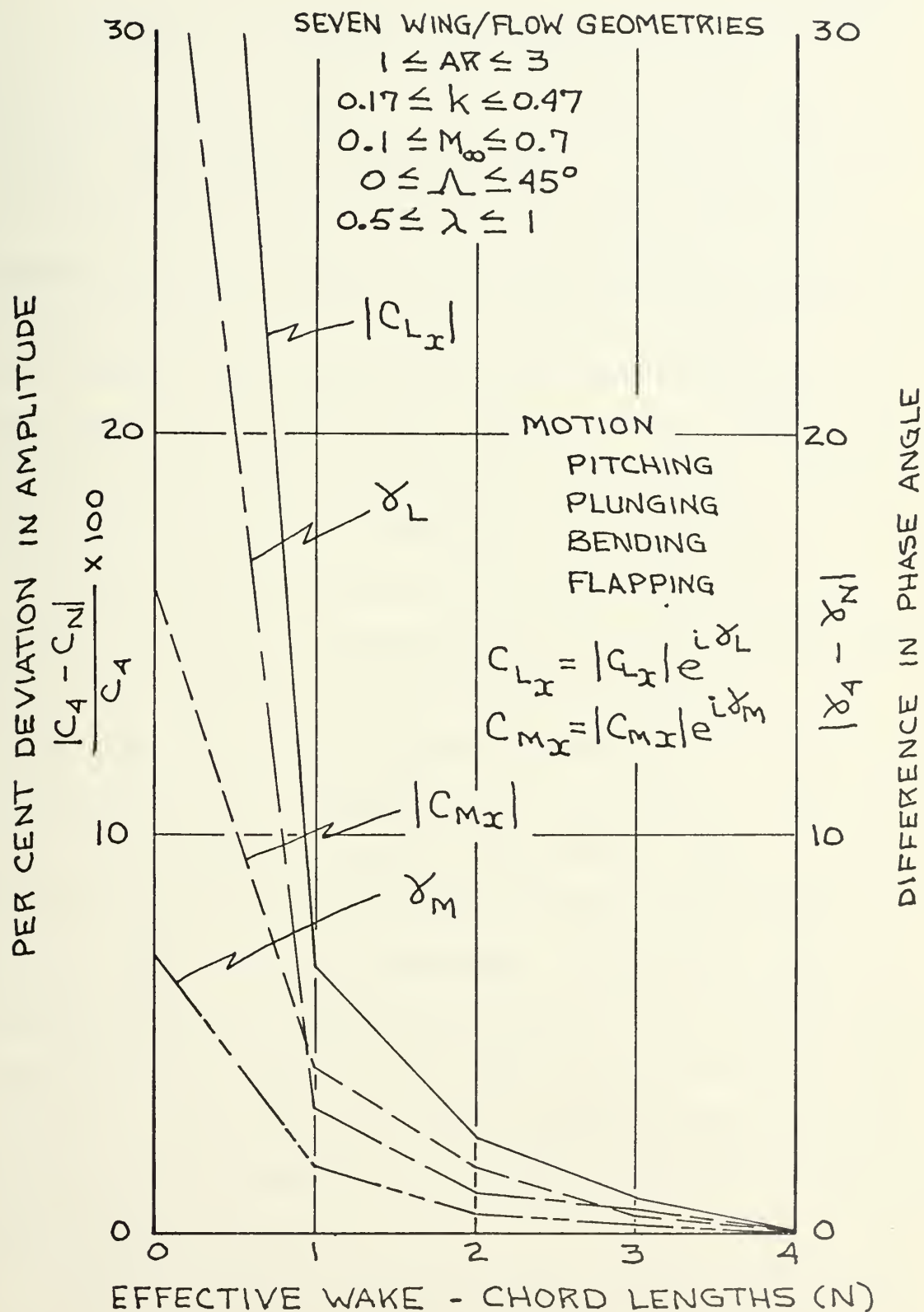




FIGURE 27  
WAKE EFFECT - MAXIMUM DEVIATION





## B. WING/BODY ANALYSIS

### 1. Comparison with Steady Analyses

A thorough literature search was made in an attempt to find previous theoretical or experimental work, in the nonsteady lifting surface field, with which to compare and validate the wing/body program results. Unfortunately, no such effort which explicitly analyzed body interference effects on an oscillating wing's pressure distribution could be found. Rodden [38] includes some body interference effects in his doublet lattice method for analyzing nonplanar configurations, by extending the lifting surface elements onto the body surface near the wing-body intersection. However, the actual interference effects are not presented.

It was therefore necessary to compare the wing/body program results with data previously obtained in the steady field. The two latest works found were presented at the AGARD conference on Aero-dynamic Interference in 1970 by Kuchemann [52] and Labrujere [53]. Both analyzed an aspect ratio six rectangular wing at a six degree angle of attack midmounted on a cylindrical body of radius approximately equal to 20% of the wing semi-span. This configuration was also theoretically analyzed by Weber [40] and experimentally investigated by Körner [54]. Each of the theoretical analyses employed a combination of surface source singularities and vortex line distributions to construct a steady kernel function method solution.

Figure 28 compares the wing/body program results, for both the wing and wing/body combination, with results



obtained from the above investigations. The discrete potential element approach spanwise loadings are seen to compare almost exactly with the theoretical curves obtained by Weber, while the experimental data of Labrujere and Körner offer good correlation. The theoretical work of Labrujere overestimates the spanwise loading, especially in the case of the wing/body combination. The good agreement between these theoretical and experimental results and the wing/body program results provides a reasonable measure of confidence in the discrete potential element analysis of this type of nonplanar configuration.

Figure 29 indicates the convergence of the wing/body program as the number of control points on the quarter circumference of the body was increased from 72 to 108. This graph is a greatly expanded representation of the wing root area effects. Outboard of the 25% semi-span point, the three grid configurations gave essentially the same results shown in Figure 28. In each case, body and wing control panels were matched as closely as practical in size and shape, so that the body grid becomes in essence an extension of the wing network on the body surface. Small variations between wing and body panel size did not effect the wing pressure distribution; however, when wing and body grids were obviously mismatched results became inconsistent.

For all the data presented in this paper, the body grid extended from one chord length upstream of the wing leading edge to one chord downstream of the effective wake termination point. Extending the body grid somewhat further in





either direction produced no appreciable effect on the results. However, decreasing the length of the body grid, to the point where the wing/wake singularity grid extended beyond the body grid, caused the wing pressure distributions to become inconsistent. This effect held for both the steady and nonsteady cases. Therefore, it would seem that the body surface which effects the wing pressure distribution, as discussed in Section IV.B.3, is concentrated in this effective length between one wing chord upstream and downstream of the wing/wake grid. Further investigation of this effect, such as by increasing the effective wake and/or the body grid length with increased number of control points, was precluded due to the accuracy limitations of the matrix inversion routine discussed in Section VI.A.2.

In addition, wing body grids within this effective body length were limited in the number of control points which could be used for the same reason. It was, therefore, not possible to investigate configurations with body radii greater than about 20% of the wing semi-span. Future work with this method would definitely require an improved complex matrix inversion procedure to allow greater range in the wing/body analysis.

An indication of the effect of body size, in the steady case, is presented in Figure 30, where spanwise loadings are plotted, with a greatly expanded ordinate, for the wing previously considered in combination with bodies of three different radii. It can be seen that the interference



effect is large even for a relatively small body radius of five per cent of the wing semi-span. This is reasonable since the body is at zero angle of attack and is providing no lift carry-through, or reinforcement, for the wing. This effect for bodies of small radius is also shown by Kuchemann's results [52].



FIGURE 28  
STEADY WING/BODY SPANWISE LOADING

$$AR=6$$

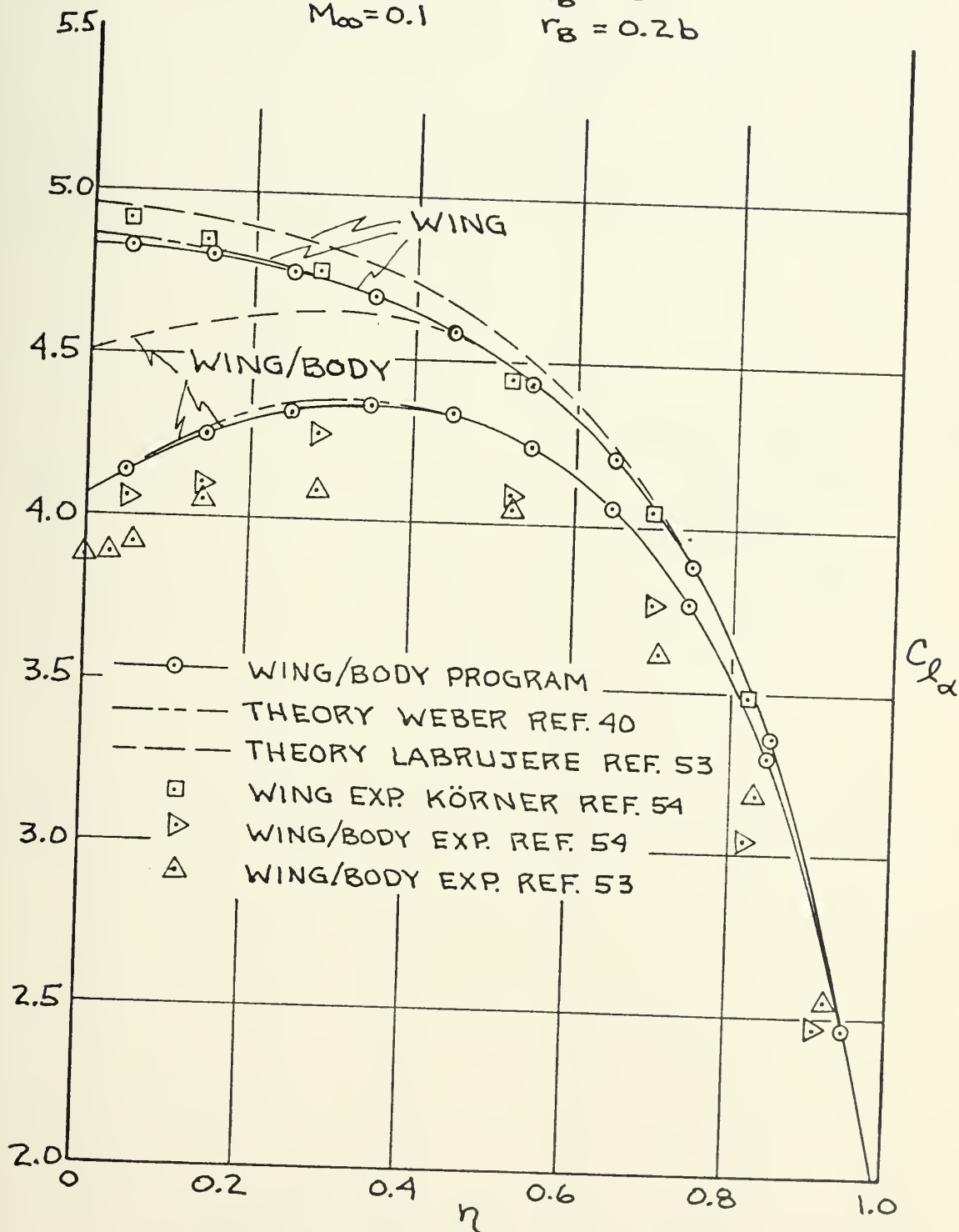
$$k=0$$

$$M_{\infty}=0.1$$

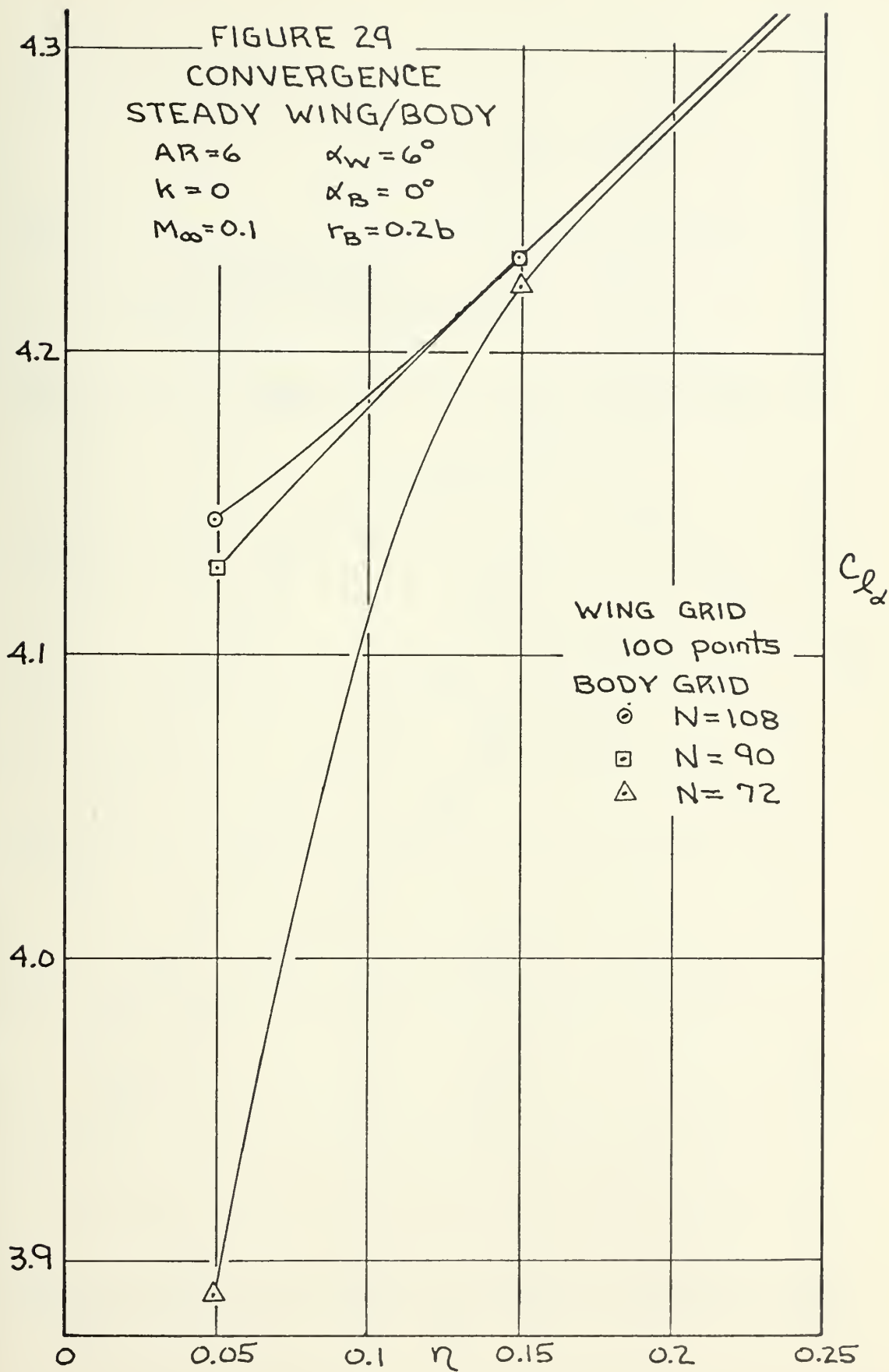
$$\alpha_w = 6^\circ$$

$$\alpha_B = 0^\circ$$

$$r_B = 0.2b$$

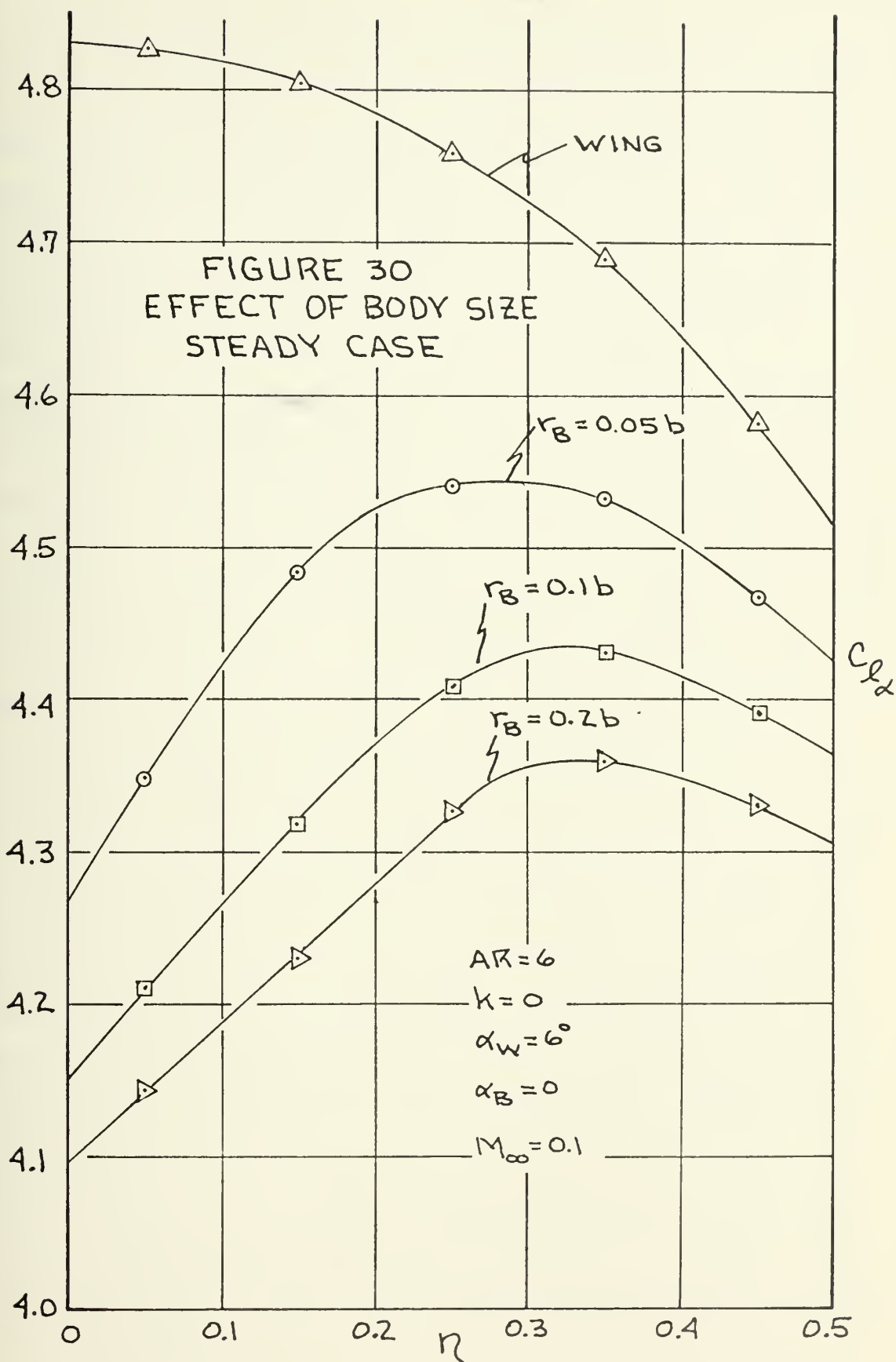














## 2. Extension to Nonsteady Interference

Investigation of wing/body interference for the non-steady case was conducted for two modes of wing motion: bending, as previously discussed; and torsional oscillations of the wing cantilevered at the root in an assumed first natural mode. In each case the coefficients were normalized with respect to the wing tip angle of attack. It should be noted that, of the types of motion normally considered in the nonsteady case, these are the only two valid for the wing/body configuration considered in this investigation.

Figure 31 presents the interference effects for the wing analyzed in Figure 16, cantilevered from a body with ten per cent semi-span radius. The decrease in sectional lift amplitude follows the steady case format, being greatest at the root and essentially disappearing as the wing tip is approached. The change in phase angle, while small, remains relatively constant until midspan and then slowly decreases. Figure 32 presents spanwise loading in the root area for wing/body configurations with body radii varying from five to twenty per cent wing semi-span. Again the trends are essentially the same as in the steady case, with a small but relatively constant phase angle difference. Wing/body interference for the torsional vibration case, with body radius equal to 20% of the wing semi-span is shown in Figure 33. These interference effects in the torsional loading follow the same trends as for the nonsteady bending mode, as well as the steady case.



The results of the wing/body program show that nonsteady interference occurs in the same way and via the same mechanism as in the steady case. Interference is greatest in the root area, decreasing towards the wing tip. The difference between the steady and nonsteady cases comes from the type of wing loading with which the body interferes. For a wing at a steady angle of attack, the wing loading is greatest in the root area, and, therefore, the interference is of relatively large magnitude. In the nonsteady case, the wing loading is smaller in the root area (since the wing is cantilevered from the body and has no motion at the root) and increases towards the tip, as the wing motion amplitude increases. Therefore, the interference effects, concentrated towards the root area, are of smaller relative magnitude for nonsteady motion, as compared to the general steady case.



FIGURE 31a  
UNSTEADY WING/BODY SPANWISE LOADING  
WING BENDING

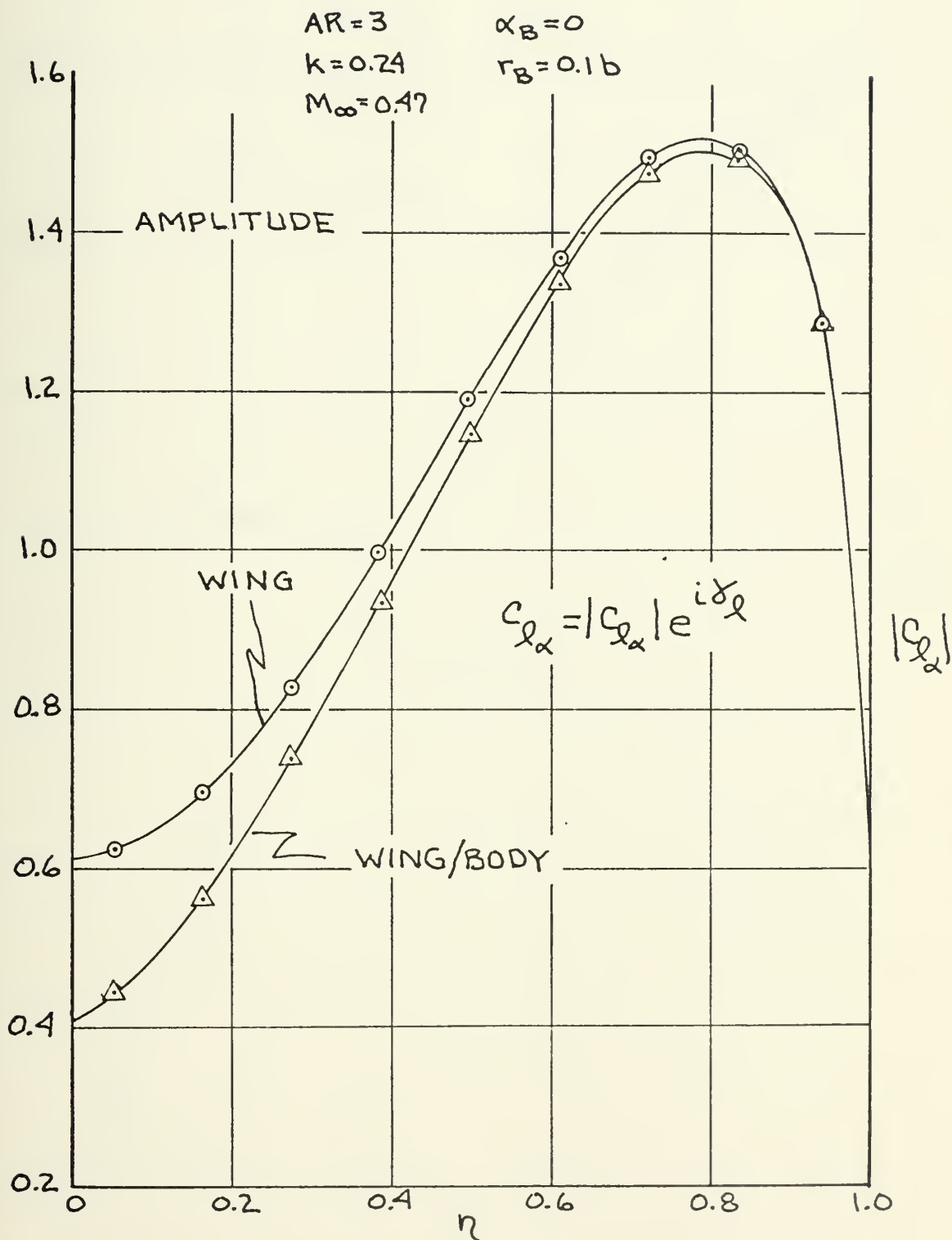






FIGURE 31b  
UNSTEADY WING/BODY SPANWISE LOADING  
WING BENDING

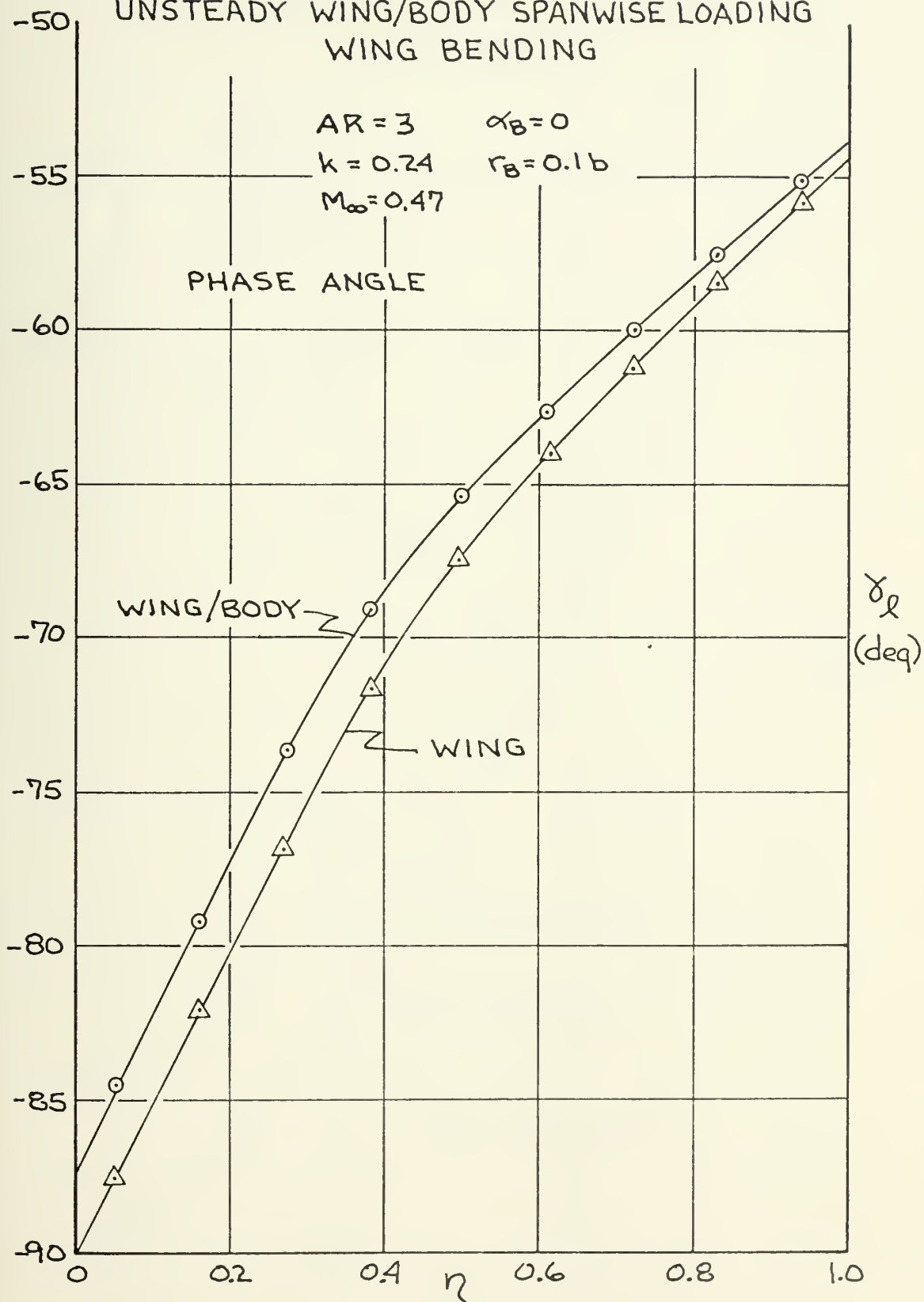




FIGURE 32a

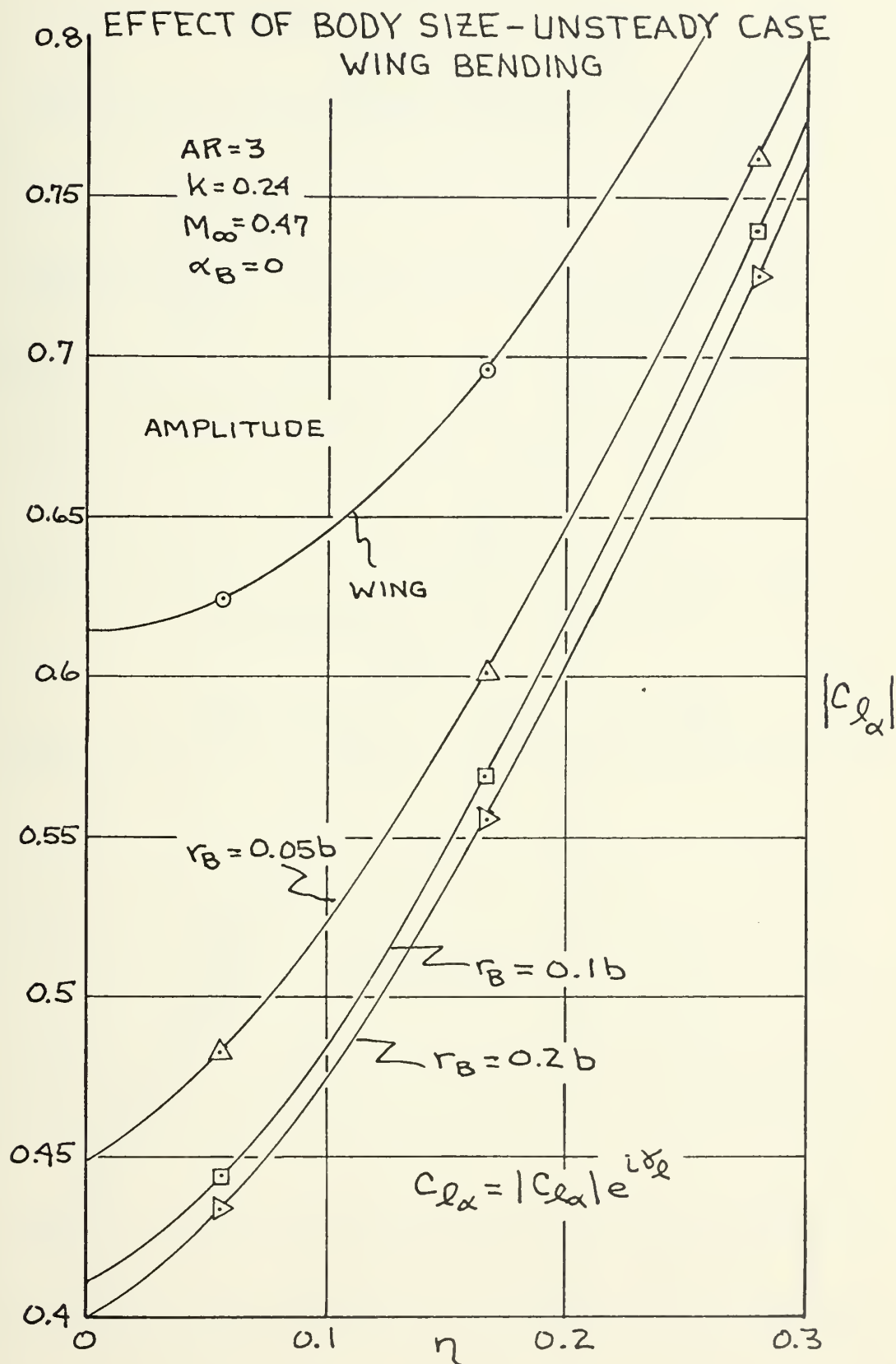




FIGURE 32b  
EFFECT OF BODY SIZE  
UNSTEADY CASE  
WING BENDING

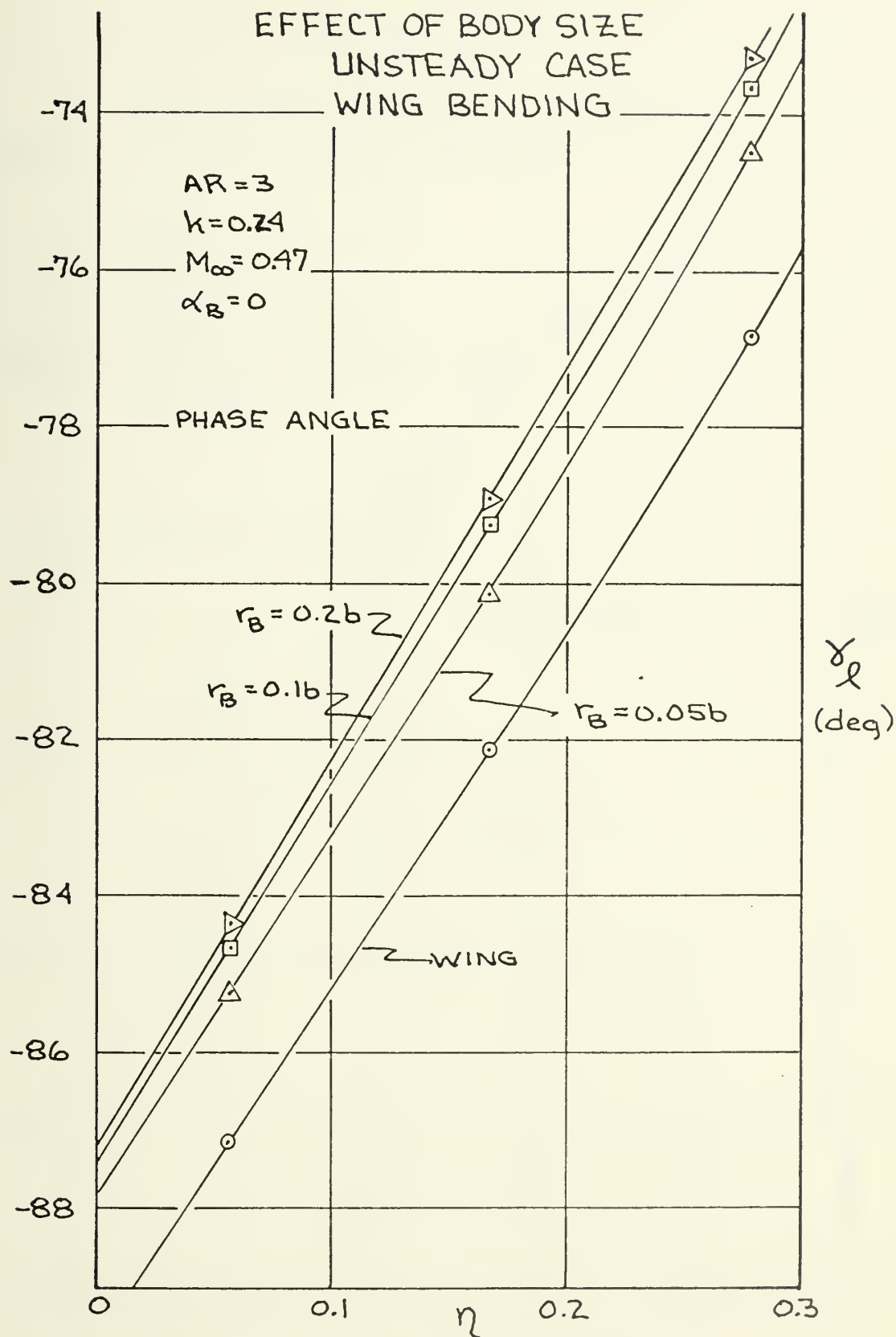
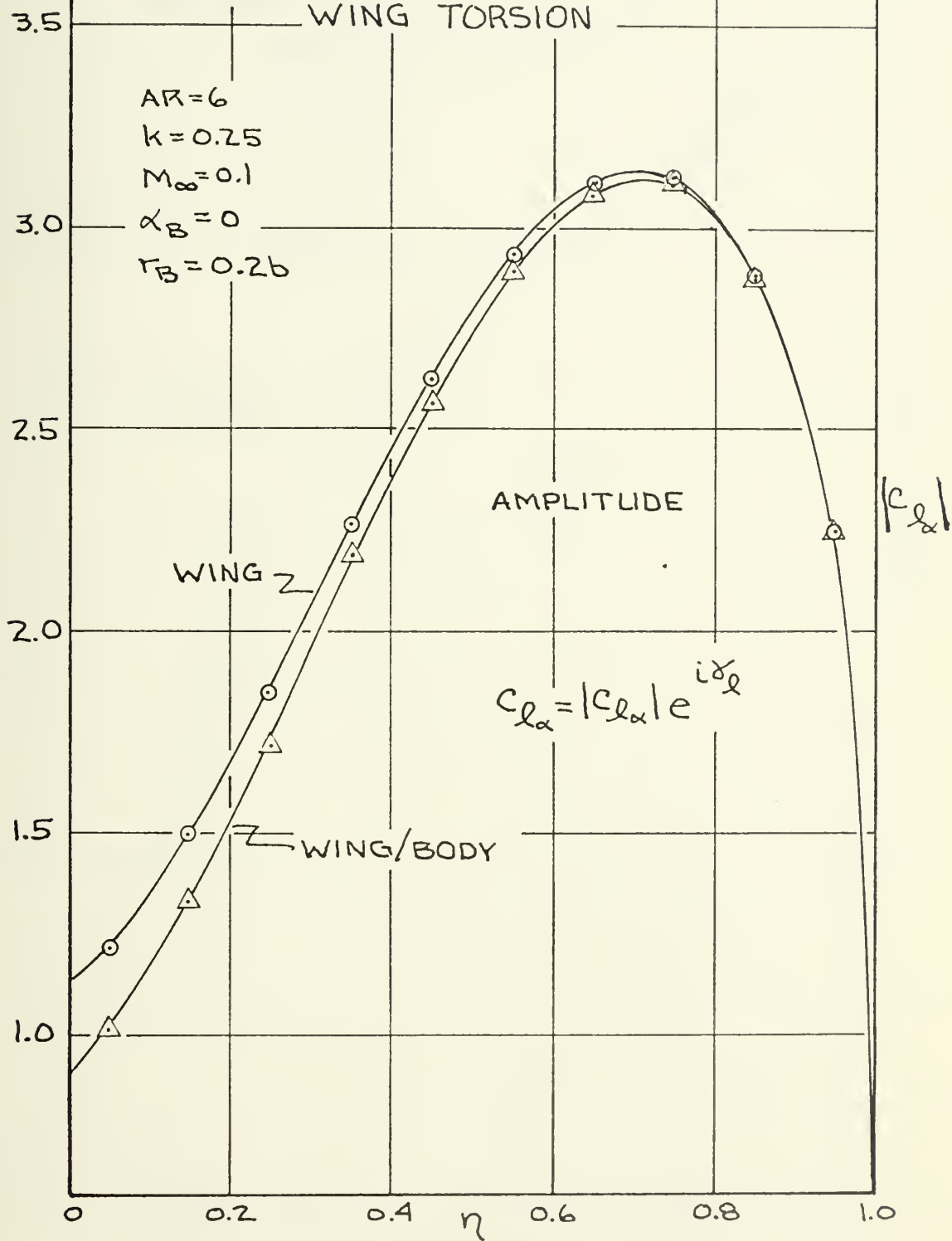




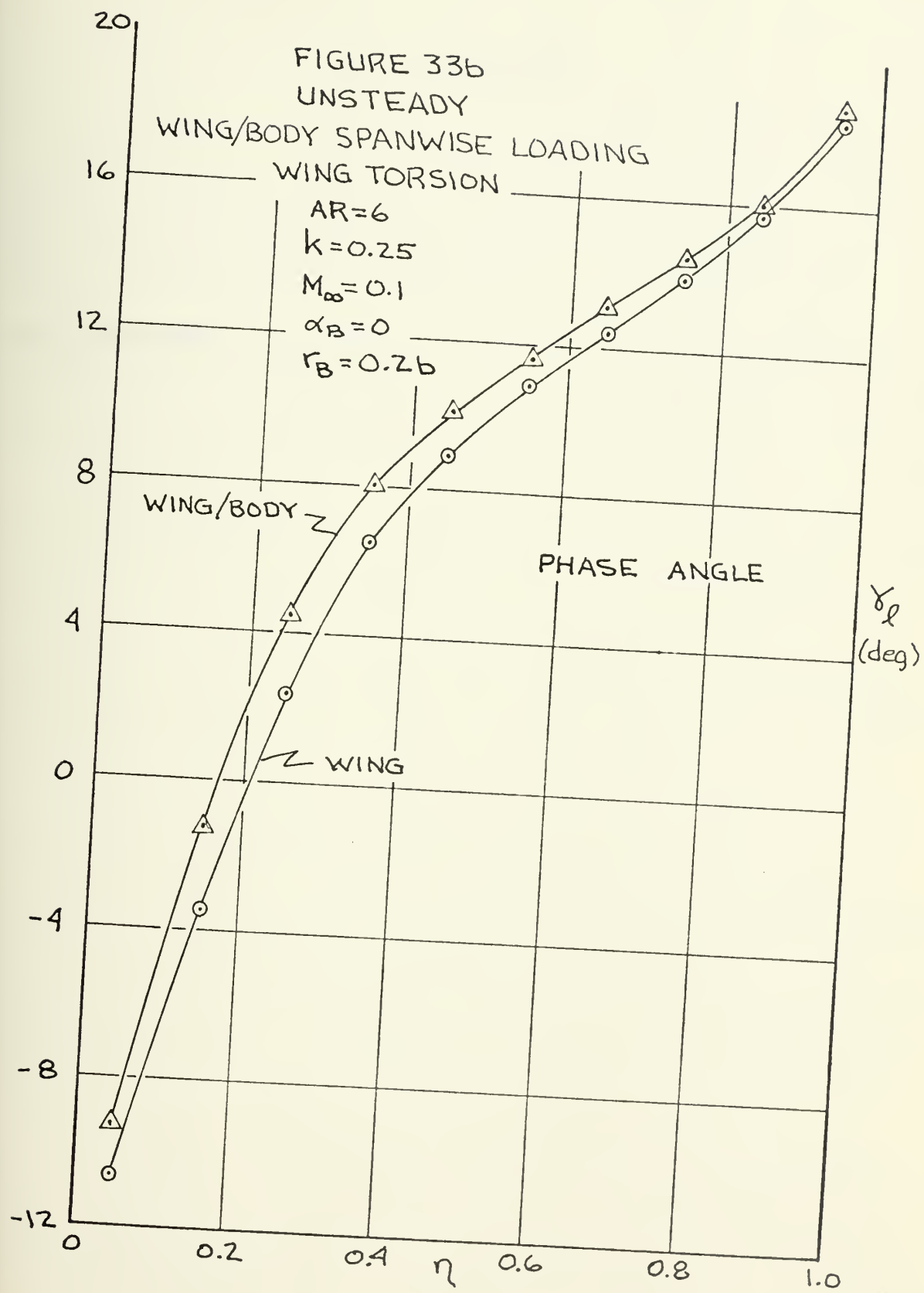
FIGURE 33a

UNSTEADY  
WING/BODY SPANWISE LOADING  
WING TORSION











## VII. CONCLUSIONS

In summary, a discrete potential element approach to subsonic numerical lifting surface theory has been developed and shown to be practical in predicting the nonsteady loading on harmonically oscillating wings. This approach was then extended to the case of an oscillating wing, cantilevered from a steady cylindrical body, to investigate interference effects and show the versatility of the basic method.

Correlation of the wing program results with those of nonsteady lifting surface theory is generally quite good over the full range of subsonic flow. Deviations, where they exist, appear to come from the different methods employed to handle the wing edge singularities in the pressure distribution, which are assumed a priori in the lifting surface theory, but in the discrete potential element approach are implicit in the boundary conditions. Primary deviation appears to rest in the handling of the wing tip pressure slope singularity, since sectional lift and pitching moment are generally overestimated in the wing tip area. Future work with the discrete potential element method should include investigation of a more adequate acknowledgement of this boundary condition in the problem formulation.

A minimum of about sixty control points is required on the semi-span wing surface to achieve convergence of the wing program results. In addition, at least six control



points are required, in both the chordwise and spanwise directions, to achieve accurate integration of the pressure distribution into sectional and wing coefficients. The wings, which can be analyzed efficiently by this method, are effectively limited to medium to small aspect ratios, because of the requirement for large numbers of control points, and consequently long computer run times, for high aspect ratio wings. The wing is further restricted to constant leading and trailing edge sweeps, and to a finite tip chord. Future development of the program capability should be pointed at removing these restrictions.

The effect of the wake on the wing loading is concentrated in the area just downstream of the wing. In all cases investigated, wing loading converged to within one per cent in an effective wake length of four root chords downstream of the trailing edge, allowing the wake singularity grid to be terminated at this finite distance from the wing. In addition, the wake effect is included in the wing kernel function matrix prior to the inversion process, through application of the boundary conditions in the wake. In this way, an historical drawback to the velocity potential formulation, the requirement to integrate the lifting surface downwash equation over both wing and wake, is removed.

Wing/body program results agree very well with both theoretical and experimental results for the steady case. Results obtained for nonsteady wing motion appear consistent



and give a good representation of interference effects. Convergence of the wing/body program is achieved with a body control panel grid of essentially the same format as the wing grid.

The effective body length which causes interference in the wing pressure loading extends approximately from one chord length upstream of the wing leading edge to one chord length downstream of the effective wake termination point. Increasing the body length modeled did not effect the pressure distribution, while decreasing this length so that the body grid did not extend beyond the wing/wake singularity grid in either the upstream or downstream directions caused inconsistent results to occur. This analysis was somewhat limited due to numerical restrictions on the allowable size of the body grid.

In the numerical analysis, the number of control points on the wing and the body was limited due to loss of computational accuracy in the matrix inversion routine of subroutine COMAT. This restricted the scope of the wing/body interference investigation both as to the length and radius of body which could be considered. Accurate solution of the wing downwash equation and inversion of the body influence coefficient matrix, is limited to coefficient matrices of order less than 110. Future wing/body analyses by this method would definitely require a more sophisticated inversion routine capable of handling much larger body grids.





Within the limitations noted, the wing/body program results show that interference effects are significant, and follow the same format, in both the steady and nonsteady cases. The decrease in wing pressure loading amplitude, caused by the body's presence, is greatest in the root area, decreasing towards the tip. Differences in phase angle, while small, exist over the entire wing. Therefore, these interference effects are of importance to three-dimensional analyses of wing/body configurations.

Future development of the discrete potential element approach should include the analysis of oscillating wings with control surfaces. This approach appears to provide a direct means of including the control surface boundary conditions, without the problems associated with properly defining singularity effects in the continuous loading formulation.



## APPENDIX A

### KERNEL FUNCTION DEVELOPMENT

For the purposes of nonsteady lifting surface analysis, a kernel function is defined as the normalwash on a surface due to a unit oscillatory acoustic singularity which satisfies the linearized convective wave equation (2.9). The singularities may be elementary radiators of zero order representing simple point sources, commonly used in supersonic analyses, or first order radiators, namely dipoles or doublets, whose axes are normal to the surface, used in subsonic analyses as in this paper. Development of the general form of the doublet kernel function was first accomplished by Küssner in 1940 [2]. The development in this appendix follows Küssner's method and specializes the results to the forms of the kernel function employed in the discrete potential element approach for both the wing and body surfaces.

In summary, the solution to the linearized wave equation for a stationary acoustic singularity is first extended to the case of a moving singularity in a space fixed coordinate system through application of a Lorentz coordinate transformation invariant with respect to the speed of sound. This solution is then transferred to the moving wing (or body) fixed coordinate system through a Galilean transformation. The results are subsequently reduced for the harmonic case



to the forms of the kernel functions necessary in the analysis discussed in Section IV.

### 1. Stationary Singularity

The perturbation analysis of Section II led to the linearized convective wave equation (2.9), which for the stationary case ( $U_\infty = 0$ ) has the familiar form

$$\nabla^2 \bar{\phi} - \frac{1}{a_\infty^2} \frac{\partial^2 \bar{\phi}}{\partial t^2} = 0 \quad (\text{A.1})$$

Since the pressure and velocity potential are linearly related by

$$\bar{p} = -\rho_\infty \frac{\partial \bar{\phi}}{\partial t} \quad (\text{A.2})$$

the perturbation pressure also satisfies the wave equation

$$\nabla^2 \bar{p} - \frac{1}{a_\infty^2} \frac{\partial^2 \bar{p}}{\partial t^2} = 0 \quad (\text{A.3})$$

Considering a stationary source at the origin of the coordinate system, equation (A.3) becomes

$$\frac{1}{r^2} \frac{\partial}{\partial r} \left( r^2 \frac{\partial \bar{p}}{\partial r} \right) - \frac{1}{a_\infty^2} \frac{\partial^2 \bar{p}}{\partial t^2} = 0 \quad (\text{A.4})$$

where

$$r = \sqrt{x^2 + y^2 + z^2}$$

This equation has the well known solution

$$\bar{p} = \frac{1}{r} F(t-r/a_\infty) + \frac{1}{r} G(t+r/a_\infty) \quad (\text{A.5})$$



where  $F$  and  $G$  are arbitrary functions. From the boundary conditions of the problem, only the solution representing outgoing waves ( $F$ ) is admitted.

Representing the oscillating source as a sphere of radius  $r_b$  expanding and contracting with a rate of flow away from the surface defined by

$$S(t) = 4\pi r_b^2 \bar{u}_r(t)$$

The momentum equation (2.2) becomes in linearized form

$$\frac{1}{r} \frac{\partial F}{\partial r} - \frac{F}{r^2} = - \rho_\infty \frac{\partial \bar{u}_r}{\partial t}$$

or

$$\frac{1}{r} \frac{\partial F}{\partial r} - \frac{F}{r^2} = - \frac{\rho_\infty}{4\pi r_b^2} \frac{dS}{dt} \text{ at } r = r_b \quad (\text{A.6})$$

If  $r_b$  is very small,  $\frac{F}{r^2}$  is much larger than  $\frac{\partial F}{\partial r}$  at  $r=r_b$ , and equation (A.6) can be taken as

$$F = \frac{\rho_\infty}{4\pi} \frac{dS(t)}{dt} \text{ at } r = r_b$$

Extending this solution to a general  $r$

$$F = \frac{\rho_\infty}{4\pi} \frac{\partial}{\partial t} S(t-r/a_\infty)$$

or

$$\bar{p} = \frac{\rho_\infty}{4\pi r} \frac{\partial}{\partial t} S(t-r/a_\infty) \quad (\text{A.7a})$$

and

$$\bar{\phi} = \frac{1}{4\pi r} S(t-r/a_\infty) \quad (\text{A.7b})$$





from equation (A.2). Equations (A.7) represent the pressure and velocity potential distributions of a stationary oscillatory source of strength S.

## 2. Moving Singularity

Consider a source moving with uniform velocity  $U_\infty$ , with respect to the surrounding fluid, in the direction of the negative x axis. If  $Q(x,y,z,t)$  is the source distribution density, the continuity equation (2.1) becomes

$$\frac{\partial \rho}{\partial t} + \nabla \cdot \rho \vec{U} = Q$$

and the linearized wave equation (A.3) becomes

$$\nabla^2 \bar{p} - \frac{1}{a_\infty^2} \frac{\partial^2 \bar{p}}{\partial t^2} = - \frac{\partial Q}{\partial t} \quad (A.8)$$

This source distribution can be represented by

$$Q(x,y,z,t) = \rho_\infty S(t) \delta(x+U_\infty t) \delta(y) \delta(z)$$

where  $\delta$  represents the familiar Dirac delta function. Making use of the linear relationship between  $\bar{p}$  and  $\bar{\phi}$  in equation (A.2), equation (A.8) may then be expressed in terms of the velocity potential as

$$\nabla^2 \bar{\phi} - \frac{1}{a_\infty^2} \frac{\partial^2 \bar{\phi}}{\partial t^2} = S(t) \delta(x+U_\infty t) \delta(y) \delta(z) \quad (A.9)$$

A Lorentz transformation, scaled with respect to the compressibility factor  $\beta$ , can now be used to reduce the right hand side of equation (A.9) to that of a stationary source. The transformed coordinate system (primed) is defined as follows:



$$\begin{aligned}
x' &= \frac{1}{\beta^2} (x + U_\infty t) \\
y' &= y/\beta \\
z' &= z/\beta \\
t' &= \frac{1}{\beta^2} \left( t + \frac{U_\infty}{a_\infty^2} x \right)
\end{aligned} \tag{A.10}$$

Performing this transformation, equation (A.9) takes the form

$$\nabla'^2 \bar{\phi} - \frac{1}{a_\infty^2} \frac{\partial^2 \bar{\phi}}{\partial t'^2} = \frac{1}{\beta^2} S(t') \delta(x') \delta(y') \delta(z') \tag{A.11}$$

Equation (A.9) has therefore been reduced to the form of the wave equation for a stationary source in the primed coordinate system, which from equation (A.7) has the solution

$$\bar{\phi}(r', t') = \frac{-1/\beta^2}{4\pi r'} S(t' - r'/a_\infty) \tag{A.12}$$

In terms of the space fixed coordinate system, the variables of equation (A.12) are

$$\begin{aligned}
r' &= \frac{1}{\beta^2} \sqrt{(x + U_\infty t)^2 + \beta^2 (y^2 + z^2)} \\
t' &= \frac{1}{\beta^2} \left( t + \frac{U_\infty}{a_\infty^2} x \right)
\end{aligned}$$

Transferring the solution (A.12) to the wing fixed coordinate system now requires the further Galilean transformation

$x = x + U_\infty t$ , which produces the final result

$$\bar{\phi}(r, t) = \frac{-1}{4\pi r} S \left[ t + \frac{1}{a_\infty \beta^2} (M_\infty x - r) \right] \tag{A.13}$$



where

$$r = \sqrt{x^2 + \beta^2(y^2 + z^2)}$$

All variables are referenced to the wing fixed coordinate system.

### 3. Wing Fixed Periodic Singularities

If an harmonically oscillating source of unit strength ( $S = 1e^{i\omega t}$ ) is located at the origin of the wing fixed coordinate system, the velocity potential distribution given by equation (A.13) is

$$\bar{\phi}_S(x, y, z, t) = - \frac{1}{4\pi r} \exp \left\{ i\omega \left[ t + \frac{1}{a_\infty \beta^2} (M_\infty x - r) \right] \right\} \quad (A.14)$$

Considering now only the spatial variation of the velocity potential of a unit source located at a general point  $(x_0, y_0, z_0)$  (time dependence  $e^{i\omega t}$  having been factored out)

$$\phi_S(x, y, z) = \frac{-1}{4\pi r} \exp \left\{ i \frac{\omega}{a_\infty \beta^2} [M_\infty(x - x_0) - R] \right\} \quad (A.15)$$

where

$$R = \sqrt{(x - x_0)^2 + \beta^2 [(y - y_0)^2 + (z - z_0)^2]}$$

The potential distribution of a dipole or doublet is related to that of a source by

$$\phi_d = \frac{\partial \phi_S}{\partial n}$$

where  $n$  is the direction of the axis of the dipole. Therefore from equation (A.15), the velocity potential of a unit dipole oriented in the  $z$  direction is



$$\phi_d(x,y,z) = \frac{\partial \phi_s}{\partial z_o} = \frac{-\beta^3}{4\pi k^3} (z-z_o) \left( 1 + i \frac{\omega}{a_\infty \beta^2} R \right) \exp \left\{ i \frac{\omega}{a\beta^2} [M_\infty(x-x_o) - R] \right\} \quad (A.16)$$

The downwash at a point on the wing  $(x,y,o)$  from such a doublet located in the plane of the wing  $(x_o,y_o,o)$  is given by

$$w(x,y,o) = \left. \frac{\partial \phi_d}{\partial z} \right|_{z=0, z_o=0}$$

or

$$w = \frac{-\beta^2}{4\pi R^3} \left( 1 + i \frac{\omega}{a_\infty \beta^2} R \right) \exp \left\{ i \frac{\omega}{a_\infty \beta^2} [M_\infty(x-x_o) - R] \right\} \quad (A.17)$$

where

$$R = \sqrt{(x-x_o)^2 + \beta^2(y-y_o)^2}$$

This is the standard form of the kernel function in cartesian coordinates normally used in the velocity potential formulation of lifting surface theory.

#### 4. Kernel Function for Wing/Body Doublets

To analyze the wing/body problem, a transformation from cartesian to cylindrical coordinates was made as discussed in Section IV.B and shown in Figure 8. Thus

$$x = x$$

$$y = r \cos \theta$$

$$z = r \sin \theta$$

relate the equations of the previous section to the  $(r,\theta,x)$  system. A unit doublet with axis in the  $z$  direction located





at  $(r_o, \theta_o, x_o)$  has a potential distribution, from equation (A.16), in the new coordinate system of

$$\phi_d(r, \theta, x) = \frac{-\beta^2}{4\pi R^3} (r \sin \theta - r_o \sin \theta_o) \left( 1 + i \frac{\omega}{a_\infty \beta^2} R \right) \exp \left\{ i \frac{\omega}{a_\infty \beta^2} [M_\infty(x-x_o) - R] \right\} \quad (A.18)$$

where

$$R = \sqrt{(x-x_o)^2 + \beta^2(r^2 + r_o^2 - 2rr_o \cos <\theta - \theta_o>)}$$

For a doublet located on the wing at  $(r_o, \theta=0 \text{ or } \pi, x_o)$ , the downwash on the wing at  $(r, \theta, x)$  is given by

$$u_\theta = \frac{1}{r} \frac{\partial \phi_d}{\partial \theta} \bigg|_{\theta=0, \theta_o=0 \text{ or } \pi}$$

which applied to equation (A.18) results in

$$u_\theta = \frac{-\beta^2}{4\pi R^3} \left( 1 + \frac{i\omega}{a_\infty \beta^2} R \right) \exp \left\{ i \frac{\omega}{a_\infty \beta^2} [M_\infty(x-x_o) - R] \right\} \quad (A.19)$$

where

$$R = \sqrt{(x-x_o)^2 + \beta^2(r^2 + r_o^2 \mp 2rr_o)}$$

- for  $\theta = 0$

+ for  $\theta = \pi$

This is of course the same as equation (A.17) in cartesian coordinates except for R which indicates the coordinate transformation.



The normalwash on a cylindrical body of radius  $r_B$ , coaxial with the  $x$  axis, at a control point,  $(r_B, \theta, x)$ , due to the wing doublet is given by

$$u_r = \left. \frac{\partial \phi_d}{\partial r} \right|_{r=r_B, \theta_0=0 \text{ or } \pi}$$

or

$$u_r = \frac{-\beta^2}{4\pi R^3} \sin \theta \left[ \left( 1 - \frac{3r_B}{R} \frac{\partial R}{\partial r} \right) \left( 1 + i \frac{\omega}{a_\infty \beta^2} R \right) + \left( \frac{\omega}{a_\infty \beta^2} \right)^2 r_B R \frac{\partial R}{\partial r} \right] \exp \left\{ i \frac{\omega}{a_\infty \beta^2} [M(x-x_0) - R] \right\} \quad (\text{A.20})$$

where

$$R = \sqrt{(x-x_0)^2 + \beta^2(r_B^2 + r_0^2 + 2r_B r_0 \cos \theta)}$$

$$\frac{\partial R}{\partial r} = \frac{\beta^2}{R} (r_B + r_0 \cos \theta)$$

$$- \text{ for } \theta = 0$$

$$+ \text{ for } \theta = \pi$$

To determine the body singularity kernel function forms, the velocity potential of a source is expressed in cylindrical coordinates. From equation (A.15)

$$\phi_s(r, \theta, x) = \frac{-1}{4\pi R} \exp \left\{ i \frac{\omega}{a_\infty \beta^2} [M_\infty(x-x_0) - R] \right\} \quad (\text{A.21})$$

where

$$R = \sqrt{(x-x_0)^2 + \beta^2(r^2 + r_0^2 - 2rr_0 \cos <\theta - \theta_0>)}$$



The potential distribution of a doublet oriented in the radial direction and located at  $(r_o, \theta_o, x_o)$  is obtained from

$$\phi_d = \frac{\partial \phi_s}{\partial r_o}$$

which applied to equation (A.21) gives

$$\begin{aligned} \phi_d(r, \theta, x) = & \frac{\beta^2}{4\pi R^3} [r_o - r \cos(\theta - \theta_o)] \left[ 1 + i \frac{\omega}{a_\infty \beta^2} R \right] \\ & \exp \left\{ i \frac{\omega}{a_\infty \beta^2} [M(x - x_o) - R] \right\} \end{aligned} \quad (A.22)$$

with  $R$  as above. From this potential formulation, the following kernel functions can be obtained for a unit doublet with axis in the radial direction, located on the body surface at  $(r_B, \theta_o, x_o)$ .

The downwash on the wing at  $(r, o, x)$  is given by

$$u_\theta = \frac{1}{r} \frac{\partial \phi_d}{\partial \theta} \bigg|_{\theta=0, r_o=r_B}$$

or

$$\begin{aligned} u_\theta = & \frac{-\beta^2}{4\pi R^3} \left\{ \left[ r \sin \theta_o + \frac{3}{R} (r_B - r \cos \theta_o) \frac{\partial R}{\partial \theta} \right] \right. \\ & \left[ 1 + i \frac{\omega}{a_\infty \beta^2} R \right] - \left( \frac{\omega}{a_\infty \beta^2} \right)^2 R (r_B - r \cos \theta_o) \frac{\partial R}{\partial \theta} \Big\} \\ & \exp \left\{ i \frac{\omega}{a_\infty \beta^2} [M(x - x_o) - R] \right\} \end{aligned} \quad (A.23)$$

where

$$R = \sqrt{(x - x_o)^2 + \beta^2 (r^2 + r_B^2 - 2rr_B \cos \theta_o)}$$



$$\frac{\partial R}{\partial \theta} = \frac{-\beta^2}{R} r r_B \sin \theta_o$$

The normalwash on the body at  $(r_B, \theta, x)$  is given by

$$u_r = \left. \frac{\partial \phi_d}{\partial r} \right|_{r=r_B, r_o=r_B}$$

or

$$\begin{aligned} u_r = \frac{-\beta^2}{4\pi R^3} & \left\{ \left[ \cos(\theta - \theta_o) + \frac{3}{R} r_B (1 - \cos <\theta - \theta_o>) \frac{\partial R}{\partial r} \right] \right. \\ & \left[ 1 + i \frac{\omega}{a_\infty \beta^2} R \right] - \left( \frac{\omega}{a_\infty \beta^2} \right)^2 R r_B (1 - \cos <\theta - \theta_o>) \frac{\partial R}{\partial r} \left\{ \right. \\ & \left. \exp \left\{ i \frac{\omega}{a_\infty \beta^2} [M_\infty (x - x_o) - R] \right\} \right\} \end{aligned} \quad (A.24)$$

where

$$R = \sqrt{(x - x_o)^2 + 2\beta^2 r_B^2 (1 - \cos <\theta - \theta_o>)}$$

$$\frac{\partial R}{\partial r} = \frac{\beta^2}{R} r_B (1 - \cos <\theta - \theta_o>)$$

Equations (A.19), (A.20), (A.23), (A.24) represent the kernel function formulations used in the discrete potential element analysis of the wing and wing/body programs.





## APPENDIX B

### INPUT INSTRUCTIONS FOR COMPUTER PROGRAMS

Instructions for preparing input data for both the wing and wing/body programs are presented in this appendix. The field location and format for each input quantity is specified. Any set of units may be used for geometric dimensions, displacements, and acoustic velocity as long as they are consistent. Any number of problems may be run in sequence, with the programs terminating when a new data set is not available to be read.

#### 1. Wing Program

a. First card: `FORMAT(3F10.4,2I10,F10.4)`

Column	1-10	11-20	21-30	40	50	51-60
Name	XM	F	A	ICH	JCH	ALPH

XM      Mach number.

F      Circular frequency (rad/sec).

A      Speed of Sound.

ICH      Indicator for second card input data.  
= 0 for new data; program reads second card.  
= 1 for same data as previous problem; no second card required.

JCH      Indicator for wing displacement input data.  
= 0 for new data; program reads third and subsequent wing displacement cards.  
= 1 for same data as previous problem or for pitching motion; no wing displacement cards required.

ALPH      Amplitude of pure pitching motion.  
> 0 for pitching motion; program computes downwash for pitching mode (JCH must equal 1).  
= 0.0 for general wing motion; program computes downwash from wing displacement input.



b. Second card: FORMAT(4I5,5F10.4)

Column	1-5	6-10	11-15	16-20	21-30	31-40	41-50	51-60	61-70
Name	N	M	MB	NC	XC	XB	BR	G11	G22

N Number of chordwise control points (maximum ten).

M Number of spanwise control points (maximum ten).

MB = 0 for wing program.

NC Significant wake length downstream from wing trailing edge (root chord lengths).

XC Wing root chord.

BR = 0 for wing program

XB Wing semi-span.

G11 Leading edge sweep angle (deg.).

G22 Trailing edge sweep angle (deg.).

G11 and G22 positive for downstream sweep.

c. Third and subsequent wing displacement cards:  
FORMAT(7F10.4)

Column	1-10	11-20	21-30	31-40	41-50	51-60	61-70
Name	Z(1)	Z(2)	Z(3)	Z(4)	Z(5)	Z(6)	Z(7)
	Z(8)	Z(9)	Z(10)		fourth card		
	Z(11)	Z(12)	Z(13)	etc.	fifth card		

Displacements (wing motion amplitudes) are read spanwise starting from the wing root at the leading edge. A new card must be started for each spanline of data (example above is for ten spanwise points).

## 2. Wing/Body Program

a. First card: same as wing program.

b. Second card: FORMAT(4I5,3F10,I5)

Column	1-5	6-10	11-15	16-20	21-30	31-40	41-50	51-55
Name	N	M	MB	NC	XC	XB	BR	MS

N Number of wing chordwise control points (maximum ten).

M Number of wing spanwise control points (maximum ten).



MB	Total number of control points on body quarter-circumference surface (maximum 130)
NC	Significant wake length downstream from wing trailing edge (chord lengths).
XC	Wing chord.
XB	Wing semi-span.
BR	Body radius.
MS	Number of control points along body quarter circumference.

c. Third and subsequent wing displacement cards: same as wing program.



APPENDIX C

COMPUTER PROGRAM FLOW DIAGRAMS





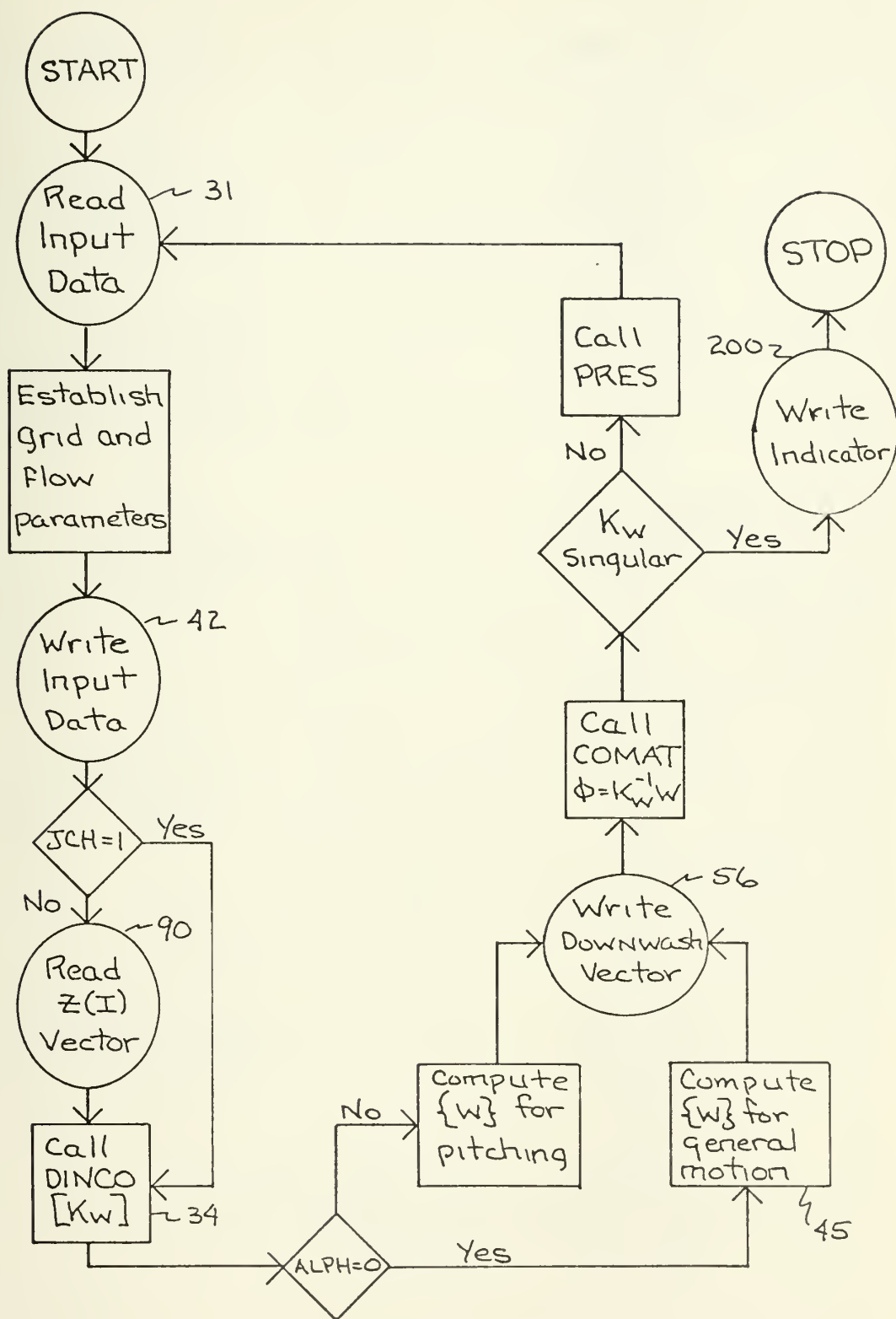


FIGURE 34

WING PROGRAM - MAIN FLOW DIAGRAM



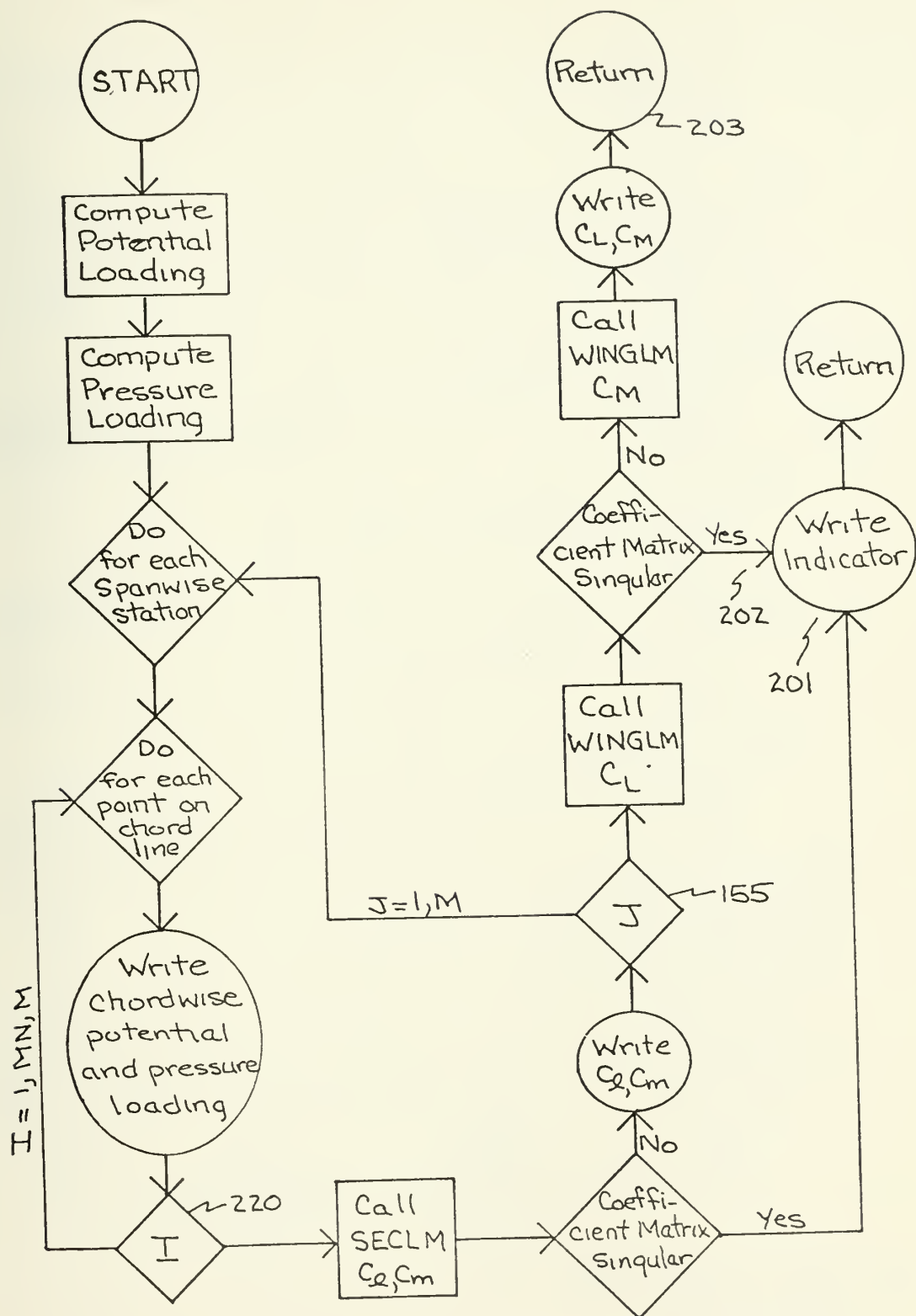


FIGURE 35

SUBROUTINE PRES FLOW DIAGRAM







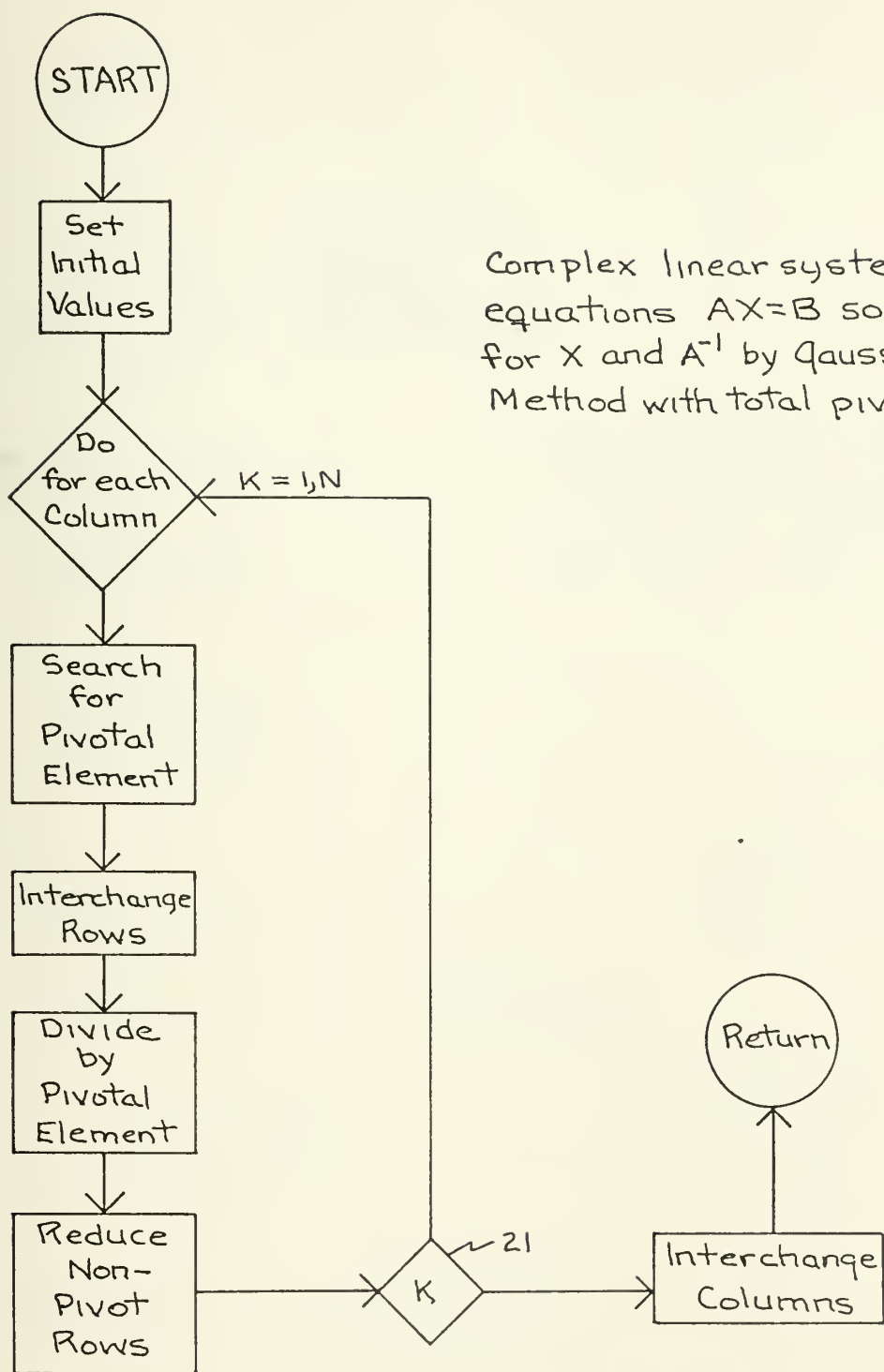


FIGURE 37

SUBROUTINE COMAT FLOW DIAGRAM





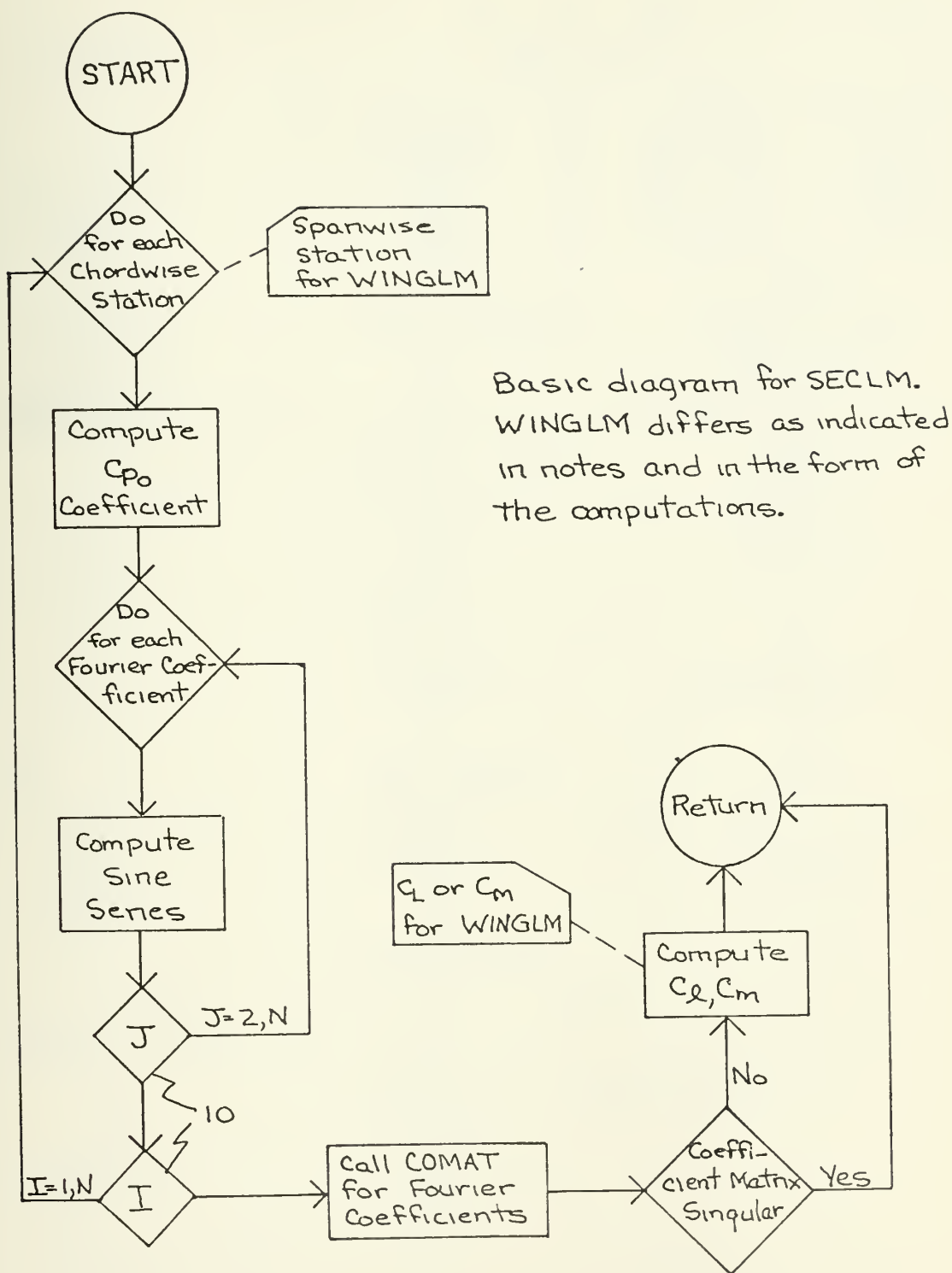


FIGURE 38

SUBROUTINES SECLM AND WINGLM FLOW DIAGRAM



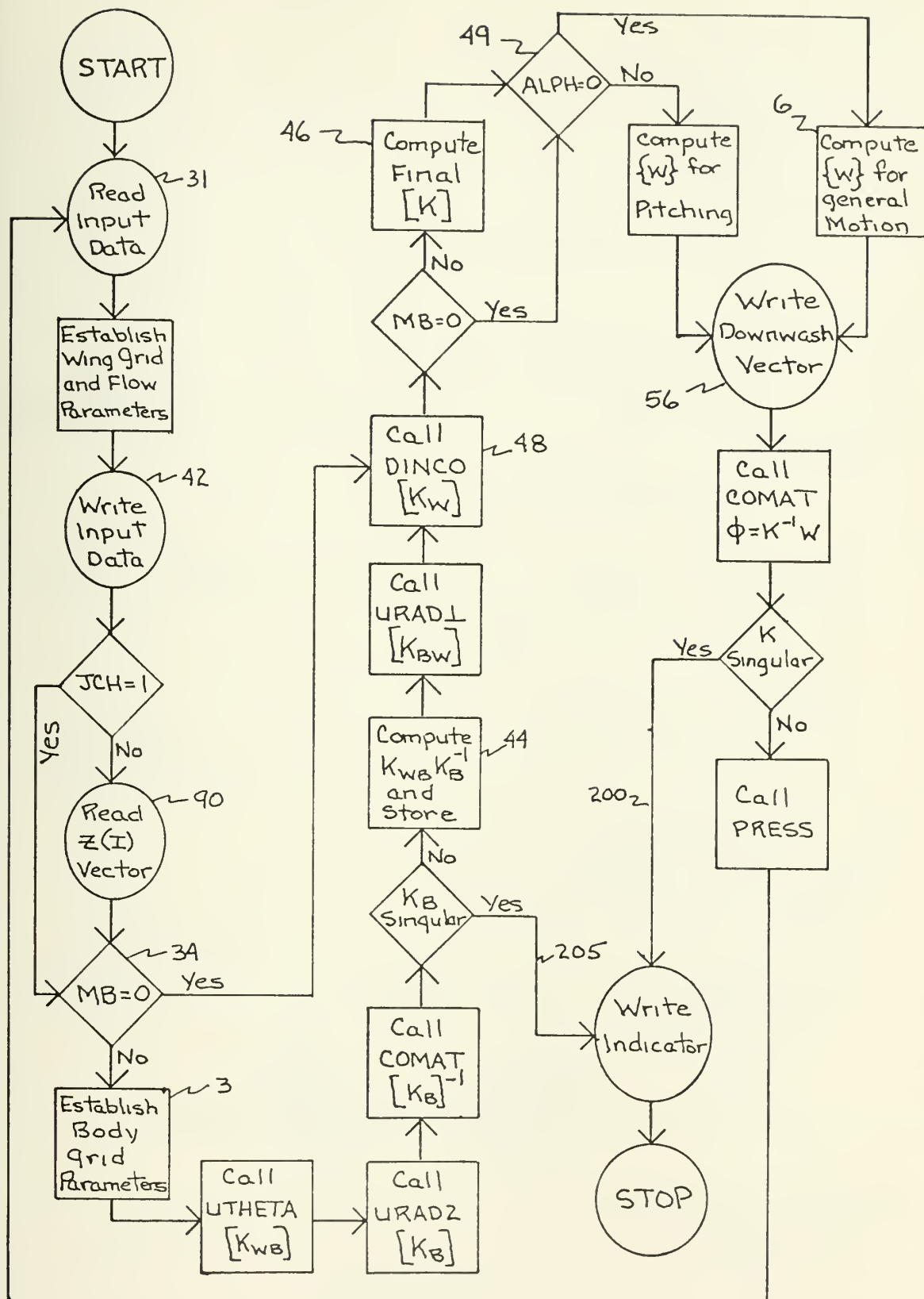


FIGURE 39  
WING/BODY PROGRAM - MAIN FLOW DIAGRAM



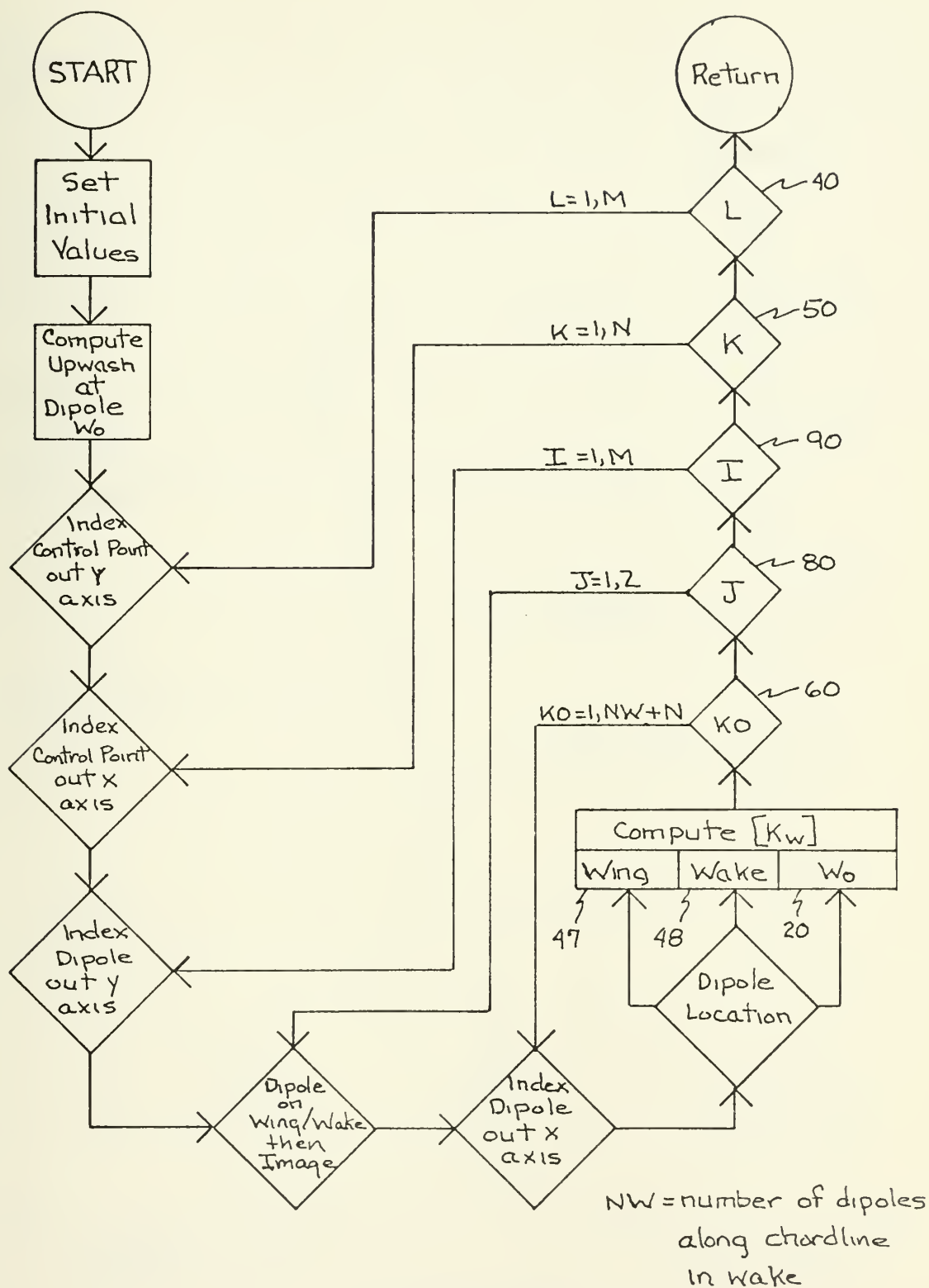


FIGURE 40

WING/BODY PROGRAM - DINCO FLOW DIAGRAM



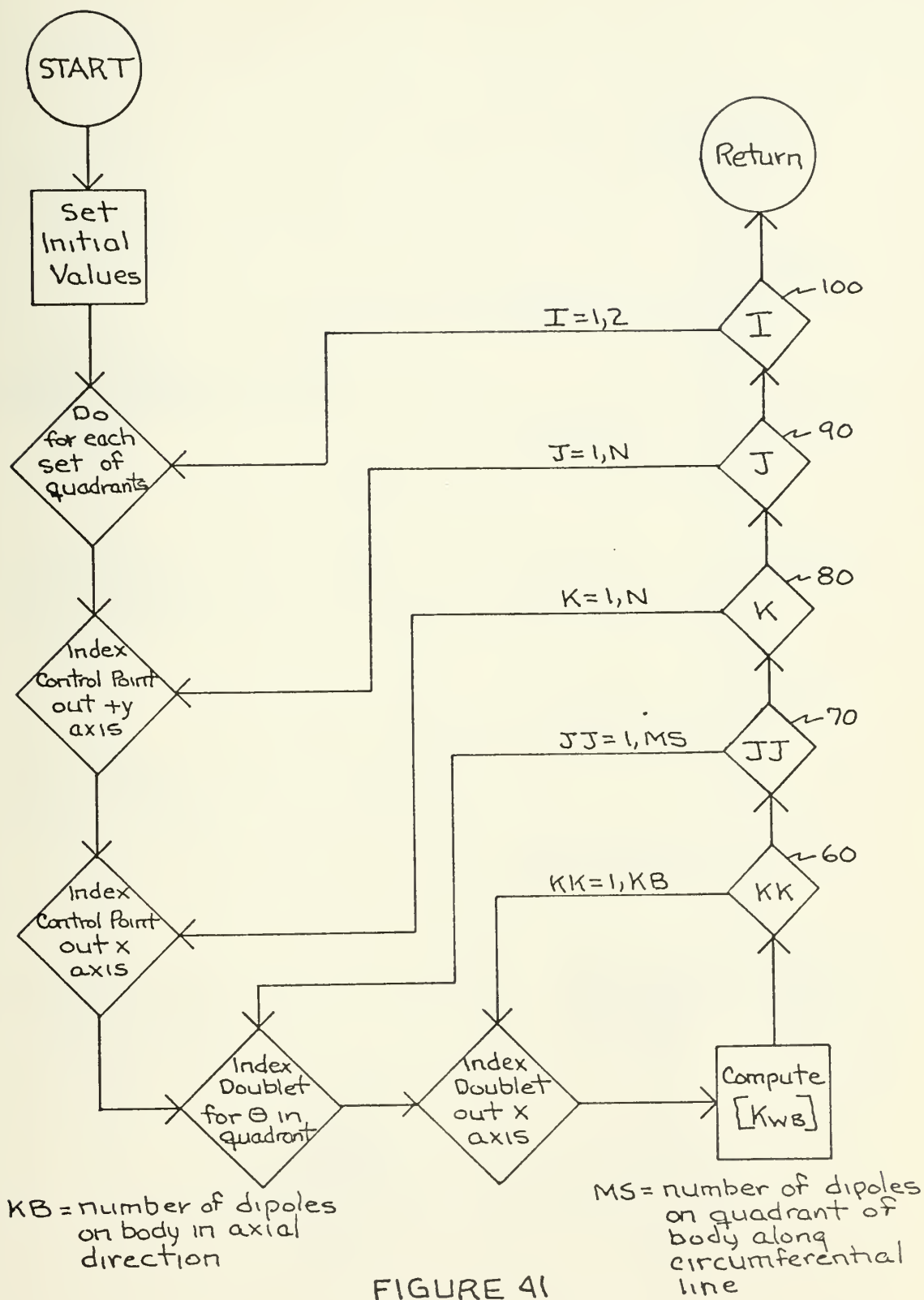


FIGURE 41

SUBROUTINE UTHETA FLOW DIAGRAM





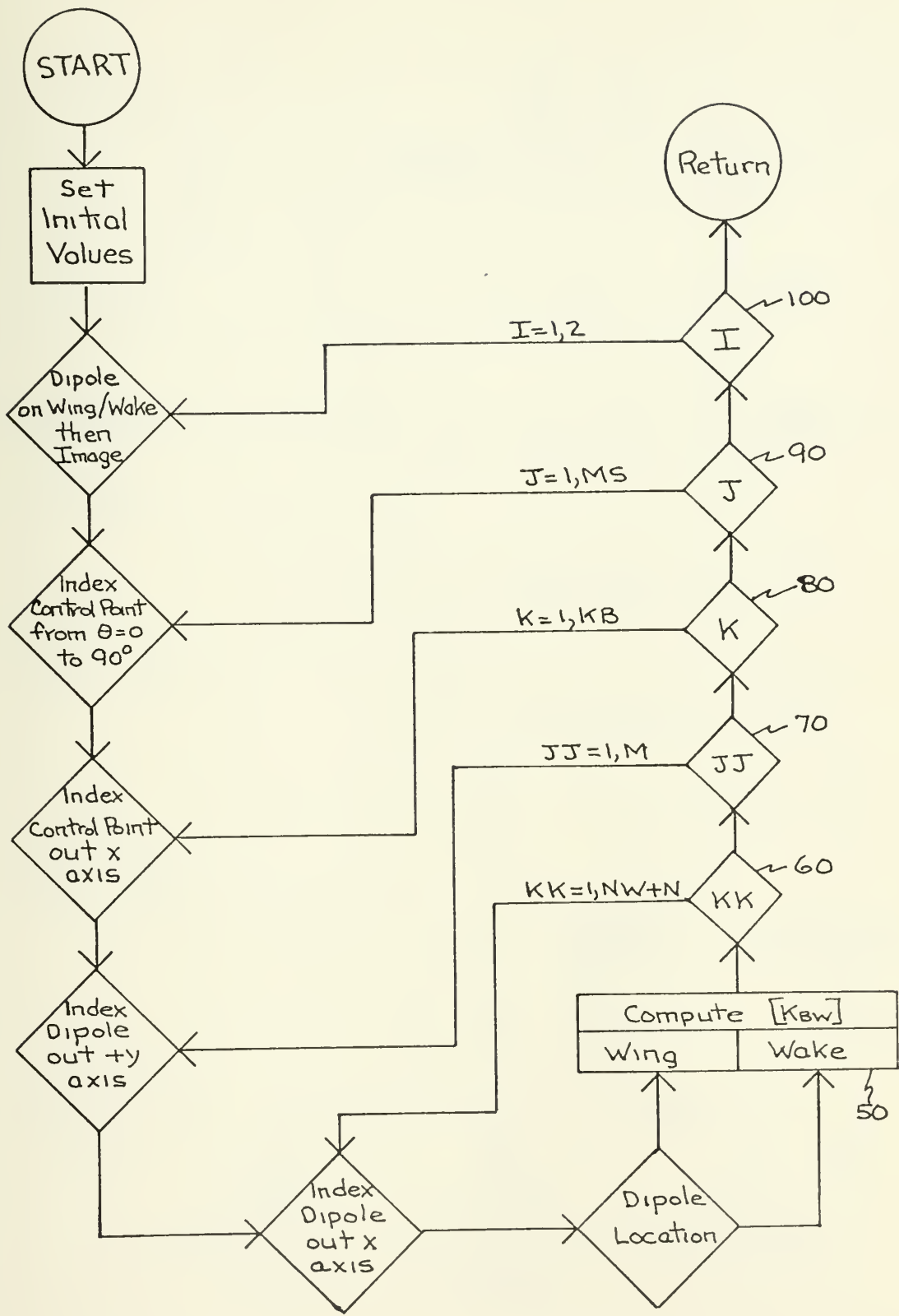


FIGURE 42  
SUBROUTINE URADL FLOW DIAGRAM



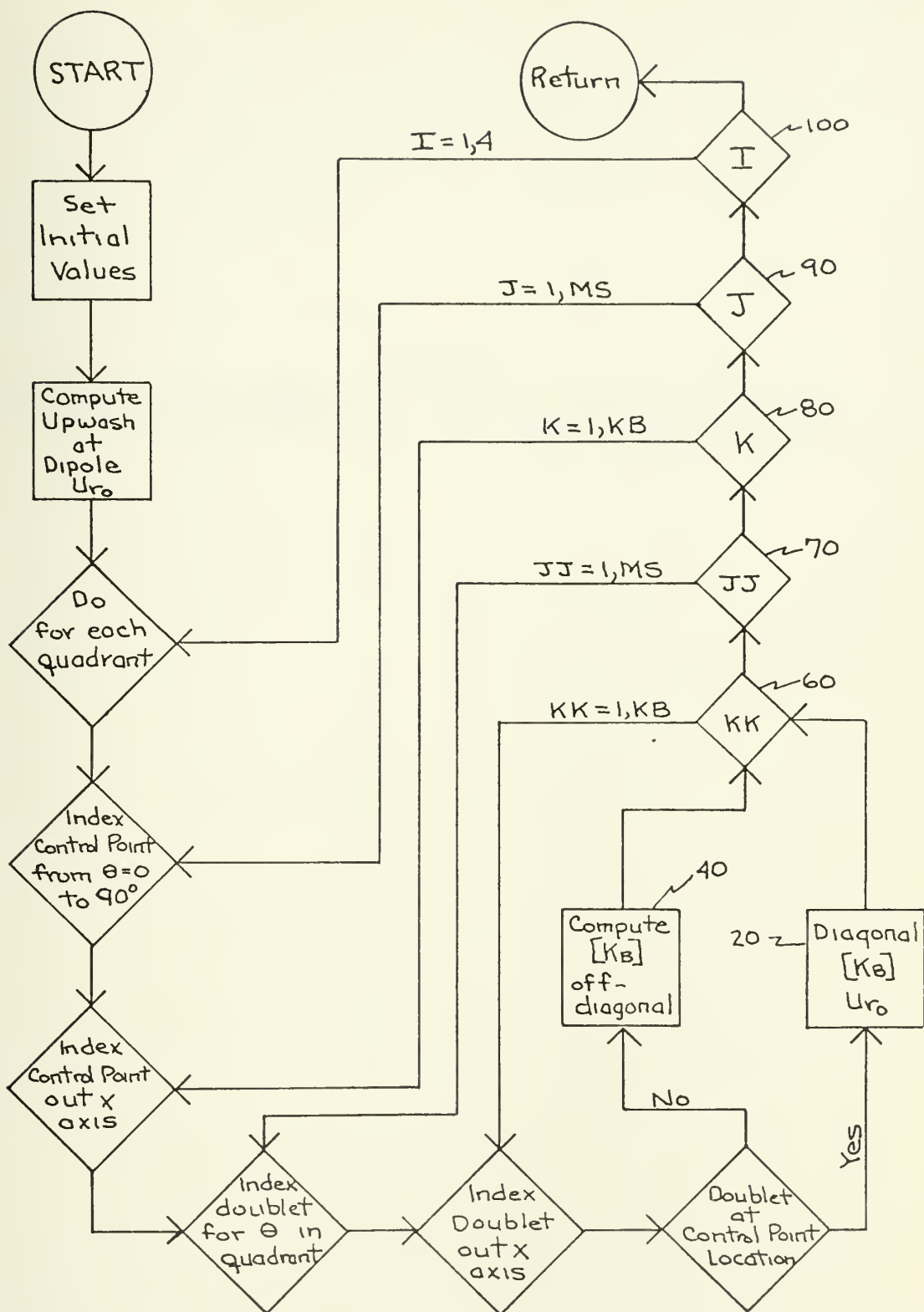


FIGURE 43  
SUBROUTINE URADZ FLOW DIAGRAM



APPENDIX D

LISTING OF THE FORTRAN CODE FOR THE WING PROGRAM



..

156





C ESTABLISH CONTROL POINT COORDINATES.

```
G1=0.017453*G11
G2=0.017453*G22
TG1=TAN(G1)
TG2=TAN(G2)-TG1
XCW=NC*XC
YINC=XB/M
DELY=YINC/2.0
K=1
DO 2 I=1,M
  Y(I)=BR+DELY
  XCI=XC+DELY*TG2
  XINC(I)=XCI/N
  DELX=XINC(I)/2.0
  NX(I)=N+XCW/XINC(I)
  NXI=NX(I)
  DO 1 J=1,NXI
    X(K)=DELY*TG1+DELX
    K=K+1
  DELX=DELX+XINC(I)
  DELY=DELY+YINC
  CHECK ON INPUT DATA
42 WRITE(6,26)
XK=(F*XC)/(2.0*XM*A)
WRITE(6,28)XM,F,A,XC,XB,N,M,NC,XK
DO 7 I=1,M
  UFAC(I)=XM*A/(2.0*XINC(I))
  CUFAC(I)=CMPLX(0.0,F/UFAC(I))
  PFAC(I)=-2.0/(XM*A*XINC(I))
7 CONTINUE
IF(JCH.EQ.1)GO TO 34
C READ WING DISPLACEMENT INPUT
DO 90 J=1,N
90 READ(5,13)(Z(I),I=J,MN,N)
WRITE(6,70)
WRITE(6,71)(Z(J),J=1,MN)
C CALL SUBROUTINE DINCO TO CALCULATE DOWNWASH INFLUENCE COEFFICIENT
C MATRIX CA
34 CALL DINCO(CA,100)
IF(ALPH.LE.0.001)GO TO 45
C CALCULATE DOWNWASH VELOCITY VECTOR FOR PITCHING MOTION
AA=0.7*XC
L=1
KK=1
DO 3 I=1,M
3 KK=1
DO 4 J=1,N
4 AB=F*(AA-X(K))
```

00000400  
00000410  
00000420  
00000430  
00000440  
00000450  
00000460  
00000470  
00000480  
00000490  
00000500  
00000510  
00000520  
00000530  
00000540  
00000550  
00000560  
00000570  
00000580  
00000590  
00000600  
00000610  
00000620  
00000630  
00000640  
00000650  
00000660  
00000670  
00000680  
00000690  
00000700  
00000710  
00000720  
00000730  
00000740  
00000750  
00000760  
00000770  
00000780  
00000790  
00000800  
00000810  
00000820  
00000830  
00000840  
00000850  
00000860  
00000870



```

CAB=CMPLX(0.0,AB)
CU5(L)=ALPH*(CAB-XM*A)
L=L+1
K=K+1
KK=KK+NX(I)
CONTINUE
45 IF(ALPH.GT.0.001)GO TO 56
C CALCULATE DOWNWASH VELOCITIES (CUN) FROM INPUT DEFLECTIONS (Z)
J=1
DO 60 K=1,M
CU5(J)=2.0*UFAC(K)*(Z(J+1)-(1.0-CUFAC(K)*DP/2.0)*Z(J))
DO 54 I=2,NXKO
J=J+1
CU5(J)=UFAC(K)*(Z(J+1)+CUFAC(K)*Z(J)-Z(J-1)*DP)
J=J+1
CU5(J)=2.0*UFAC(K)*((1.0+CUFAC(K)/2.0)*Z(J)-Z(J-1)*DP)
J=J+1
CONTINUE
56 C PRINT OUT DOWNWASH VELOCITY MATRIX
WRITE(6,72)
WRITE(6,30)(CU5(J),J=1,MN)
C CALL SUBROUTINE COMAT TO SOLVE SYSTEM OF EQUATIONS FOR DIPOLE
C STRENGTHS(CUN). CA MATRIX IS INVERSE OF INPUT COEFFICIENT MATRIX
C KI IS INDICATOR WHICH EQUALS 2 IF CA IS SINGULAR
CALL COMAT(MN,1,CA,CU5,CD,KI,100)
IF(KI.EQ.2)GO TO 200
C CALL SUBROUTINE PRES TO CALCULATE AND PRINT PRESSURE DISTRIBUTIONS,
C AND SECTIONAL AND WING LIFT AND MOMENT VALUES.
CALL PRES(C5,CPH5,P5,P6,CP5,XX5,CL5,CM5,XET5,CU5)
GO TO 31
200 WRITE(6,40)
140 STOP
C * * * * *
C * * * * *
C * * * * *

```

```

00000880
00000890
00000900
00000910
00000920
00000930
00000940
00000950
00000960
00000970
00000980
00000990
00001000
00001010
00001020
00001030
00001040
00001050
00001060
00001070
00001080
00001090
00001100
00001110
00001120
00001130
00001140
00001150
00001160
00001170
00001180
00001190
00001200
00001210
00001220
00001230

```

```

SUBROUTINE PRES(CP,CPHI,PA,PP,CPS,XXI,CLW,CMW,XETA,CUN)
C
C SUBROUTINE PRES CALCULATES AND WRITES WING PRESSURE COEFFICIENT
C DISTRIBUTIONS, AND SECTIONAL AND WING LIFT AND MOMENT COEFFICIENTS.
C
C IMPLICIT COMPLEX (C)
C REAL*8 DP
C DIMENSION CP(MN),CPHI(MN),PA(MN),PP(MN),CPS(N2),XXI(N2),CLW(N2),
C 1CMW(N2),XETA(N2),CUN(MN)

```

```

00001240
00001250
00001260
00001270
00001280
00001290
00001300
00001310
00001320
00001330

```







```

XCI=XC+(YINC/2.0+(J-1)*YINC)*TG2
XSCF=XINC(J)/XCI
XSC=XSCF/2.0
DO 220 K=1,N
  CPS(K)=CP(I)
  XXI(K)=XSC
  WRITE(6,66) XSC,CUN(I),CP(I),PA(I),PP(I)
  I=I+1
  XSC=XSC+XSCF
220 K=N+1
C CALL SUBROUTINE SECLM FOR SECTIONAL LIFT AND MOMENT COEFFICIENTS
CALL SECLM(CPS,XXI,K,CSL,CSM,KK1)
IF(KK1.EQ.2) GO TO 201
SLA=CABS(CSL)
SLP=57.29578*ATAN2(AIMAG(CSL),REAL(CSL))
SMA=CABS(CSM)
SMP=57.29578*ATAN2(AIMAG(CSM),REAL(CSM))
WRITE(6,76) SLA,SLP,SMA,SMP
CLW(J)=XCI*CSL
CMW(J)=(CSM+CSL*((XC*0.5-DELY*TG1)/XCI-0.5))*XCI**2
XETA(J)=ETA
DELY=DELY+YINC
ETA=ETA+ETAF
XMEAN=XC+XB*TG2/2.0
JJ=M+1
C CALL SUBROUTINE WINGLM FOR WING LIFT COEFFICIENT
CALL WINGLM(CLW,XETA,JJ,CL,KK2)
IF(KK2.EQ.2) GO TO 202
CL=CL/XMEAN
XLA=CABS(CL)
XLP=57.29578*ATAN2(AIMAG(CL),REAL(CL))
C CALL SUBROUTINE WINGLM FOR WING MOMENT COEFFICIENT
CALL WINGLM(CMW,XETA,JJ,CM,KK2)
CM=CM/(XMEAN*XC)
XMA=CABS(CM)
XMP=57.29578*ATAN2(AIMAG(CM),REAL(CM))
WRITE(6,78) XLA,XLP,XMA,XMP
RETURN
203 WRITE(6,41)
201 GO TO 203
202 WRITE(6,39)
GO TO 203
END
C ** *
C ** *
C ** *

```





```

SUBROUTINE DINCO(CAL,MAX1)
C
C SUBROUTINE DINCO CALCULATES THE DOWNWASH INFLUENCE COEFFICIENT MATRIX
C OF THE WING DUE TO WING AND WAKE SINGULARITIES.
C
      IMPLICIT COMPLEX(C)
      REAL*8 DP
      COMPLEX W01,WW0
      DIMENSION CAL(MAX1,MN)
      COMMON/COM1/CUFAC(10),X(1500),Y(10),XINC(10),UFAC(10),PFAC(10)
      COMMON/COM2/F,A,MB,NC,XC,XB,MN,MNW,DP,N2
      COMMON/COM3/B,XM,S,N,NW,BR,YINC,M,NXKO,TG2,TG1
      COMMON/COM4/NX(15)
      EX(X,R)=S*(XM*X-R)
      CFAC(R,Z)=-B/(12.5663*R*Z)
      C1(X,R)=CMPLX(0.0,EX(X,R))
      C2(S,R)=CMPLX(1.0,S*R)
      B=1.0-XM**2
      S=F/(A*R)
C INITIALIZE MATRICES TO ZERO
      DO 132 I=1,MN
      DO 132 J=1,MN
132      CAL(I,J)=(0.0,0.0)
C CALCULATE DOWNWASH MATRIX
C INDEXING DOUBLET LOCATION OUT POSITIVE Y AXIS
      KK=1
      LL=1
      DO 100 I=1,M
      K2=LL+N-1
      WAKE=-F*XINC(I)/(XM*A)
      CWAKE=CMPLX(0.0,WAKE)
      CWEX=CEXP(CWAKE)
C CALCULATE UPWASH AT SINGULARITY
      WW0=0.0
      X0=0.0
      DO 1 L=1,101
      DO 6 K=1,2
      Y0=0.0
      DO 2 J=1,101
      IF(L+J-2,2,3)
      RSQ=X0**2+B*Y0**2
      R0=SQRRT(RSQ0)
      W01=CFAC(R0,RSQ0)*C2(S,R0)*CEXP(C1(X0,R0))
      IF((L.EQ.1).OR.(J.EQ.1))GO TO 4
      WW0=WW0-2.0*W01
      GO TO 2
4      WW0=WW0-W01

```



```

2      Y0=Y0+YINC
6      X0=-X0
1      X0=X0+XINC(I)
      WWO=CABS(WWO)
      L1=1
      JJ=1
C INDEX CONTROL POINT OUT Y AXIS
      DO 50 L=1,M
      L2=JJ
C INDEX CONTROL POINT ALONG X AXIS
      DO 40 K=1,N
C DOUBLET ON WING/WAKE THEN IMAGE
      W=-2.0
      DO 80 J=1,2
      K3=1
C INDEX DOUBLET ALONG X AXIS
      I1=KK
      I2=LL
      NXI=NX(I)
      DO 60 KO=1,NXI
      XX=X(L2)-X(I1)
      RSQ=XX**2+B*(Y(L)**2+Y(I)**2+W*Y(L)*Y(I))
      IF(RSQ.LE.0.001)GO TO 20
      R=SQRT(RSQ)
      IF(KO-N)47,47,48
C DOWNWASH FROM WING DOUBLET
47      CAL(L1,I2)=CAL(L1,I2)+CFAC(R,RSQ)*C2(S,R)*CEXP(C1(XX,R))
      GO TO 60
C DOWNWASH FROM WAKE DOUBLET
48      CAL(L1,K2)=CAL(L1,K2)+CFAC(R,RSQ)*C2(S,R)*CEXP(C1(XX,R))*CWEX**K3
      K3=K3+1
      GO TO 60
20      CAL(L1,I2)=WWO
      I2=I2+1
60      I1=I1+1
80      W=+2.0
      L2=L2+1
40      L1=L1+1
50      JJ=JJ+NX(L)
      LL=1+NX+1
100      KK=KK+NX(I)
125      RETURN
C * * * * *
C * * * * *
C * * * * *

```



```

SUBROUTINE COMAT(N,M,A,B,D,I,MAX)
C
C SUBROUTINE COMAT SOLVES THE COMPLEX MATRIX EQUATION AX=B
C FOR X AND GIVES THE INVERSE OF A.
C
      INTEGER C,H,R,Q,Z
      COMPLEX A,B,D,TT,P
      REAL*8 DP
      DIMENSION A(MAX,N),B(MAX,M),C(100,3)
      DP=1.0
      D = (1.0,0.0)
      DO 20 J=1,N
        DO 20 C(J,3) = 0
      C SEARCH FOR PIVOT ELEMENT
      DO 21 K=1,N
        TT = (0.0,0.0)
        T = 0.0
        DO 4 J=1,N
          IF (C(J,3).EQ. 1) GO TO 4
          DO 5 H=1,N
            IF (C(H,3) - 1) 15,5,12
            IF (T.GE. CABS(A(J,H))) GO TO 5
          15 R = J
          Q = H
          T = CABS(A(J,H))
          5 CONTINUE
        4 CONTINUE
        C(Q,3) = C(Q,3) + 1
        C(K,1) = R
        C(K,2) = Q
      C INTERCHANGE ROWS TO PUT PIVOT ELEMENT ON DIAGONAL
      IF (R.EQ. Q) GO TO 11
      D = -D
      DO 8 L=1,N
        TT = A(R,L)
        A(R,L) = A(Q,L)
        8 A(Q,L) = TT
      IF (M.LE. 0) GO TO 11
      DO 2 L=1,M
        TT = B(R,L)
        B(R,L) = B(Q,L)
        2 B(Q,L) = TT
      DIVIDE PIVOT ROW BY PIVOT ELEMENT
      11 P = A(Q,Q)
      A(Q,Q) = (1.0,0.0)
      DO 13 L=1,N
        13 A(Q,L) = A(Q,L)/P

```



```

00003710
00003720
00003730
00003740
00003750
00003760
00003770
00003780
00003790
00003800
00003810
00003820
00003830
00003840
00003850
00003860
00003870
00003880
00003890
00003900
00003910
00003920
00003930
00003940
00003950
00003960
00003970
00003980
00003990
00004000
00004010
00004020
00004030
00004040
00004050
00004060

IF (M.LE. 0) GO TO 1
DO 3 L = 1,M
  3 B(Q,L) = B(Q,L)/P
C REDUCE NON-PIVOT ROWS
  1 DO 21 Z = 1,N
    IF (Z.EQ.Q) GO TO 21
    TT = A(Z,Q)
    A(Z,Q) = (0.0,0.0)
    DO 16 L = 1,N
      16 A(Z,L) = A(Z,L) - A(Q,L)*TT*DP
    IF (M.LE. 0) GO TO 21
    DO 17 L = 1,M
      17 B(Z,L) = B(Z,L) - B(Q,L)*TT*DP
  21 CONTINUE
C INTERCHANGE COLUMNS
  DO 19 II = 1,N
    L = N + 1 - II
    IF (C(L,1).EQ. C(L,2)) GO TO 19
    R = C(L,1)
    Q = C(L,2)
    DO 7 K = 1,N
      TT = A(K,R)
      A(K,R) = A(K,Q)
      7 A(K,Q) = TT
  19 CONTINUE
  DO 18 K = 1,N
    IF (C(K,3).NE. 1) GO TO 12
  18 CONTINUE
  I = 1
  50 RETURN
  12 I = 2
  GO TO 50
END
C *
C *
C *

```

```

00004070
00004080
00004090
00004100
00004110
00004120
00004130
00004140
00004150
00004160

SUBROUTINE WINGLM(CP,XI,N1,CLX,KK)
C
C SUBROUTINE WINGLM PERFORMS SPANWISE INTEGRATION OF SECTIONAL VALUES
C EXPRESSED AS MODIFIED FOURIER SERIES
C
  COMPLEX CP,CX,CLX,CD
  DIMENSION CP(N1),XI(N1),CX(12,12)
  CP(N1)=0.0
  XI(N1)=1.0

```





```

DO 10 I=1,N1
  THET=ARCCOS(1.0-2.0*XI(I))
  CX(I,1)=COS(THET/2.0)
DO 10 J=2,N1
  JJ=J-1
  CX(I,J)=SIN(JJ*THET)
10 CALL COMAT FOR FOURIER SERIES COEFFICIENTS. IF KK=2 CX IS SINGULAR.
C CALL COMAT(N1,1,CX,CP,CD,KK,12)
  IF(KK.EQ.2) GO TO 50
  CLX=0.66667*CP(1)+0.785398*CP(2)
  RETURN
50
END
C ** *
C ** *
C ** *

```

```

SUBROUTINE SECLM(CP,XI,N1,CLX,CMX,KK)
C
C SUBROUTINE SECLM PERFORMS CHORDWISE INTEGRATION OF PRESSURE
C COEFFICIENTS EXPRESSED AS FOURIER SERIES WITH LEADING EDGE
C SINGULARITY TO OBTAIN SECTIONAL AND MOMENT COEFFICIENTS.
C

```

```

  COMPLEX CP,CX,CLX,CMX,CD
  DIMENSION CP(N1),XI(N1),CX(12,12)
  CP(N1)=0.0
  XI(N1)=1.0
DO 10 I=1,N1
  THET=ARCCOS(1.0-2.0*XI(I))
  CX(I,1)=COTAN(THET/2.0)
DO 10 J=2,N1
  JJ=J-1
  CX(I,J)=SIN(JJ*THET)
10 CALL COMAT FOR FOURIER SERIES COEFFICIENTS. IF KK=2 CX IS SINGULAR.
C CALL COMAT(N1,1,CX,CP,CD,KK,12)
  IF(KK.EQ.2) GO TO 50
  CLX=0.785398*(2.0*CP(1)+CP(2))
  CMX=0.196349*(2.0*CP(1)+2.0*CP(2)-CP(3))
  CMX=0.5*CLX-CMX
  RETURN
50
END
C ** *
C ** *
C ** *

```



APPENDIX E

LISTING OF THE FORTRAN CODE FOR THE WING/BODY PROGRAM



# DISCRETE POTENTIAL ELEMENT WING/BODY PROGRAM

```

C WING/BODY PROGRAM COMPUTES THE NONSTEADY LOADING ON AN HARMONICALLY
C OSCILLATING PLANAR WING MIDMOUNTED ON A CYLINDRICAL FUSELAGE
C
C
10      IMPLICIT COMPLEX(C)
13      REAL*8 DP
15      DIMENSION CA(100,100),CKI(130),CU5(100),C5(100),
26      1CPH5(100),Z(100),P5(100),P6(100),CP5(12),XX5(12),
28      2XET5(12),CKBW(130,100),CKB(130,130),CKWB(100,130),
      COMMON/COM2/F,A,MB,NC,XC,XB,MN,MNW,KB,MS,DELTH
      COMMON/COM3/XM,S,XINC,N,NW,BR,YINC,M
      COMMON/COM4/CUFAC,DP,MPI,MNPN,MNPI,N2
      EQUIVALENCE (CKB(1),CA(1)),(CKB(10001),CKBW(1))
      FORMAT(3F10.4,2I10,F10.4)
13      FORMAT(7F10.4)
15      FORMAT(4I5,3F10.4,I5)
26      FORMAT(1H1,ON CYLINDRICAL FUSELAGE,/)
28      1FMOUNT(//,MACHNO=F8.3,SPEED OF SOUND=F8.3,FPS,/,FREQUENCY=F8.3,CHORD=
      1,F8.3,FT,/,SEMI-SPAN=F8.3,FT,/,SPANWISE INCREMENT=F8.3,FT,/,
      2,F8.3,FT,/,SEMI-SPAN=F8.3,FT,/,SPANWISE INCREMENT=F8.3,FT,/,
      3,F8.3,FT,/,SEMI-SPAN=F8.3,FT,/,SPANWISE INCREMENT=F8.3,FT,/,
      4,SIGNIFICANT WAKE=F8.3,FT,/,CHORDS,/,REDUCED FREQUENCY=F8.3,
      5F8.3,/,BODY RADIUS=F8.3,/)
30      FORMAT(5(IPE13.3,IPE11.3))
38      FORMAT(//,COEFFICIENT OF PRESSURE,/)
40      FORMAT(//,DOWNWASH VELOCITY INFLUENCE COEFFICIENT MATRIX IS
      1SINGULAR,/)
41      FORMAT(//,BODY NORMALWASH INFLUENCE COEFFICIENT MATRIX (CKB) IS
      1SINGULAR,/)
70      FORMAT(//,INPUT Z MATRIX,/)
71      FORMAT(10(IPE12.3,))
72      FORMAT(//,DOWNWASH VELOCITY MATRIX,/)
74      FORMAT(//,CHECK ON COMAT, SHOULD EQUAL DOWNWASH VELOCITY MATRIX
      1,/)
      DP=1.0
      N2=12
C READ INPUT DATA
31      READ(5,10)XM,F,A,ICH,JCH,ALPH

```



```

32 IF(ICH.EQ.1)GO TO 42
   READ(5,15)N,M,MB,NC,XC,XB,BR,MS
   XINC=XC/(2*N)
   YINC=XB/(2*M)
   MN=M*NC
   NW=N*NC
   MPI=M+1
   MNMN=MN-M
   MNP1=MNMN+1
   C CHECK ON INPUT DATA
42 WRITE(6,26)
   B=1.0-XM**2
   S=F/(A*B)
   XK=(F*XC)/(2.0*XM*A)
   UFAC=XM*A/(2.0*XINC)
   CUFAC=CMPLX(0.0,F/UFAC)
   WRITE(6,28)XM,F,A,XC,XB,XINC,YINC,NC,XK,BR
   IF(JCH.EQ.1)GO TO 34
   C READ WING DISPLACEMENT INPUT
   K=M
   DO 90 J=1,MN,M
     READ(5,13)(Z(I),I=J,K)
90   K=K+M
     WRITE(6,70)
     WRITE(6,71)(Z(J),J=1,MN)
34   IF(MB.EQ.0)GO TO 48
   C INCORPORATE BODY EFFECT.
   C ESTABLISH BODY GRID
3   DELTH=C.785398/MS
   KB=MB/MS
   MB=KB*MS
   C CALL SUBROUTINE UTHETA TO CALCULATE DOWNWASH INFLUENCE COEFFICIENTS
   C ON WING DUE TO BODY SINGULARITIES.
     CALL UTHETA(CKWB,100,130)
   C CALL SUBROUTINE URAD2 TO CALCULATE NORMALWASH IC'S ON BODY DUE TO
   C BODY SINGULARITIES.
     CALL URAD2(CKB,130)
   C CALL COMAT TO CALCULATE INVERSE OF CKB. IF KK=2, CKB IS SINGULAR.
     CALL COMAT(MB,0,CKB,CB,CD,CK,130)
     IF(KK.CQ.2)GO TO 205
     DO 43 I=1,MN
     DO 45 J=1,MB
       CKI(J)=0.0
45     CKI(J)=CKI(J)+CKWB(I,K)*CKB(K,J)
     DO 44 J=1,MB
44     CKWB(I,J)=CKI(J)

```





```

43 CONTINUE
C CALL SUBROUTINE URAD1 TO CALCULATE NORMALWASH ON BODY DUE TO WING.
CALL URAD1(CKBW,130)
48 CONTINUE
C CALL SUBROUTINE DINCO TO CALCULATE DOWNWASH INFLUENCE COEFFICIENT
C MATRIX CA
CALL DINCO(CA,100)
IF(MB.EQ.0)GO TO 49
C COMBINE BODY IC MATRICES WITH WING IC MATRIX.
DO 46 I=1,MN
DO 46 J=1,MN
DO 46 K=1,MB
46 CA(I,J)=CA(I,J)-.5*CKWB(I,K)*CKWB(K,J)
49 CONTINUE
IF(ALPH.LE.0.001)GO TO 6
C CALCULATE DOWNWASH VELOCITY VECTOR FOR PITCHING MOTION
AA=0.5*XC
X=XINC
I=0
DO 5 K=1,N
AB=F*(AA-X)
CAB=CMPLX(0.0,AB)
CU5K=ALPH*(CAB-XM*A)
DO 4 J=1,M
I=I+1
4 CU5(I)=CU5K
5 X=X+2.0*XINC
6 CONTINUE
C CALCULATE DOWNWASH VELOCITIES (CUN) FROM INPUT DEFLECTIONS (Z)
IF(ALPH.GT.0.001)GO TO 56
DO 50 J=1,M
50 CU5(J)=UFAC*(Z(J+M)-(1.0-CUFAC*DP)*Z(J))
55 CU5(J)=(UFAC/2.0)*(Z(J+M)+(2.0-CUFAC)*Z(J)-Z(J-M)*DP)
60 CU5(J)=UFAC*(1.0+CUFAC)*Z(J)-Z(J-M)*DP
56 CONTINUE
C PRINT OUT DOWNWASH VELOCITY MATRIX
WRITE(6,72)
WRITE(6,30) (CU5(J),J=1,MN)
C CALL SUBROUTINE COMAT TO SOLVE SYSTEM OF EQUATIONS FOR DIPOLE
C STRENGTHS(CUN). CA MATRIX IS INVERSE OF INPUT COEFFICIENT MATRIX
C KI IS INDICATOR WHICH EQUALS 2 IF CA IS SINGULAR
CALL COMAT(MN,1,CA,CU5,CD,KI,100)
IF(KI.EQ.2)GO TO 200
C CALL SUBROUTINE PRES TO CALCULATE AND PRINT PRESSURE DISTRIBUTIONS,
C AND SECTIONAL AND WING LIFT AND MOMENT VALUES.
CALL PRES(C5,CPH5,P5,P6,CP5,XX5,CL5,CM5,XET5,CU5)

```

```

00000880
00000890
00000900
00000910
00000920
00000930
00000940
00000950
00000960
00000970
00000980
00000990
00001000
00001010
00001020
00001030
00001040
00001050
00001060
00001070
00001080
00001090
00001100
00001110
00001120
00001130
00001140
00001150
00001160
00001170
00001180
00001190
00001200
00001210
00001220
00001230
00001240
00001250
00001260
00001270
00001280
00001290
00001300
00001310
00001320
00001330
00001340
00001350

```



```

200 GO TO 31
205 WRITE(6,40)
205 WRITE(6,41)
140 STOP
C ** * * * * * * * * * * * * * * * * * * * * * *
C ** * * * * * * * * * * * * * * * * * * * * * *
C ** * * * * * * * * * * * * * * * * * * * * * *
C ** * * * * * * * * * * * * * * * * * * * * * *
00001360
00001370
00001380
00001390
00001400
00001410
00001420
00001430

```

```

C SUBROUTINE PRES(CP,CPHI,PA,PP,CPS,XXI,CLW,CMW,XETA,CUN)
C
C SUBROUTINE PRES CALCULATES AND WRITES WING PRESSURE COEFFICIENT
C DISTRIBUTIONS, AND SECTIONAL AND WING LIFT AND MOMENT COEFFICIENTS.
C

```

```

C IMPLICIT COMPLEX (C)
C REAL*8 DP
C DIMENSION CP(MN),CPHI(MN),PA(MN),PP(MN),CPS(N2),XXI(N2),CLW(N2),
C 1CMW(N2),XETA(N2),CUN(MN)
C COMMON/COM2/F,A,MB,NC,XC,XB,MN,MNW,KB,MS,DELTH
C COMMON/COM3/B,XM,S,XINC,N,NW,BR,YINC,M
C COMMON/COM4/CFAC,DP,MPI,MNMN,MNPI,N2
C FORMAT(///,' SPANWISE COEFFICIENT MATRIX SINGULAR',///)
C 39 FORMAT(///,' CHORDWISE COEFFICIENT MATRIX SINGULAR',///)
C 41 FORMAT(///,' ETA =',F8.4///4X,'X/C',12X,'DCUBLET POTENTIAL STRE
C 64 NGTH',9X,'PRESSURE COEFFICIENT',4X,'PRESSURE AMPLITUDE',5X,
C 2,PHASE ANGLE,/)
C 66 FORMAT(F10.4,2(1PE20.3),2(1PE20.3)/)
C 76 FORMAT(/,' SECTION LIFT COEFFICIENT: AMPLITUDE =',1PE13.3,
C 1, AMPLITUDE =',1PE13.3,' SECTION MOMENT COEFFICIENT: ',
C 2, AMPLITUDE =',1PE13.3,' PHASE ANGLE =',1PE13.3/)
C 78 FORMAT(///,' WING LIFT COEFFICIENT: AMPLITUDE =',1PE13.3,
C 1, PHASE ANGLE =',1PE13.3,' WING MOMENT COEFFICIENT: ',
C 2, AMPLITUDE =',1PE13.3,' PHASE ANGLE =',1PE13.3///)
C COMPUTE WING VELOCITY POTENTIAL DISTRIBUTION
C AR2=8.0*XINC*YINC
C DO 85 J=1,MN
C 85 CPHI(J)=-CUN(J)/AR2
C COMPUTE WING PRESSURE COEFFICIENT DISTRIBUTION.
C PFAC=-1.0/(XM*A*XINC)
C DO 100 J=1,M
C 100 CP(J)=PFAC*(CPHI(J+M)+2.0*CUFAC*CPHI(J))
C DO 110 J=MP1,MNMN
C 110 CP(J)=PFAC*(CPHI(J+M)+2.0*CUFAC*CPHI(J)-CPHI(J-M)*DP)
C DO 120 J=MNPI,MN
C 120 CP(J)=PFAC*((2.0*CUFAC+1.0/CEXP(CUFAC))*CPHI(J)-CPHI(J-M)*DP)
C NORMALIZE CP WITH RESPECT TO ANGLE OF ATTACK AMPLITUDE

```



```

ALH=-0.1 J=1,MN
DO 210 CP(J)=CP(J)/ALH
210 C COMPUTE PRESSURE COEFFICIENT AMPLITUDE AND PHASE ANGLE
DO 230 J=1,MN
230 PA(J)=ABS(CP(J))
PP(J)=57.29578*ATAN2(AIMAG(CP(J)),REAL(CP(J)))
XSCF=2.0*XINC/XC
ETAF=2.0*YINC/XB
ETA=ETAF/2.0
C COMPUTE AND WRITE RESULTS FOR EACH SPANWISE STATION
DO 155 J=1,M
WRITE(6,64)ETA
XSC=XSCF/2.0
K=1
C WRITE CHORDWISE PRESSURE DISTRIBUTIONS
DO 220 I=J,MN,M
CPS(K)=CP(I)
XXI(K)=XSC
WRITE(6,66) XSC,CUN(I),CP(I),PA(I),PP(I)
K=K+1
220 XSC=XSC+XSCF
C CALL SUBROUTINE SECLM FOR SECTIONAL LIFT AND MOMENT COEFFICIENTS
CALL SECLM(CPS,XXI,K,CSL,CSM,KK1)
IF(KK1.EQ.2) GO TO 201
SLA=ABS(CSL)
SLP=57.29578*ATAN2(AIMAG(CSL),REAL(CSL))
SMA=CBS(CSM)
SMP=57.29578*ATAN2(AIMAG(CSM),REAL(CSM))
WRITE(6,76)SLA,SLP,SMA,SMP
CLW(J)=CSL
CMW(J)=CSM
XETA(J)=ETA
155 ETA=ETA+ETAF
C CALL SUBROUTINE WINGLM FOR WING LIFT COEFFICIENT
JJ=M+1
CALL WINGLM(CLW,XETA,JJ,CL,KK2)
IF(KK2.EQ.2) GO TO 202
XLA=ABS(CL)
XLP=57.29578*ATAN2(AIMAG(CL),REAL(CL))
C CALL SUBROUTINE WINGLM FOR WING MOMENT COEFFICIENT
CALL WINGLM(CMW,XETA,JJ,CM,KK2)
XMA=CBS(CM)
XMP=57.29578*ATAN2(AIMAG(CM),REAL(CM))
WRITE(6,78)XLA,XLP,XMA,XMP
203 RETURN
201 WRITE(6,41)
GO TO 203

```



```

202 WRITE(6,39)
GO TO 203
END
C ** * * * * * * * * * * * * * * * * * * * * * *
C ** * * * * * * * * * * * * * * * * * * * * * *
C ** * * * * * * * * * * * * * * * * * * * * * *
00002300
00002310
00002320
00002330
00002340
00002350

SUBROUTINE DINCO(CAL,MAX1)
00002360
00002370
00002380
00002390
00002400
00002410
00002420
00002430
00002440
00002450
00002460
00002470
00002480
00002490
00002500
00002510
00002520
00002530
00002540
00002550
00002560
00002570
00002580
00002590
00002600
00002610
00002620
00002630
00002640
00002650
00002660
00002670
00002680
00002690
00002700
00002710
00002720
00002730
00002740
00002750

SUBROUTINE DINCO CALCULATES THE DOWNWASH INFLUENCE COEFFICIENT MATRIX
OF THE WING DUE TO WING AND WAKE SINGULARITIES.

IMPLICIT COMPLEX(C)
COMPLEX W01,W0
DIMENSION CAL(MAX1,MN)
COMMON/COM2/F,A,MB,NC,XC,XB,MN,MNW,KB,MS,DELTH
COMMON/COM3/B,XM,S,XINC,N,NW,BR,YINC,M
EX(X,R)=S*(XM*X-R)
CFAC(R,Z)=-B/(12.5663*R*Z)
C1(X,R)=CMPLX(0.0,EX(X,R))
C2(S,R)=CMPLX(1.0,S*R)
NXKO=NW+N
WAKE=-F*2.0*XINC/(XM*A)
CWAKE=CMPLX(0.0,WAKE)
CWEX=CEXP(CWAKE)
C INITIALIZE MATRICES TO ZERO
DO 132 I=1,MN
DO 132 J=1,MN
132 CAL(I,J)=(0.0,0.0)
C CALCULATE UPWASH AT SINGULARITY
W0=0.0
X0=0.0
DO 1 I=1,101
DO 6 K=1,2
Y0=0.0
DO 2 J=1,101
IF(I+J-2)2,2,3
RSQ0=X0**2+B*Y0**2
RO=SQRT(RSQ0)
W01=CFAC(RO,RSQ0)*C2(S,RO)*CEXP(C1(X0,RO))
IF((1.EQ.1).OR.(J.EQ.1))GO TO 4
W0=W0-2.0*W01
GO TO 2
W0=W0-W01
Y0=Y0+2*YINC
X0=-X0
4
2
6

```





```

1      XO=XO+2*XINC
      WWO=CABS(WWO)
C  CALCULATE DOWNWASH MATRIX
      XDI=2.0*XINC
      YDI=2.0*YINC
C  INDEX CONTROL POINT OUT Y AXIS
      Y=BR+YINC
      DO 40 L=1,M
      L1=L
C  INDEX CONTROL POINT ALONG X AXIS
      XCP=0.0
      DO 50 K=1,N
      INDEXING DOUBLET LOCATION OUT POSITIVE Y AXIS
      RO=BR+YINC
      DO 90 I=1,M
      K2=MN-M+I
C  DOUBLET ON WING/WAKE THEN IMAGE
      W=-2.0
      DO 80 J=1,2
      I1=I
      K3=1
C  INDEX DOUBLET ALONG X AXIS
      XD=0.0
      DO 60 KO=1,NXKO
      X = XCP-XD
      RSQ=X**2+BB*(Y**2+RO**2+W*Y*RO)
      IF(RSQ.LE.0.001)GO TO 20
      R=SQRT(RSQ)
      IF(KO-N)47,47,48
C  DOWNWASH FROM WING DOUBLET
47      CAL(L1,I1)=CAL(L1,I1)+CFAC(R,RSQ)*C2(S,R)*CEXP(C1(X,R))
      I1=I1+M
      GO TO 60
C  DOWNWASH FROM WAKE DOUBLET
48      CAL(L1,K2)=CAL(L1,K2)+CFAC(R,RSQ)*C2(S,R)*CEXP(C1(X,R))*CWEX**K3
      K3=K3+1
      GO TO 60
20      CAL(L1,I1)=WWO
      I1=I1+M
      XD=XD+XDI
      W=+2.0
      RO=RO+YDI
      L1=L1+M
      XCP=XCP+XDI
      Y=Y+YDI
125    RETURN
      END
C  * * * * *

```







```
C INDEX DOUBLET IN X DIRECTION
K3=1
DO 60 KK=1,NXKO
X=XCP-XD
RSQ=X**2+R1
R=SQR(T(RSQ))
DR=B*(BR+W*RO*T1/2.0)/R
C3=(1.0-(3.0*BR*DR))/R
C4=S**2*BR*DR
IF(KK.GT.N)GO TO 50
C NORMALWASH ON BODY FROM WING DOUBLET
CAL(J1,K1)=CAL(J1,K1)+CFAC(R,RSQ)*T2*(C3*C2(S,R)+C4)*CEXP(C1(X,R))
KI=K1+M
GO TO 60
C NORMALWASH ON BODY FROM WAKE DOUBLET
50 CAL(J1,K2)=CAL(J1,K2)+CFAC(R,RSQ)*T2*(C3*C2(S,R)+C4)*CEXP(C1(X,R))
1*CWEX**K3
60 XD=XD+2.0*XINC
70 DRO=DRO+2.0*YINC
80 J1=J1+MS
90 XCP=XCP+XDI
100 THE=THE+2.0*DELTH
W=2.0
RETURN
END
C * * * * *
C * * * * *
C * * * * *
SUBROUTINE URAD2(CB,MAX)
C
C SUBROUTINE URAD2 CALCULATES NORMALWASH INFLUENCE COEFFICIENTS ON
C BODY DUE TO BODY SINGULARITIES.
C
IMPLICIT COMPLEX(C)
REAL COS
COMPLEX WO1,WVO
DIMENSION CB(MAX,MAX)
COMMON/COM2/F,A,M,B,NC,XC,XB,MN,MNW,KB,MS,DELTH
COMMON/COM3/B,XM,S,XINC,N,NW,BR,YINC,M
EX(X,R)=S*(XM*X-R)
CFAC(R,Z)=-B/(12.5663*R*Z)
C1(X,R)=CMPLX(0.0,EX(X,R))
C2(S,R)=CMPLX(1.0,S*R)
C INITIALIZE MATRIX TO ZERO
```



```

30      DO 30 I=1,MB
        DO 30 J=1,MB
          CB(I,J)=0.0
          THEO I=DELTH
          XDI=6*XC/KB
          YDI=BR*2.0*DELTH
        C CALCULATE UPWASH AT SINGULARITY
          WOI=0.0
          THE=0.0
          MS1=4*MS
          X=XDI
          DO 210 I=1,MS1
            T3=BR*(1.0-COS(THE))
            R1=2.0*B*T3*BR
            DO 220 J=1,101
              RSQ=X**2+R1
              R=SQRT(RSQ)
              IF(I.EQ.1)GO TO 202
              DR=B*T3/R
              C3=COS(THE)+3.0*DR*T3/R
              C4=S**2*DR*T3
              GO TO 204
            202      C3=1.0
            204      C4=0.0
            C5=C*FAC(R,RSQ)*(C3*C2(S,R)-C4)
            WOI=WOI-C5*CEXP(C1(X,R))
            IF(X.LE.0.001)GO TO 220
            WOI=WOI-C5*CEXP(C1(-X,R))
            220      X=X+XDI
            X=0.0
            210      THE=THE+2.0*DELTH
              WWO=CABS(WOI)
              WW=1.0
            C COMPUTE URADIAL FOR QUADRANTS 1 & 2, THEN FOR QUADRANTS 3 & 4
              W=1.0
              DO 100 I=1,4
                THE=DELTH
                IF(I-2)14,14,12
              12      W=-1.0
              14      CONTINUE
            C INDEX CONTROL POINTS FROM 0 TO 90 DEGREES
              DO 90 J=1,MS
                J1=J
                XCP=0.0
            C INDEX CONTROL POINT ALONG X AXIS
              DO 80 K=1,KB
                THEO=THEO I
            C INDEX DOUBLET FROM 0 TO 90 DEGREES

```





```

DO 70 JJ=1,MS
K1=JJ
T3=BR*(1.0-COS(THE-THEO))
R1=2.0*B*T3*BR
XD=0.0
C INDEX DOUBLET IN X DIRECTION
DO 60 KK=1,KB
X=XCP-XD
RSQ=X**2+R1
IF(RSQ.LE.0.001)GO TO 20
R=SQRT(RSQ)
IF(T3.LE.0.001)GO TO 38
DR=B*T3/R
C3=COS(THE-THEO)+3.0*DR*T3/R
C4=S**2*DR*T3
GO TO 40
38 C3=1.0
C4=0.0
40 CB(J1,K1)=CB(J1,K1)+W*CFAC(R,RSQ)*(C3*C2(S,R)-C4)*CEXP(C1(X,R))
GO TO 55
20 CB(J1,K1)=WWO
55 K1=K1+MS
60 XD=XD+XDI
70 THEO=THEO+WW*2.0*DELTH
80 J1=J1+MS
90 XCP=XCP+XDI
THE=THE+2.0*DELTH
WW=-WW
IF(I-2)95,100,92
THEOI=- (3.141593-DELTH)
95 GO TO 100
92 THEOI=DELTH
100 THEOI=-THEOI
RETURN
END
C * * * * *
C * * * * *
C * * * * *

```

```

SUBROUTINE UTHETA(CWB,MAX1,MAX2)
C
C SUBROUTINE UTHETA CALCULATES DOWNWASH INFLUENCE COEFFICIENTS ON WING
C DUE TO BODY SINGULARITIES.
C
C IMPLICIT COMPLEX(C)
C REAL COS

```



```

DIMENSION CWB(MAX1,MAX2)
COMMON/COM2/F,A,MB,NC,XC,XB,MN,MNW,KB,MS,DELTH
COMMON/COM3/B,XM,S,XINC,N,NW,BR,YINC,M
EX(X,R)=S*(XM*X-R)
CFAC(R,Z)=+B/((12.5663*R*Z))
C1(X,R)=CMPLX(0.0,EX(X,R))
C2(S,R)=CMPLX(1.0,S*R)
XDI=6*XC/KB
C INITIALIZE MATRIX TO ZERO
DO 33 I=1,MN
DO 33 J=1,MB
CWB(I,J)=0.0
THEO(I)=DELTH
33
WV=1.0
C COMPUTE UTHETA FOR DOUBLET IN QUADRANTS 1 & 2, THEN FOR QUADRANTS 3
C AND 4
DO 100 I=1,2
Y=BR+YINC
C INDEX CONTROL POINT OUT Y AXIS
DO 90 J=1,M
J1=J
W=2.0/Y
R2=B*(Y**2+BR**2)
XCP=XC-XINC
C INDEX CONTROL POINT ALONG X AXIS
DO 80 K=1,N
THEO=THEO1
C INDEX DOUBLET AROUND CIRCUMFERENCE
DO 70 JJ=1,MS
K1=JJ
T1=Y*COS(THEO)
T2=Y*SIN(THEO)
T3=BR-T1
R1=R2-2.0*B*BR*T1
XD=0.0
C INDEX DOUBLET IN X DIRECTION
DO 60 KK=1,KB
X=XCP-XD
RSQ=X**2+R1
R=SQR1(RSQ)
DR=-B*BR*T2/R
C3=-T2-3.0*DR*T3/R
C4=S**2*R*DR*T3
CWB(J1,K1)=CWB(J1,K1)+W*CFAC(R,RSQ)*((C3*C2(S,R)+C4)*CEXP(C1(X,R)))
K1=K1+MS
XD=XD+XDI
THEO=THEO+WW*2.0*DELTH
J1=J1+M
60
70
00005100
00005110
00005120
00005130
00005140
00005150
00005160
00005170
00005180
00005190
00005200
00005210
00005220
00005230
00005240
00005250
00005260
00005270
00005280
00005290
00005300
00005310
00005320
00005330
00005340
00005350
00005360
00005370
00005380
00005390
00005400
00005410
00005420
00005430
00005440
00005450
00005460
00005470
00005480
00005490
00005500
00005510
00005520
00005530
00005540
00005550
00005560
00005570

```



80	XCP=XCP+2.0*XINC	00005580
90	Y=Y+2.0*YINC	00005590
92	WW=-1.0	00005600
100	THEOI=3.141593-DELTH	00005610
	RETURN	00005620
	END	00005630
*	*	00005640
C	*	00005650
C	*	00005660

```
C SUBROUTINE COMAT(N,M,A,B,D,I,MAX)
C
C SUBROUTINE COMAT SOLVES THE COMPLEX MATRIX EQUATION AX=B
C FOR X AND GIVES THE INVERSE OF A.
C C C
00005670
00005680
00005690
00005700
00005710
00005720
00005730
```

```

INTEGER C,H,R,Q,Z
COMPLEX A,B,D,TT,P
REAL*8 DP
DIMENSION A(MAX,N),B(MAX,M),C(130,3)
00005730
00005740
00005750
00005760
00005770

```

```

01 1,0,0,0,0)
D = (1,0,0,0)
DO 20 J = 1,N
20 C(J,3) = 0
C SEARCH FOR PIVOT ELEMENT
DO 21 K = 1,N
TT = (0.0,0.0)
T = 0.0
DO 4 J = 1,N
IF (C(J,3) .EQ. 1) GO TO 4
DO 5 H = 1,N
IF (C(H,3) - 1) 15,5,12
15 IF (T .GE. CABSA(A(J,H))) GO TO 5
00005780
00005790
00005800
00005810
00005820
00005830
00005840
00005850
00005860
00005870
00005880
00005890
00005900

```

[illegible]

```

C(K,Z) = Q
C INTERCHANGE ROWS TO PUT PIVOT ELEMENT ON DIAGONAL
IF (R.EQ. Q) GO TO 11
D = -D
DO 8 L = 1,N
TT = A(R,L)
A(R,L) = A(Q,L)

```









```

SUBROUTINE WINGLM(CP,XI,N1,CLX,KK)
C
C
C SUBROUTINE WINGLM PERFORMS SPANWISE INTEGRATION OF SECTIONAL VALUES
C EXPRESSED AS MODIFIED FOURIER SERIES
C
      COMPLEX CP,CX,CLX,CD
      DIMENSION CP(N1),XI(N1),CX(12,12)
      CP(N1)=0.0
      XI(N1)=1.0
      DO 10 I=1,N1
        THET=ARCCOS(1.0-2.0*XI(I))
        CX(I,1)=COS(THET/2.0)
        DO 10 J=2,N1
          JJ=J-1
          CX(I,J)=SIN(JJ*THET)
10    CALL COMAT FOR FOURIER SERIES COEFFICIENTS. IF KK=2 CX IS SINGULAR.
C
      CALL COMAT(N1,1,CX,CP,CD,KK,12)
      IF(KK.EQ.2) GO TO 50
      CLX=0.66667*CP(1)+0.785398*CP(2)
      RETURN
50    END
C
C
C

```

```

SUBROUTINE SECLM(CP,XI,N1,CLX,CMX,KK)
C
C
C SUBROUTINE SECLM PERFORMS CHORDWISE INTEGRATION OF PRESSURE
C COEFFICIENTS EXPRESSED AS FOURIER SERIES WITH LEADING EDGE
C SINGULARITY TO OBTAIN SECTIONAL AND MOMENT COEFFICIENTS.
C
      COMPLEX CP,CX,CLX,CMX,CD
      DIMENSION CP(N1),XI(N1),CX(12,12)
      CP(N1)=0.0
      XI(N1)=1.0
      C COMPUTE TRIG VALUES FOR CP=A(0)*TAN(THETA/2)+ SUM OF A(N)*SIN(N*THETA)
      DO 10 I=1,N1
        THET=ARCCOS(1.0-2.0*XI(I))
        CX(I,1)=COTAN(THET/2.0)
        DO 10 J=2,N1
          JJ=J-1
          CX(I,J)=SIN(JJ*THET)
10    CALL COMAT FOR FOURIER SERIES COEFFICIENTS. IF KK=2 CX IS SINGULAR.
C
      CALL COMAT(N1,1,CX,CP,CD,KK,12)
      IF(KK.EQ.2) GO TO 50

```







## LIST OF REFERENCES

1. Landahl, M. T. and Stark, V. J. E., "Numerical Lifting-Surface Theory - Problems and Progress," AIAA Journal, v. 6, no. 11, p. 2049-2060, November 1968.
2. Küssner, H. G., "Allgemeine Tragflächentheorie," Lustfahrtforschung, v. 17, no. 11/12, p. 370-378, 10 December 1940. (translated NACA Tech. Memo. 979, 1941).
3. NACA Report 1234, On the Kernel Function of the Integral Equation Relating the Lift and Downwash Distributions of Oscillating Finite Wings in Subsonic Flow, by C. E. Watkins, H. L. Runyan, and D. S. Woolston, 1955.
4. Stark, V. J. E., Calculation of Lifting Forces on Oscillating Wings, Ph.D. Thesis, Royal Institute of Technology, Stockholm, 1964.
5. Laschka, B., "Zur Theorie der harmonisch schwingenden tragenden Fläche bei Unterschallanströmung," Z. Flugwiss., v. 11, p. 265-292, July 1963.
6. Air Force Flight Dynamics Laboratory Technical Report 69-2, Some New Concepts in Oscillatory Lifting Surface Theory, by J. C. Houbolt, June 1969.
7. Ashley, H., "Some Considerations Relative to the Prediction of Unsteady Air Loads on Lifting Configurations," Journal of the Aeronautical Sciences, v. 8, no. 10, p. 747-756, October 1971.
8. Haviland, J. K., "Downwash-Velocity Potential Method for Lifting Surfaces," AIAA Journal, v. 9, no. 11, p. 2268-2269, November 1971.
9. Garrick, I. E., Nonsteady Wing Characteristics, sec. F, v. VII, Aerodynamic Components of Aircraft at High Speeds, p. 658-759, Princeton Univ. Press, 1957.
10. Liepmann, H. W. and Roshko, A., Elements of Gasdynamics, p. 178-201, Wiley and Sons, 1957.
11. Landahl, M., "Pressure Loading Functions for Oscillating Wings with Control Surfaces," AIAA Journal, v. 6, no. 2, p. 345-348, February, 1968.
12. Van Dyke, M., Perturbation Methods in Fluid Mechanics, Academic Press, 1964.



13. Miles, J. W., The Potential Theory of Unsteady Supersonic Flow, p. 4-15, Cambridge Univ. Press, 1959.
14. Küssner, H. G., "Zusammenfassender Bericht über den instationären Auftrieb von Tragflügeln," Luftfahrtforschung, v. 13, p. 410-424, 1936.
15. von Kármán, Th. and Sears, W. R., "Airfoil Theory for Non-Uniform Motion," Journal of the Aeronautical Sciences, v. 5, p. 379-390, 1938.
16. Aeronautical Research Council, Great Britain R and M 3157, A Method for Calculating the Lifting Forces on Wings (Unsteady Subsonic and Supersonic Lifting Surface Theory), by J. R. Richardson, 1960.
17. NASA Report R-48, A Systematic Procedure for Determining Aerodynamic Forces on Oscillating or Steady Finite Wings at Subsonic Speeds, by C. E. Watkins, D. S. Woolston, and H. J. Cunningham, 1959.
18. Rodden, W. P. and Rebell, J. D., "The Status of Unsteady Aerodynamic Influence Coefficients," AIAA Journal, v. 1, no. 3, p. 724-725, March 1963.
19. Stark, V. J. E., "On the Approximation of the Normal Velocity on Oscillating Wings," AIAA Journal, v. 4, no. 12, p. 2236-2239, December 1966.
20. Royal Aircraft Establishment, Great Britain Technical Report 67103, An Application of Flax's Variational Principle to Lifting Surface Theory, by D. E. Davies, April 1967.
21. Ashley, H., Widnall, S., and Landahl, M. T., "New Directions in Lifting-Surface Theory," AIAA Journal, v. 3, no. 1, p. 3-16, January, 1965.
22. Aeronautical Research Council, Great Britain R and M 2470, The Calculation for Wings of Any Plan Form in Non-Uniform Motion, by W. P. Jones, 1952.
23. Biot, M. A., "Some Simplified Methods in Airfoil Theory," Journal of the Aeronautical Sciences, v. 9, p. 186-190, 1942.
24. van Spiegel, E., "Boundary Value Problems in Lifting Surface Theory," Verslagen en Verhandelingen, v. 22, National Luchtvaartlaboratorium, Amsterdam, 1959.
25. NACA TN 3694, Method for Calculating the Aerodynamic Loading on an Oscillating Finite Wing in Subsonic and Sonic Flow, by H. L. Runyan and D. S. Woolston, August 1956.





26. Rowe, W. S., "Collocation Method for Calculating the Aerodynamic Pressure Distributions on a Lifting Surface Oscillating in Subsonic Compressible Flow," AIAA Symposium on Structural Dynamics and Aeroelasticity, p. 31-45, September 1965.
27. Aeronautical Research Council, Great Britain R and M 2884, Methods for Calculating the Lift Distribution of Wings, by H. Multhopp, 1955.
28. Truckenbrody, E., "Tragflächentheorie bei incompressibler Stromung," Jahrbuch 1953 der Wissenschaftlichen Gesellschaft für Luftfahrt E. V. (WGL), Braunschweig, p. 40-65, 1954.
29. Wieghardt, K., "Über die Auftriebsverteilung des einfachen Rechteckflügels über die Tiefe," Zeitschrift für Angewandte Mathematik und Mechanik, v. 19, no. 5, p. 257-270, 1939.
30. Boeing Co. Report D6-9244, Theoretical Characteristics of Arbitrary Wings by a Non-Planar Vortex Lattice Method, by P. E. Rubbert, 1964.
31. Grumman Aircraft Engineering Corp, Report ADR 01-02-64.1, A Lifting Surface Method for Calculating Load Distributions and the Aerodynamic Influence Coefficient Matrix for Wings in Subsonic Flow, by J. Dulmovits, 1964.
32. Flygtekniska Forskingsanstalten (FFA) Report 105, Vortex Lattice Method for Calculation of Quasi Steady State Loadings on Elastic Wings in Subsonic Flow, by S. Hedman, 1966.
33. Albano, E. and Rodden, W. P., "A Doublet-Lattice Method for Calculating Lift Distributions on Oscillating Surfaces in Subsonic Flows," AIAA Journal, v. 7, no.2, p. 279-285, February 1969; errata v. 7, no. 11, p. 2192, November 1969.
34. Aeronautical Research Council, Great Britain R and M 3422, Generalised Aerodynamic Forces on a T-Tail Oscillating Harmonically in Subsonic Flow, by D. E. Davies, 1966.
35. Landahl, M. T., "Kernel Function for Nonplanar Oscillating Surfaces in a Subsonic Flow," AIAA Journal, v. 5, no. 5, p. 1045-1046, May 1967.
36. Air Force Flight Dynamics Laboratory Technical Report 54-152 Pt. I, Unsteady Aerodynamics for Advanced Configurations. Part I - Application of the Subsonic Kernel Function to Nonplanar Lifting Surfaces, by H. T. Vivian and L. V. Andrew, May 1965.



37. Laschka, B., Interfering Lifting Surfaces in Subsonic Flow, paper presented at AGARD Structures and Materials Panel Meeting, 29th, Istanbul, Turkey, 28 September 1969.
38. Rodden, W. P., Giesing, J. P., and Kalman, T. P., New Developments and Applications of the Subsonic Doublet-Lattice Method for Nonplanar Configurations, paper presented at AGARD symposium on Unsteady Aerodynamics for Aeroelastic Analyses of Interfering Surfaces, Tonsberg Oslofjorden, Norway, 3 November 1970.
39. Milne-Thomson, L. M., Theoretical Hydrodynamics, p. 206-220, MacMillan Co., 1955.
40. Aeronautical Research Council, Great Britain R and M 2872, An Extension of Multhopp's Method of Calculating the Spanwise Loading of Wing-Fuselage Combinations, by J. Weber, D. A. Kirby, and D. J. Kettle, 1956.
41. Woodward, F. A., "Analysis and Design of Wing-Body Combinations at Subsonic and Supersonic Speeds," Journal of Aircraft, v. 5, no. 6, p. 528-534, November-December 1968.
42. McCormick, J. M. and Salvadori, M. G., Numerical Methods in FORTRAN, Prentice-Hall, 1964.
43. Laschka, B. and Schmid, H., Unsteady Aerodynamic Forces on Coplanar Lifting Surfaces in Subsonic Flow (Wing-Horizontal Tail Interference), paper presented at the AGARD Structures and Materials Panel Meeting, Ottawa, Canada, 25 September 1967.
44. Pao Tan Hsu, Some Recent Developments in the Flutter Analysis of Low-Aspect-Ratio Wings, paper presented at the National Specialists Meeting on Dynamics and Aeroelasticity, Fort Worth, Texas, 6 November 1958.
45. MIT Aeroelastic and Structures Research Laboratory Technical Report 51-2, Theoretical and Experimental Pressure Distributions on Low Aspect Ratio Wings Oscillating in an Incompressible Flow, by W. R. Laidlaw, September 1954.
46. Laschka, B., Über Ergebnisse der experimentellen der instationären Luftkräfte Stand der Forschung in Deutschland, Wiss. Ges. für Luft- und Raumfahrt Nonstationary Aerodyn., p. 135-198, October 1965. (reproduced in NASA N66-20003).



47. NACA TN D-344, Experimental Determination of the Pressure Distribution on a Rectangular Wing Oscillating in the First Bending Mode for Mach No.'s from 0.24 to 1.30, by H. C. Lessing, J. L. Troutman, and G. P. Menees, December 1960.
48. NASA TR R-48, A Systematic Kernel Function Procedure for Determining Aerodynamic Forces on Oscillating or Steady Finite Wings at Subsonic Speeds, by C. E. Watkins, D. S. Woolston, and H. J. Cunningham, 1959.
49. NACA TN 1194, Effect of Finite Span on the Airload Distributions for Oscillating Wings. I - Aerodynamic Theory of Oscillating Wings, by E. Reissner, 1947.
50. NACA TN 1195, Effect of Finite Span on the Airload Distributions for Oscillating Wings. II - Methods of Calculation and Examples of Application, by E. Reissner and J. E. Stevens, 1947.
51. NACA TN 4302, Analytical and Experimental Investigation of Aerodynamic Forces and Moments of Low-Aspect-Ratio Wings Undergoing Flapping Oscillations, by D. S. Woolston, S. A. Clevenson, and S. A. Leadbetter, May 1958.
52. Kuchemann, D., "Some Remarks on the Interference Between a Swept Wing and a Fuselage," Proceedings of AGARD Conference #71 on Aerodynamic Interference, Report no.1, 28 September 1970.
53. Labrujere, T. E., Loeve, W., and Slooff, J. W., "An Approximate Method for the Calculation of the Pressure Distribution on Wing-Body Combinations at Subcritical Speeds," Proceedings of AGARD Conference 371 on Aerodynamic Interference, Report no. 11, 28 September 1970.
54. DFVLR-Bericht Nr 0562, Untersuchungen zur Bestimmung der Druckverteilung an Flügel-Rumpfkombinationen. Teil I: Messergebnisse für Mitteldeckeranordnung aus dem 1,3 m - Windkanal, by H. Körner, 1969.



# INITIAL DISTRIBUTION LIST

	No. Copies
1. Defense Documentation Center Cameron Station Alexandria, Virginia 22314	2
2. Library, Code 0212 Naval Postgraduate School Monterey, California 93940	2
3. Chairman, Department of Aeronautics Naval Postgraduate School Monterey, California 93940	1
4. Professor L. V. Schmidt, Code 57Sx Department of Aeronautics Naval Postgraduate School Monterey, California 93940	1
5. Office of Naval Research Dr. A. Laufer, Chief Scientist 1030 E. Green St. Pasadena, California 91109	1
6. Dr. Alan Somoroff, Code AM-21 Naval Air Development Center Warminster, Pennsylvania 18974	1
7. Naval Air Systems Command Code NAIR 320D Washington, D.C. 20360	1
8. Naval Air Development Center SAED, Systems Analysis Division Code SRS Warminster, Pennsylvania 18974	1
9. Naval Air Systems Command Mr. G. P. Maggos, Code NAIR 530214 Washington, D.C. 20360	1
10. CDR Richard L. Breckon 2393 No. Allen Ave. Altadena, California 91001	2





## DOCUMENT CONTROL DATA - R &amp; D

(Security classification of title, body of abstract and indexing annotation must be entered when the overall report is classified)

ORIGINATING ACTIVITY (Corporate author)

Naval Postgraduate School  
Monterey, California 93940

2a. REPORT SECURITY CLASSIFICATION

Unclassified

2b. GROUP

REPORT TITLE

A DISCRETE POTENTIAL ELEMENT APPROACH TO  
NONSTEADY SUBSONIC LIFTING SURFACE THEORY

DESCRIPTIVE NOTES (Type of report and, inclusive dates)

Doctorate Thesis; June 1972

AUTHOR(S) (First name, middle initial, last name)

Richard Louis Breckon; Commander, United States Navy

REPORT DATE

June 1972

7a. TOTAL NO. OF PAGES

190

7b. NO. OF REFS

54

CONTRACT OR GRANT NO.

9a. ORIGINATOR'S REPORT NUMBER(S)

PROJECT NO.

9b. OTHER REPORT NO(S) (Any other numbers that may be assigned  
this report)

DISTRIBUTION STATEMENT

Approved for public release; distribution unlimited.

SUPPLEMENTARY NOTES

12. SPONSORING MILITARY ACTIVITY

Naval Postgraduate School  
Monterey, California 93940

ABSTRACT

A discrete potential element approach to subsonic numerical lifting surface theory has been developed and shown to be practical in predicting the nonsteady loading on harmonically oscillating, medium to low aspect ratio wings. A unique method of including the wake effect in the wing kernel function matrix prior to solution of the singular integral downwash equation was devised, thus greatly simplifying the velocity potential formulation. In addition, termination of the effective wake a finite distance downstream of the wing was investigated, with wing loading found to converge to within one per cent in an effective wake length of four root chords.

This discrete element method has also been extended to the case of an oscillating wing, cantilevered from a cylindrical fuselage, to investigate nonplanar interference effects. This interference in wing loading, while of relatively small magnitude, does exist in both pressure amplitude and phase angle distributions, and is, therefore, of importance in three-dimensional stability analyses of wing/body configurations.



KEY WORDS	LINK A		LINK B		LINK C	
	ROLE	WT	ROLE	WT	ROLE	WT
UNSTEADY AERODYNAMICS						
AEROELASTICITY						
SUBSONIC AERODYNAMICS						
LIFTING SURFACE THEORY						



26 OCT 73  
1 JUN 76

19369  
23355

134784

Thesis  
B80309  
c.1

Breckon

A discrete potential  
element approach to non-  
steady subsonic lifting  
surface theory.

26 OCT 73  
1 JUN 76

19369  
23355

Thesis  
B80309  
c.1

Breckon

A discrete potential  
element approach to non-  
steady subsonic lifting  
surface theory.

134784

thesB80309

A discrete potential element approach t



3 2768 002 07222 5

DUDLEY KNOX LIBRARY